VIBRATORY ANALYSIS
OF TILLAGE OPERATION

A THESIS

Submitted to the College of Graduate Studies

in Partial Fulfillment of the Requirements

for the Degree of

Doctor of Philosophy

in the

Department of Agricultural and Bioresource Engineering

University of Saskatchewan

Saskatoon, Saskatchewan

by

Ji Zhang

Spring 1997

UNIVERSITY OF SASKATCHEWAN

College of Graduate Studies and Research

SUMMARY OF DISSERTATION

Submitted in Partial Fulfillment of the Requirements for the

DEGREE OF DOCTOR OF PHILOSOPHY
by

Ji Zhang

Department of Agricultural and Bioresource Engineering
University of Saskatchewan

Spring 1997

Examining Committee:

Dr. D.J. Pennock	Dean/~~Associate Dean~~/Dean's Designate, Chair College of Graduate Studies and Research
Dr. D. I. Norum	Chair of Advisory Committee, Department of Agricultural and Bioresource Engineering
Dr. R. L. Kushwaha	Supervisor, Department of Agricultural and Bioresource Engineering
Dr. P. R. Ukrainetz	Department of Mechanical Engineering
Dr. R. J. Ford	Department of Agricultural and Bioresource Engineering
Dr. D. Wulfsohn	Department of Agricultural and Bioresource Engineering

External Examiner:

Dr. K. C. Watts
Department of Agricultural Engineering
Technical University of Nova Scotia
P. O. Box 1000
Halifax, Nova Scotia B3J 2X4

VIBRATORY ANALYSIS OF TILLAGE OPERATION

Energy conservation in agricultural operation is becoming increasingly important for the viability of the modern agricultural industry. The endless desire for increased productivity in agricultural operations is arousing intensive search for more efficient ways of soil and earth moving process than the conventional tractive methods. Vibratory tillage operation has been investigated for the possibility to realize more effective soil cutting.

For the forced oscillatory soil cutting, it has been found that soil cutting resistance decreases as vibratory amplitude and frequency increase. However, the soil resistance reduction was achieved at a substantial increase in total power consumption. Two sources of energy provide the required energy to the forced oscillatory soil cutting process: the oscillator driver and the tractor drawbar power. An optimum frequency and amplitude were suggested for the energy conservation in a given circumstance.

For the general soil cutting during agricultural field operation, numerous investigations have found that the simple tools carry horizontal forces which fluctuate in a periodic manner. This indicates that the actual soil cutting is a process of vibration. Since the tillage tool oscillation is caused by the soil resistance, this phenomenon is called the self-excited vibration.

A tillage tool operating on agricultural soil was considered as a cantilever beam subjected to the fluctuating soil cutting resistance. A lateral vibration equation was used to describe the motion of the shank.

$$\frac{\partial^2}{\partial x^2}[EI(x)\frac{\partial^2 w}{\partial x^2}(x,t)] + \rho A(x)\frac{\partial^2 w}{\partial t^2}(x,t) - P\frac{\partial^2 w}{\partial x^2}(x,t) = f(x,t)$$

The analytical solution of the above equation for soil-shank system does not exist as the shank is not uniform and/or the soil resistance is discontinuous. However, the finite element analysis can be used to solve this problem by using the variational method.

A finite element model was developed to simulate the response of the deflection, velocity and acceleration of the shank and tillage tool when the soil resistance was applied at the end of the shank. It was found that the responses of the displacement, velocity and acceleration of the blade were associated with the natural frequency of the system and the applied frequency of the soil cutting resistance. The soil cutting resistance will cause the movement of the shank-tool assembly. In turn the position of the tillage tool will affect the soil cutting resistance. A transient soil cutting model was developed to obtain the relationship between the soil cutting resistance and the movement of the tillage tool. The values of the acceleration of the tillage tool calculated through the finite element method were compared with the results of the soil bin measurement. There was a good correlation between the measured data and the model estimation values. The verification of the model was in good agreement in terms of acceleration for the first few points of comparison. A higher sampling rate provided a better agreement between the test data and the model estimations. This analysis provided a guidance for the shank-tool assembly design in considering the vibration effect.

BIOGRAPHICAL

1962	Born in Hunan, China.
1981	B. Sc, (Agric. Eng.); Gansu Agricultural University, Lanzhou, China.
1981-1983	Assistant Engineer, Gansu Agricultural University, Lanzhou, China.
1984-1989	Instructor, Gansu Agricultural University, Lanzhou, China.
1989-1990	Visiting Scholar, University of Saskatchewan, Saskatoon, Canada.
1992	M. Sc, University of Saskatchewan, Saskatoon, Canada.
1992-1996	Ph. D. Student, University of Saskatchewan, Saskatoon, Canada.

HONOR

University Graduate Scholarship, University of Saskatchewan. Nov. 93-Oct. 94

PERMISSION TO USE

The author has agreed that the library, University of Saskatchewan, may make this thesis freely available for inspection. Moreover, the author has agreed that permission for extensive copying of this thesis for scholarly purposes may be granted by the Professors who supervised the thesis work recorded herein or, in their absence, by the head of the Department or the Dean of the College in which the thesis work was done. It is understood that due recognition will be given to the author of the thesis and to the University of Saskatchewan in any of the material in this thesis. Copying for publication or any other use of the thesis for financial gain without approval by the university of Saskatchewan and the author's permission is prohibited.

Requests for permission to copy or to make any other use of the material in this thesis in whole or in part should be addressed to:

Head of the Department of Agricultural and Bioresource Engineering
University of Saskatchewan
57 Campus Dr.
Saskatoon, Saskatchewan
Canada, S7N 5A9

ABSTRACT

A forced oscillatory soil cutting model was proposed with consideration for the energy requirement of the oscillator system and the soil cutting resistance related to the drawbar power of the tractor. A comparison between energy consumption in the cutting process for oscillatory and non-oscillatory cases was presented. Two sources of energy provide the required energy to the oscillatory soil cutting process: the oscillator driver and the tractor drawbar power. An optimum frequency was suggested for a given condition to realize a more effective soil cutting process.

A tillage tool operating on agricultural soil was considered as a cantilever beam subjected to the fluctuating soil cutting resistance. A finite element model was developed to simulate the response of the deflection, velocity and acceleration of the shank and tillage tool when the soil resistance was applied at the end of the shank. It was found that the responses of the displacement, velocity and acceleration of the blade were associated with the natural frequency of the system and the applied frequency of the soil cutting resistance. It is known that the soil cutting resistance will cause movement of the tool. In turn, the position of the tillage tool will affect the soil cutting resistance. A transient soil cutting model was developed to obtain the relationship between the soil cutting resistance and the movement of the tillage tool. The values of the acceleration of the tillage tool calculated through the finite element method were compared with the results of soil bin measurements. There was a good correlation between the measurement data and the model estimation values. The verification of the model was in good agreement in terms of acceleration for the first few points of comparison. A higher sampling rate provided a better agreement between the test data and the model estimations.

ACKNOWLEDGMENTS

The author wishes to thank R. L. Kushwaha for his assistance and guidance during the preparation of this thesis. The author would also like to express his appreciation for the much needed advice and critics from other members of the supervisory committee, R. J. Ford, D. Wulfsohn, K. Williams, P. R. Ukrainetz and D. I. Norum.

Finally, thanks goes to my wife, Ying Zhang, for her moral support in preparing this thesis. My appreciation also goes to my son, Milton Zhang, for his understanding and encouragement.

TABLE OF CONTENTS

LIST OF TABLES

LIST OF FIGURES

LIST OF SYMBOLS

a	velocity ratio (dimensionless)
A(x)	cross section of the beam (m^2)
A_0	Fourier coefficient
A_n	Fourier coefficient
B_n	Fourier coefficient
b	damping coefficient (Ns/m)
B	tool width (m)
c	cohesion strength (kPa)
C_1	constant
C_2	constant
C_3	constant
C_4	constant
C_m	constant in Burger model
d	tool operating depth (m)
E	Young's modulus (kPa)
E_{dr}	drawbar energy consumption (W)
E_k	value related to the stiffness of the spring element (kPa)
E_m	value related to the stiffness of the spring element (kPa)
E_{os}	energy consumption of oscillator (W)
E_{st}	non-oscillatory energy consumption in a time period (W)
f	force per unit length (N/m)
F	transverse point load (N)
F_0	driving force (N)

F_{dr} average drawbar force (N)

[F] force matrix (N)

G shear modulus (kPa)

I moment of inertia of the cross section (m^4)

k spring constant (N/m)

k_t Timoshenko's shear coefficient (dimensionless)

[K] stiffness matrix (N/m)

l length of shank (m)

L oscillatory amplitude (m)

M bending moment (Nm)

m mass (kg)

[M] mass matrix (kg)

N_γ dimensionless factor due to gravity term

N_c dimensionless factor due to cohesion term

N_q dimensionless factor due to gravity term

P axial force (N)

P_γ force due to gravity term (kN)

P_b applied pressure to the top surface of a semi-infinite body (kPa)

P_c force due to cohesion term (kN)

P_{ca} force due to adhesion term (kN)

P_{dr} drawbar power (J)

P_{os} power required to drive oscillator (J)

P_{st} power required for non-oscillatory operation (J)

P_t force on the tool (kN)

P' force on the imaginary blade (kN)

q surcharge on the soil surface (kPa)

Q boundary conditions

R(t)	soil cutting resistance (N)
s	exponential coefficient, root of equation (dimensionless)
S	area on which the pressure is applied (m^2)
t	time (s)
t_0	time zero from which the tool is about to move forward (s)
t_1	time blade meets the untilled soil (s)
t_2	time blade begins to move backward (s)
t_3	time blade begins to move forward again (s)
T(t)	time dependent function
U	deflection of shank (m)
$\dot{U}$	velocity of shank (m/s)
$\ddot{U}$	acceleration of shank (m/s^2)
V	shear force (N)
V_c	constant velocity of carriage (m/s)
w	transverse displacement of beam (m)
W(x)	space dependent function
x	displacement (m)
x'	velocity (m/s)
x''	acceleration (m/s^2)
x(f)	function in frequency domain
x(t)	function in time domain
Z	depth of impression of the loaded area into the semi-infinite body (m)
α	rake angle of the tool from horizontal (degree)
β	parameter of the Newmark numerical method (dimensionless)
β	angle of soil failure zone (degree)
γ	parameter of Newmark numerical method (dimensionless)
γ'	soil specific weight (kN/m^3)

δ angle of soil-metal friction (degree)

Δt increment in time t (s)

ε strain

ζ yield stress in shear (Pa)

η viscosity pertaining to shear stress above ζ (Ns/m)

θ phasor keeping tool speed equal to zero (rad)

θ_1 slope of the shank at finite element node 2 (rad)

θ_2 slope of the shank at finite element node 4 (rad)

λ_k values related to the viscosity of the dashpot element (kPa·s)

λ_m values related to the viscosity of the dashpot element (kPa·s)

ν Poisson's ratio for the soil

ξ damping ratio

ρ density of shank (kg/m^2)

σ stress (Pa)

σ_n normal stress on the sliding plane (Pa)

τ soil shear strength (Pa)

τ_c period of cycle (s)

ϕ phase angle (rad)

ϕ' internal frictional angle of material (degree)

υ test function

ψ shear strain

ω driving force frequency (rad/s)

ω_n natural frequency of the system (rad/s)

CHAPTER 1

INTRODUCTION AND OBJECTIVES

1.1 Introduction

Tillage is a basic practice in the crop production system. It is a process of mechanical manipulation of the soil by changing bulk density, soil aggregate size distribution and other physical properties of the soil. The objectives of proper tillage are to provide a suitable environment for seed germination, root growth, weed control, soil-erosion control, and moisture control.

A major portion of the energy consumption in an agricultural operation can be attributed to the movement of soil by tillage tools. Even though the tool operating depth seldom exceeds 100 mm, the areas involved are large and the quantity of soil moved each year is enormous (Kushwaha and Roy 1989). Tillage requires well over half of the engine power expended on North American farms, and it has been estimated that more than 250 billion tons of soil are moved each year in United States alone (Buckingham 1976).

Tillage operations also result in large friction and wear loss to the implement. A strategy for tribology in Canada (NRC 1986) states that the total annual losses in the agricultural sector due to friction and wear amount to $1.26 billion. The share for tillage operations is estimated to be more than $32 million. Because of the high cost of energy and significant losses due to friction and wear, energy conservation in agricultural practice is becoming increasingly important for the viability of the modern agricultural industry. Any tillage practice which does not return more than its cost by increasing and improving soil conditions should be eliminated or changed. Contrary to previous beliefs, soil needs

to be worked only enough to assure optimum crop production and weed control. Any tillage activity beyond that is of questionable value.

An analysis of soil tool interaction reveals that practically all tillage tools consist of some device for applying pressure to the soil, often by means of inclined planes, or wedges, or their combination. The soil in the path of these tools is subjected to compressive stresses which result in shear failure of the soil. Since the soil is strongest in compression, it becomes obvious that tillage tools have to impart excessive energy to the soil for altering the soil conditions. A device that will shear by a mode in which the soil is weakest is yet to be developed and would be welcomed.

The endless desire for increased productivity in agricultural operations is arousing intensive search for more efficient ways of soil cutting and earth moving processes than the conventional tractive methods. Among the methods of energy applications being considered are:

a. Forced vibration of the soil cutting device
b. Rotary cutting techniques
c. High speed soil cutting techniques.

For better operation and economical energy consumption, research efforts in the development of soil-engaging tools with their prime movers have been conducted in parallel with the new research area called soil dynamics to meet the challenges of finding new techniques for efficient energy consumption in cutting and moving soil. Today, the role of soil dynamics in solving problems and developing technology is recognized as being important around the world. Soil dynamics is an engineering discipline that is studied and practiced worldwide.

Tool oscillation for soil cutting has been utilized since the beginning of recorded history. The earliest farmer moved his stick plow back and forth when he encountered a rough spot in the soil in order to move the plow forward. In oscillating the plow, the primary goal was to reduce the soil cutting resistance rather than simply to increase the man power for a unit soil movement.

Conventional tillage implements usually have soil-working tools which do not move relative to the implement frame. Their draft requirements are comparatively high as they are always in contact with the soil. The power for operating these implements is transmitted through the traction of the vehicle. To improve the tractive efficiency the tractor drive wheels are ballasted with additional weights. However, this practice causes severe soil compaction, which is detrimental to efficient cropping of plants. Several investigators have reported that oscillating soil cutting tools have lower draft requirements and smaller soil aggregates than do other non-oscillating counterparts such as moldboard plows and cultivator sweeps when working under identical conditions. Therefore, an oscillating soil cutting tool may reduce the number of operations to prepare an acceptable seedbed and minimize soil compaction, thus providing a better physical environment for plant growth.

It is well known that the vibrating action facilitates penetration in certain conditions of soils. The exact nature of the phenomenon is complex and is not fully understood. In certain soils, there appears to be a thixotropic transformation during agitation of soil material (Kezdi 1974). In sand there is a tendency for particles to separate by agitation, a phenomenon known as liquefaction (Mogami and Kubo 1953). The vibration environment reduces the skin friction due to some type of fluidization at the

interface. A vibratory shear surface appears due to vibration, which facilitates soil-tool penetration under the action of the applied loads.

It has been recognized that the average draft of a tillage implement can be reduced by induced vibration. However, to realize this goal some extra power has to be added to drive the tillage tool for vibration. Draft power plus the power needed to drive the vibrator constituted the total power consumption. It is common practice to evaluate the efficiency of the vibratory soil working process by comparing them with the corresponding quasi static process. Only a limited amount of experimental data on the total power consumption has been published (Butson and MacIntyre 1981). The results of experimental studies of different authors led to contradictory evaluations of the energy consumption of the cyclic soil working process in comparison with their quasi static counterparts. So, some investigators came to a conclusion that the total power requirement was low for vibrating the tillage tool (Gunn and Tramontini 1955; Hendrick and Buchele 1963; Dubrovskii 1968). Others came to a contrary opinion (Smith et al. 1972; Butson and MacIntyre 1981), while other investigators found that the energy consumption for both these processes was identical (Eggenmuller 1958; Verma 1971). They concluded that the energy required to oscillate the tool is nearly equal to the draft energy reduction. These contradictions create significant difficulties in development of more sophisticated soil working machinery.

When a tillage tool operates it carries transverse loads that will induce bending of the shank. The soil resistance acting on the shank of the tillage tool becomes stored by the mechanism of deformation known as strain or elastic energy through the entire stressed volume. Numerous researchers have found that tillage tools acting on agricultural soils encounter periodic fluctuations. These fluctuations will induce the shank of the tillage tool to move back and forth relative to the tool implement. This phenomenon indicates

that the actual tillage tool operation is accompanied by a vibration process. Since this vibration is excited by soil resistance, it is called the self-excited vibratory process.

The self-excited vibration has been reported by a number of researchers (Dubrouskii 1968; Upadhyaya et al. 1987). However, their research work was only limited in recognition of this phenomenon. A further investigation of the self-excited vibration of tillage operation is essential for the better understanding of the soil tool interaction and for the potential possibility of utilization of these vibratory characteristics to realize a more efficient soil cutting operation and to reduce tillage energy consumption. The ultimate goal in tillage system research is the development of scientific knowledge to the extent that the performance of a tillage tool design, the forces, and the final soil conditions can be accurately predicted when initial conditions of the soil, operating conditions, and design parameters of a tillage tool are known.

It can be seen that in general, there is a reduction in the soil resistance for the force oscillatory operation. However, there are so many contradictions in the energy requirement for the oscillatory soil cutting operation. The magnitude of the reduction (increase) of the energy requirement and the effect of the oscillation parameters vary in such large quantities that only qualitative information should be gained. This study is an effort to clarify the energy requirement contradictions through the theoretical investigation.

More attention has been given in the investigation of the self-excited vibration for the better understanding of the soil tool interaction and for the potential possibility of utilization of these vibratory characteristics to realize a more efficient soil cutting operation.

This thesis is organized into eight chapters. The first chapter is an introduction and objectives. Chapter 2 gives the literature review of the oscillatory soil cutting and self-excited soil cutting operation. The literature review summarizes the published work to these subjects. Chapter 3 investigates the soil properties and soil dynamics and how these characteristics affect the soil failure. The analysis of soil cutting energy consumption in the oscillatory and non-oscillatory cases are discussed is chapter 4. An oscillatory model is introduced to study the effect of different parameters on the forces and energy requirements in soil cutting. Chapter 5 describes the differential equation governing the motion of the transverse vibratory beam. Finite element model is developed to obtain the responses of the vibratory shank under the transverse soil cutting resistance in chapter 6. The parameters affecting the motion of the shank under the soil cutting resistance are also investigated. Chapter 7 presents the soil bin test and model verification results. Chapter 8 gives summary, conclusions and recommendations for future work.

1.2 Objectives

The overall objective of this project was to study the vibratory phenomenon of soil-tool interaction. The specific objectives of this study were:

. To develop a dynamic model to predict the energy consumption of forced oscillatory tillage operation.

. To develop a finite element model to simulate the response of the tillage shank when the vibrating system is self excited by the soil cutting resistance.

. To study the tillage tool parameters that affect soil cutting operation.

. To carry out the soil bin test to verify the vibratory response of the tillage tool under the action of fluctuating soil cutting resistance.

CHAPTER 2

LITERATURE REVIEW

2.1 Forced Vibratory Soil Cutting

The use of vibration to reduce the force needed to drive piles into the ground was first reported in 1935 in Russian (Buston and MacIntyre 1981). Since the early 1950s there has been increasing interest in the application of vibration to soil cutting and tillage machinery, and research has been carried out in a number of countries. Experimental work, mainly in soil bins, has concentrated on demonstrating the level of draft reduction that can be achieved, and relating this to the vibration parameters.

Some basic studies to determine the effects of vibratory load on soil strength were made by civil engineers in the 1950's. It was recognized early that there are some changes in the physical properties of the soil near the zone of vibration due to vibratory loading. Mogami and Kubo (1953) investigated the effect of vibration on soil strength. They related the reduction of strength in the presence of vibration to what they called "liquefaction" from their results on sand and loamy soils. Winterkorn (1954) referred to this as a macromeritic liquid state (liquid dispersed in macroparticulates). They concluded that the shearing strength of soil diminishes with an increase in vibration. Cooper and McCreery (1958) found similar results in clay soil. However, the physical explanation of the phenomenon was given as a thixotropic effect due to the change of bound water to free water. The change of bound water into free water was then concluded to be the reason for rapid decrease in the shearing strength.

An investigation on the feasibility of the application of oscillatory motion to agricultural machines in North American was conducted by Gunn and Tramontini (1955). A tractor with a pitman drive providing the appropriate frequency and amplitude to a sub-soiler was developed and tested. The results indicated that the draft was reduced only when a dimensionless parameter ($v/\omega e$) was less than one, where v is the tractor speed, ω is the pitman angular velocity, and e is the crack eccentricity. A pitman drive was a positive drive composed of a crack slider mechanism used to transfer the angular motion to the reciprocating form.

Savchenko (1958) reported that the coefficient of internal friction of sand decreased with an increase in amplitude and/or frequency of vibration. Tests on clay soils indicated greater reduction of shear strength by increasing the frequency and amplitude, but very little reduction was observed at amplitudes greater than 0.6 mm.

Eggenmuller (1958) performed a series of tests in which the basic objective was to reduce draft by throwing soil upward so that the tool moved forward into the uncut soil free of friction without lifting any soil during this forward motion. Results indicated that relatively small amplitudes of movement resulted in a considerable reduction in draft. A draft reduction of up to 40% to 50% was obtained with the same total power input. A maximum draft reduction of 75% was reported.

Shkurenko (1960) studied the effect of oscillation on the cutting resistance of soil. His results showed that at fairly high speeds of oscillation, there was a considerable reduction in the cutting resistance in the range of 50% to 60% and the effect of forward speed was found to be relatively small.

Kondner (1960), in a study on vibratory, unconfined compression tests on clay soil, found that the maximum stress required to cause failure was 20 - 50% of that obtained by non-vibratory, unconfined compression tests. The variation was dependent upon the moisture content of the clay soil. He explained that in the non-vibrating, unconfined compression test there is sufficient time for the clay particles and their diffuse double layers of bound water to reorient themselves within the free water phase into more stable arrangements. But there is not sufficient time for a complete distortion of very viscous water. Under the vibratory loading, the vibratory energy is a form of activation energy which must reach a certain value before it sufficiently energizes the layers of very viscous, bound water in order to cause their breakdown. When this energy state is reached, the effective viscosity of the bound water is greatly reduced and yield or failure takes place.

Panagiotopoulos (1962) investigated the effect of oscillation on bulldozer blades by testing two sizes of blades under frequencies of 18 and 46 Hz. Three cutting angles of blades, 45, 60, 68 degrees were selected. It was found that the maximum reduction of the cutting resistance was obtained when the cutting angle was 45 degrees and the frequency was very close to the natural frequency. The power was reduced by 43% at a frequency of 42 Hz and amplitude of 5 mm.

Mackson (1962) tried to reduce the soil - metal friction by utilizing electro-osmosis lubrication. Mink et al. (1964) tried the air lubrication method. The electric potential was large and the power for air compression was too high. Both methods have been shown to be completely uneconomical.

Encouraged by the successful application of vibrations to the reduction of soil cutting resistance, researchers at Bell Telephone Laboratories started active research for developing vibratory cable plows (Boyd and Nalezny 1967). The immediate goal was to

produce a light weight vibratory plow that can bury short distance service cables economically. Conventional cable plows cannot be used to bury service cables economically because of their size and time required for set up. Plowing for burying telephone cables at about 0.5 to 0.6 meters deep by lightweight low traction vehicles led to the development of commercial vibrating plows utilizing harmonic oscillation. Reasonable penetration rates and drawbar forces were obtained with blade vibration in the direction of penetration. A mathematical model was presented by Boyd and Nalezny (1967) for vibratory soil cutting. They considered a lumped parameter model which consisted of a spring and Coulomb friction to simulate soil cutting by plow blades vibrating horizontally. The spring represented blade and soil elasticity, the Coulomb friction represented the soil strength. The model neglected the mass of the blade-soil combination and neglected angular velocity effects on soil cutting resistance. The results indicated that the average force can be reduced by increasing the frequency, amplitude and system stiffness for a sinusoidal oscillating blade in a compacted sand at a given cutting speed. For practical design values of these parameters, the force can be reduced to 25% of the non-vibrating cutting force. They attributed the force reductions to the small portion of the cycle time at which the blade is in contact with the soil.

Senator (1967) proposed a model of flexible soil penetrator composed of two masses joined by an elastic member with a light damper. Coulomb friction was used to characterize the soil resistance. He concluded that this penetrator had the advantage over a rigid penetrator of equal mass.

Considerable research efforts have been reported in developing vibrating plows in the USSR. Dubrovskii (1968) reported the first vibratory plow actuated by an electro-magnetic drive. The plow operated at a speed of 4.95 km/h at vibrating frequency of 50 Hz and 2 to 3 mm amplitude. A reduction of 29% in draft was obtained. The reduction in

draft constituted 24.7% when the implement was driven at the speed 2.14 km/h. By increasing the frequency to 100 Hz, no reduction in draft was observed which may be interpreted as moving further from the natural frequency of the soil tool system. By studying the vibration of cultivator, the study also showed that the vibration lead to a significant reduction in draft (up to 60%) at 40% reduction of total energy consumption. The vibratory working implements were less adhesive to soil and less jammed up with weedy vegetation. Besides, the wearing and blunting of vibratory tool edges were also less than that of non-vibratory tools.

Senator and Warren (1971) investigated the penetration rates for harmonically forced fore-aft vibrating plows. The soil resistance was represented by two parameters, namely unpenetrated and penetrated soil resistance. The result was a quantitative prediction of penetration rates as a function of harmonic force amplitude and static bias force.

Sulatisky and Ukrainetz (1972) reported that draft force reductions as high as 80% were achieved when the blade was vibrated at frequencies up to 30 Hz and amplitudes up to 12 mm. Percent draft reduction increased with the amount of power available at the vibration actuator. Generally, the overall power required to vibrate and pull the blade through the soil was greater than that required to pull a static blade under the same conditions.

Choa and Chancellor (1973) introduced combined Coulomb friction and viscous damping to present the soil resistance to blade penetration. They determined the coefficient of viscous damping of soil by drawing a sub-soiler into the soil several times at a depth of 250 mm without vibration and varying forward speed.

Brown (1978) presented theoretical and experimental analysis on a bulldozer and reported that the tractive force was reduced by 20% to 30% in the presence of oscillation.

Buston and MacIntyre (1981) described a series of soil bin experiments in which the draft and total power requirements of a soil-cutting blade system were measured. Sinusoidal excitation at frequencies up to 50 Hz and amplitudes up to 8 mm was applied with forward speeds from 0.54 km/h to 1.98 km/h. A draft reduction of more than 50% was reported but only achieved at a substantial increase in total power consumption. Draft power plus the power needed to drive the vibrator constituted the total power consumption. Only a limited amount of experimental data on the total power consumption have been published, but this may indicate that there is often a substantial increase in the overall power consumption when vibration is applied.

Garber (1983) and Spektor (1987) presented theoretical analysis of energy expenditure in cycle-loading versus quasi-static soil processes. They concluded that no unilateral preference statement can be drawn, thus justifying the contradictions in experimental results available. They showed that the existence of an optimal cycle-loading regime, challenging the quasi-static regime, strongly depended on the character of the loading-unloading curves defining the tool-soil system under consideration.

Gupta and Rajput (1993) studied the effect of amplitudes and frequencies on soil break up by an oscillating tillage tool. It was reported that the oscillating tillage tool produced smaller soil aggregates than non-oscillating tillage operation. At a given oscillation amplitude, increasing the frequency above the natural frequency of the soil did not often increase soil break-up. For the range tested, soil break-up increased with increasing amplitude. They optimized the frequency and oscillation amplitude on the basis of maximum clod surface produced per unit of energy input. Maximum utilization of

energy occurred at an oscillation frequency close to the natural frequency of soil. At this frequency of oscillation (i.e. 12.15 Hz), the clod surface produced per unit energy input was nearly maximum at all oscillation amplitudes. An optimum oscillation amplitude for the tool was found to be 9.5 mm for Kharagpur soil under the given circumstances.

Szabo et al. (1994) investigated the effectiveness of a vibrating bulldozer on draft force reduction. As much as 93% draft force reduction was achieved compared with the conventional quasi static counterparts. The combination of vibratory frequency and amplitude significantly affected draft force reduction. In the range of 17.4 - 49 for the velocity ratios, 17.4 was found optimal for combination wet non-cohesive soils while 48 was most effective for dry cohesive soils. In dry soil, the maximum force reduction was measured at higher frequencies, 60-70 Hz while wet soil had optimal values between 20-30 Hz. This investigation indicates that the velocity ratios for the optimal draft reduction are higher than the value suggested by the previous researchers in their tillage oscillating operation.

2.2 Self-Excited Vibratory Soil Cutting

Numerous researchers have found that simple tools acting on agricultural soils sustain horizontal forces which fluctuate in a periodic way. This phenomenon indicates that the actual soil cutting is a process of vibration. This type of soil cutting is widely used, particularly during the operation in compact soil. The methods describing soil cutting forces are usually static. They are based on the static equilibrium of the forces at soil failure. The soil behavior between two subsequent soil failures are not considered. In reality, soil cutting is a discrete process which is dependent upon the soil clods forming and the dynamic system of the implements. The soil cutting force is likely a periodic wave form. The soil cutting force is primarily due to the movement of the tillage

implement. Contrary to the forced vibration, this kind of process is called the self-excited vibration.

Several researchers have noticed this important phenomenon and consequent investigation has been carried out in the periodic wave form of soil cutting and its cause.

Siemens et al. (1965) measured the forces on model tools and photographed the soil cross-section through a glass plate. Draft force for a tillage tool in a soil bin varied ± 33% of the mean draft value. The horizontal distances between failure planes ranged from 25-50 mm.

Olson and Weber (1966) found that the horizontal distance variation between failure planes was 32-42 mm, and that the draft force variation was ±25% of the mean value.

Gill and Vanden Berg (1967) noticed that periodic failure planes also occur ahead of disk tools with the horizontal distance between failure planes approximately 50 mm.

Young et al. (1984) analyzed the power spectra of force variations on triangular-shaped vertical tines operated in a soil bin at depths ranging from 50 to 150 mm. The most common horizontal distances between planes of failure at the instant of highest draft ranged from 100 to 400 mm and increased with depth. In some other cases, the horizontal distances between planes of failure were usually less than the working depth of the tool. They concluded that the predominant vibration was not random and corresponded to the rate of shear plane developed. No frequencies were identified above 10 Hz. The major frequency was about 2 Hz.

Summers et al. (1985) performed the auto correlation function and power spectral density function of the soil force variations for four common types of tillage implements. They concluded that the draft and vertical force resulting from tillage tool-soil interactions appeared to be deterministic at frequencies of 1.43 to 9.99 Hz with a superimposed random component.

Stanford and Young (1986) did a power spectral density analysis of draft variations of rigid cultivator tines. The type and the predominant frequency of the soil failure were found by examining the normalized power spectrum.

Upadhyaya et al. (1987) found that soil-tool force varied in a periodic fashion and, at the extreme, this force variation was in the order of ±50% of a mean draft force value. Available evidence indicated that the physical distance between force peaks wavelength was in the range of 10-400 mm. An examination of the dynamic nature of the tillage tool draft indicated that the failure pattern and fracture distance depended on soil type and condition, and tillage tool speed. They also observed successive failure planes ahead of a disk plow in the range of 12-35 mm.

Licsko and Harrison (1988) analyzed oscillating soil forces of a half-scaled experimental plow to find the predominant frequency. They performed the spectral density analysis of the horizontal and vertical forces signals and concluded that the cyclic shearing failure of the soil ahead of the tool was less than 10 Hz.

Singh et al. (1991) studied the cyclic variations of the draft of a moldboard plow and its effect on the draft control system of a tractor. They found two different predominant frequencies, low and high. The low frequency corresponded to the actual soil failure frequency, while the high frequency corresponded to the breaking of the soil mass

into sub-blocks at the moldboard surface. They concluded that the fracture length was approximately 1 ± 0.2 m and remained almost the same at all plowing speeds and depths.

Boccafogli et al. (1992) observed cyclic phenomena of soil cutting forces from the time domain signals. At low cutting speed, the amplitudes of cycles increased with time. They used a modified power spectral density analysis to locate the predominant frequencies. The results showed that rupture distance increased with an increase in forward speed and reached a stationary value after a few cycles.

Salokhe et al. (1994) performed the power spectral density analysis of the draft and torque signals of a disk tiller. They concluded that the dominant spatial frequency of the periodic variation of draft was about 2.5 - 5.5 cycles/m, while the frequency for torque was 3.3 - 4.3 cycles/revolution of the disk. Secondary dominant frequencies were found in the power spectrum of both draft and torque. A physical explanation was still required for the amplitude of the power spectrum at frequencies other than the principal one.

Noticing the discontinuous process of soil cutting, Malaguti (1995) tried to employ auto regressive techniques to describe soil cutting process. It was found that sixth order auto regressive models fitted in a robust way some harmonics of soil cutting periodicity. As soil cutting frequency depended on cutting depth and speed, a recursive auto-regressive technique could be used to build adaptive filtering and control to use in soil cutting analysis and control in the field.

CHAPTER 3

SOIL PROPERTIES AND SOIL DYNAMICS

The study of soil-tool interaction can be dated back to the last of the 19th century (Goryachkin 1898) and the early 20th century (Nichols 1925). Since then, many investigations have been conducted using empirical and analytical methods and a large number of research papers has been published since 1950. In spite of advances made in recent years, very little of knowledge about soil mechanics has been applied to design of equipment and analysis of tool behavior in soil. Most of the technological advances in soil equipment manipulation have evolved by field experiment and by trial and error. In most cases the important properties characterizing the soil have not been properly recorded.

3.1 Classification of Soils

Theoretically three types of soils are well recognized. There are cohesionless, cohesive and frictional soils.

Shear strength of cohesionless soil is governed by

$$\tau = \sigma_n \tan\phi' \qquad (3.1)$$

where:

τ = soil shear strength (kPa),

σ_n = normal stress on the sliding plane (kPa), and

ϕ' = angle of internal friction of the material (degrees).

Dry sand is usually designated as a purely frictional material, which exhibits little or no cohesion. The angle of internal friction, ϕ', can have a magnitude varying from 18 to 55 degrees (McKyes 1989), depending on the density of the sand and the properties of its constituent particles.

Cohesive soils demonstrate negligible friction and have practically constant shear strength regardless of normal total pressure on the failure plane. Undrained saturated fine grained soils belong to this type. The shear strength can range from nearly zero, for very wet and loosely consolidated soil, to over 280 kPa for a highly consolidated fine grained soil. The sliding failure for these soils is governed by

$$\tau = c \tag{3.2}$$

where:

c = cohesion, the part of strength independent of normal pressure (kPa).

Soils, containing a mixture of coarse and fine materials, and which are partially saturated with water, will possess both frictional and cohesive shear strength properties. For such soils the maximum shear stress is given by,

$$\tau = C + \sigma_n \tan\phi' \tag{3.3}$$

The agricultural soils usually belong to this group. Fig. 3.1 shows the σ-τ plots for the three types of soils.

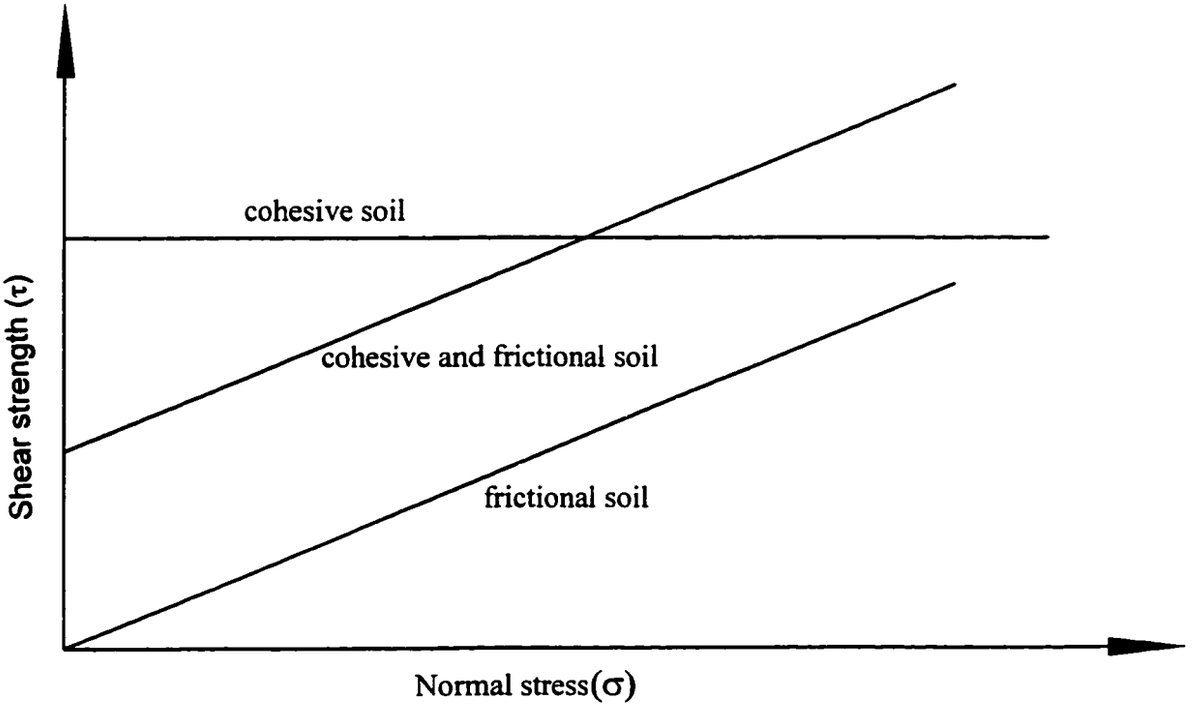

Figure 3.1 Classification of soils

3.2 Soil Failure Characteristics

Since agricultural soils exhibit elastic, plastic, elastoplastic, viscoelastic, and viscoplastic characteristics, their failure behaviors are more complex than those of construction materials. For the oscillatory operation the soil failure is not a continuous process. The soil distorts corresponding to the cyclic motion of the vibration. Several mathematical models have been used to describe the failure characteristics of different types of soils as given in the following section.

3.2.1 Coulomb friction model

Soil will not fail until the stress is greater than the yield stress σ_s. The stress σ does not generate a strain ε when the stress of the soil is less than the yield stress σ_s. The σ_s represents the minimum stress under which strain does not occur.

In oscillating operation, the carriage moves at constant velocity V_c and the tillage tool oscillates relative to the implement. When the blade moves backward the soil resistance is zero. Figure 3.2 illustrates this model for both non-oscillating and oscillating cases.

3.2.2 Elasto-plastic model

In the elasto-plastic model, the soil deforms according to Hooke's law in the elasto stress region. The material undergoes plastic deformation when the state of stress reaches the yield criterion. Figure 3.3 shows the force-time curves for non-oscillating and oscillating cases.

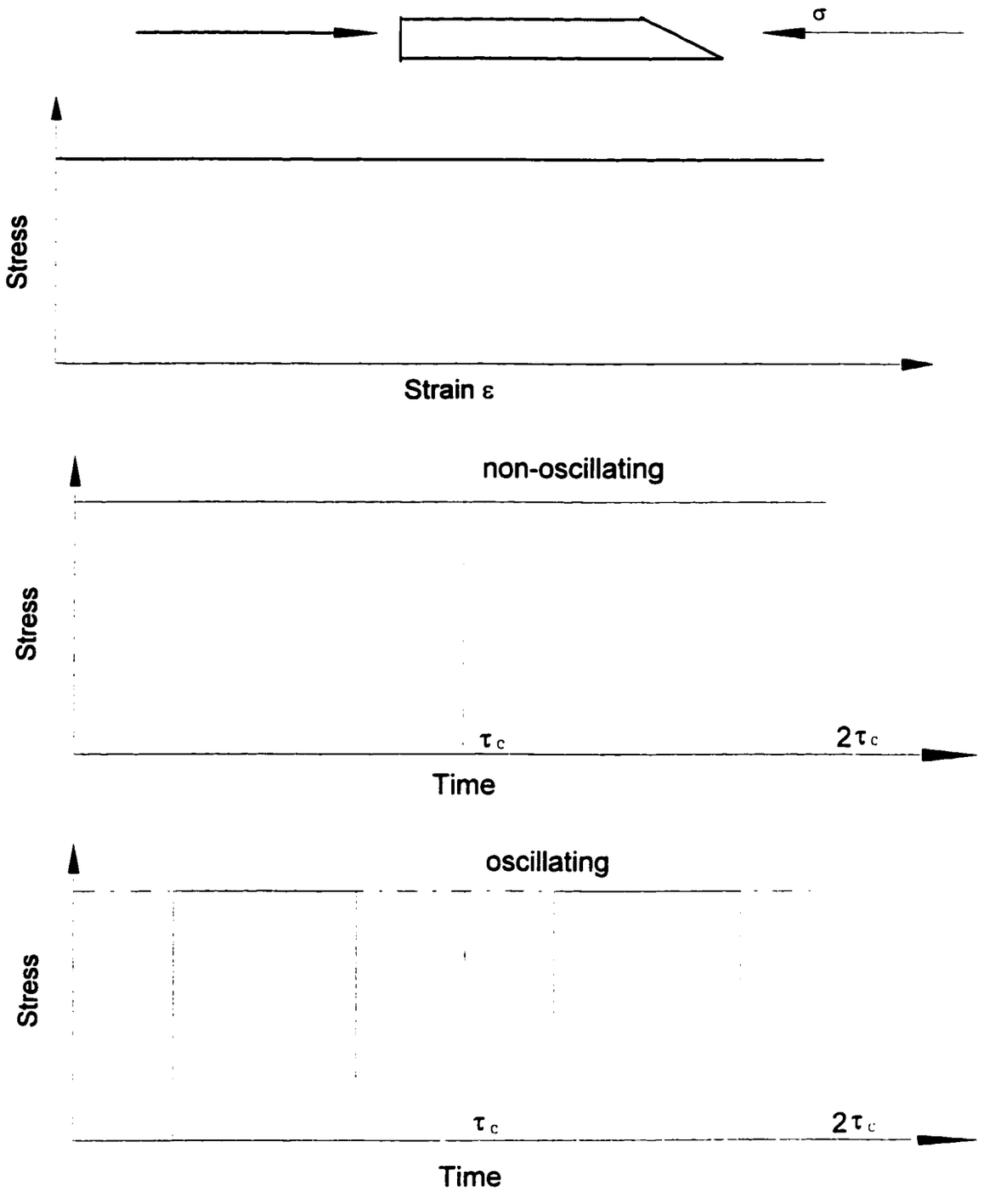

Figure 3.2 Coulomb frictional model

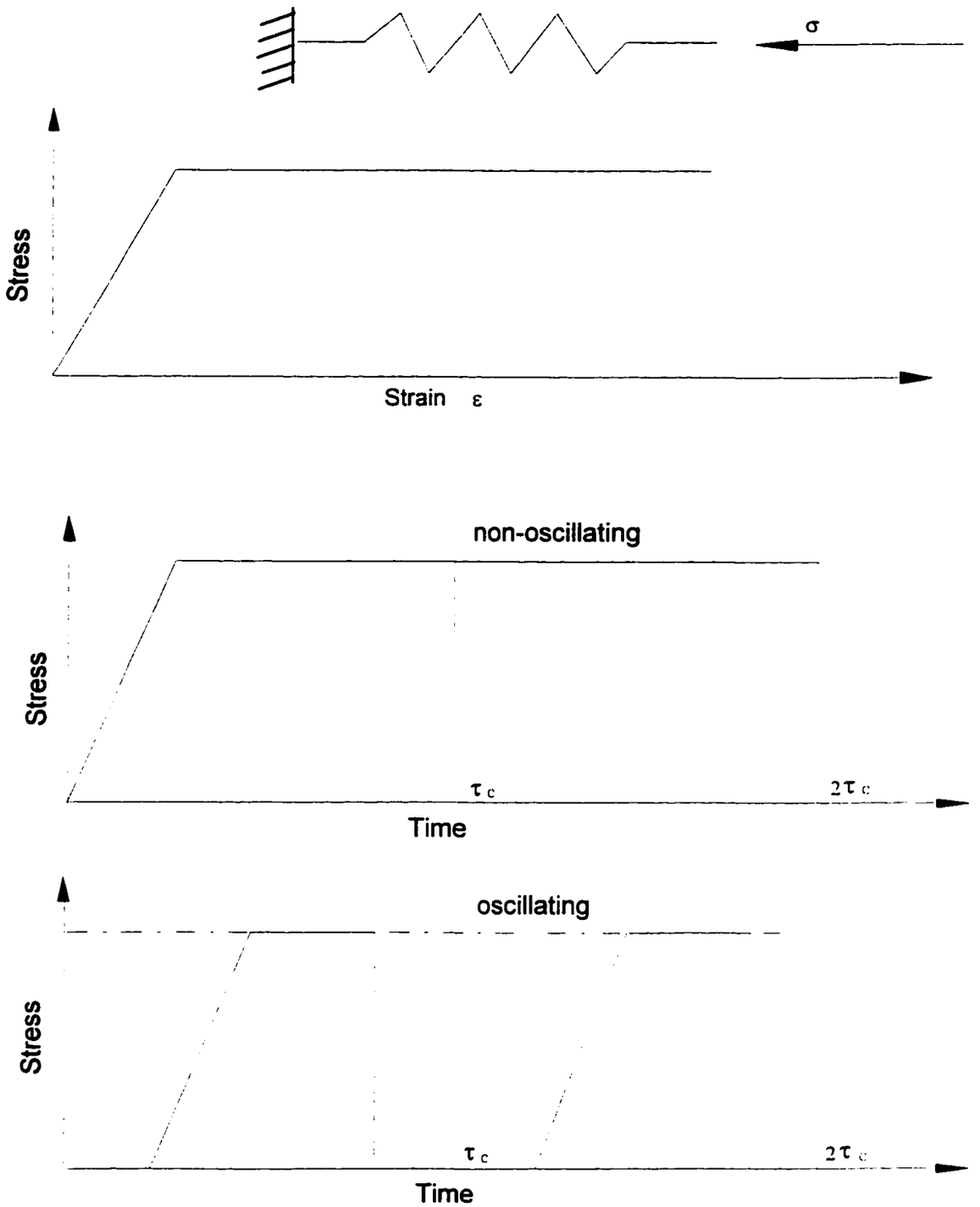

Figure 3.3 Elasto-plastic model

3.2.3 Viscoelastic and viscoplastic model

In many cases, the stress-strain data obtained at quasistatic speeds in laboratory and field test with agricultural soil are considered to be applicable to traction and tillage processes at conventional field speeds. However, many researchers have investigated the effects of time in the stress strain relationships for agricultural soils. Due to the non-elastic behavior of soils, the soil sometimes presents a visco-elastic performance which can be represented by an elastic part and a damping part. Although several combinations of these parts could be used, two theoretical cases are described here.

(a) Bingham model (Fig. 3.4) (Kezdi 1974)

$$\tau = \zeta + \eta \frac{d\varepsilon}{dt} \tag{3.4}$$

where:

ζ $= c + \sigma_n \tan\phi'$, and

η = viscosity pertaining to shear strain above ζ (Pa.s).

Saturated cohesive soils may be described as having visco-plastic characteristics, i.e., they do not deform until a certain level of shear stress is reached. Once the level of shear stress has been reached, any further increase in shear stress is found to be related to the time rate of shear strain.

(b) Burger model (Fig. 3.5) (Ji et al. 1986)

$$Z = \frac{C_m P_b}{\sqrt{A}} \left[\frac{1}{E_M} + \frac{1}{E_k} \left(1 - e^{-\frac{E_k}{\lambda_k} t}\right) + \frac{t}{\lambda_M} \right] \tag{3.5}$$

where:

C_m = a constant for a given process,

P_b = applied load to the top surface of a semi-infinite body (kN),

A = area on which the pressure is applied (m^2),

E_M, E_K = values related to the stiffness of the respective spring elements (kPa),

λ_M, λ_k = values related to the viscosity of the respective dashpot elements (kPa·s),

t = time (s),

Z = depth of impression of the loaded area into the semi-infinite body (m).

$$E_M = \frac{E_1}{1-\nu^2}$$

$$E_k = \frac{E_2}{1-\nu^2}$$

$$\lambda_M = \frac{\lambda_1}{1-\nu^2}$$

$$\lambda_k = \frac{\lambda_2}{1-\nu^2}$$

where:

ν = Poisson's ratio for the soil,

λ_1, λ_2 = viscosity of the respective dashpot elements (kPa·s).

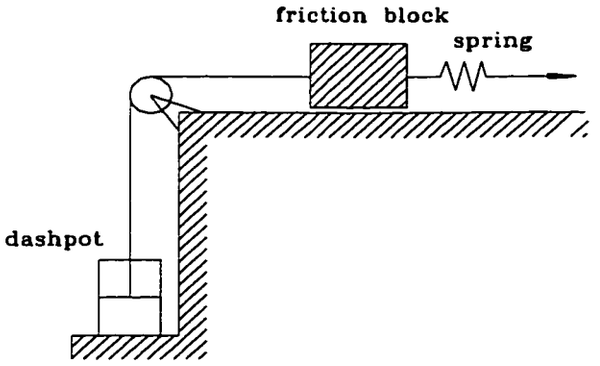

Figure 3.4 Representation of a Bingham body

with a viscous element and a Coulomb friction element (Kezdi 1974)

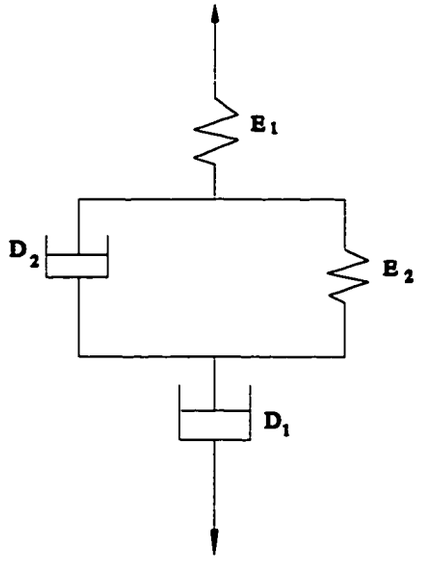

Figure 3.5 Representation of a Burger model
with spring and viscous elements (Ji et al. 1986)

3.3 Non-oscillatory Soil Resistance Models

Failure of soil under the effect of forces exerted by the cutting blades occurs along a specific failure zone. When the blade force is sufficiently large to overcome the soil resistance, shear failure occurs and continues with additional blade displacement. The soil resistance can be predicted by using the general earth pressure equation first proposed by Reece (1965).

$$P_t = (\gamma d^2 N_\gamma + cdN_c + qdN_q)B \tag{3.6}$$

where:

P_t = force on the tool (kN),

γ = soil gravity (kN/m^3),

d = tool operating depth (m),

B = tool width (m),

c = cohesion of the soil (kPa),

q = surcharge on the soil surface (kPa),

N_γ = dimensionless factor due to gravity term,

N_c = dimensionless factor due to cohesion term,

N_q = dimensionless factor due to surcharge term.

In Eq. 3.6, soil cutting resistance was contributed by the gravity, cohesion and surcharge terms.

3.3.1 Simple wedge model

A wide variety of techniques now exist for calculation of soil cutting resistance based on the different failure zone assumption. Considerable work has been done to determine all these dimensionless numbers to predict soil cutting resistance. A great number of soil cutting models was reviewed by Kushwaha et al. (1993).

McKyes and Ali (1977) proposed a model for three dimensional soil cutting calculation for a narrow tillage tool. In their model (Fig. 3.6) a straight bottom failure zone was assumed with a failure wedge composed of a center wedge and side crescents. The surface side failure crescents were assumed to be circular. Using the technique of mechanics of equilibrium soil resistance can be developed as a function of failure angle β, soil characteristics and tool parameters as given below:

$$P_t = \frac{[(\frac{1}{2}\gamma d^2 \frac{r}{d}(1+\frac{2s}{3w}) + qd\frac{r}{d}(1+\frac{s}{w}))\sin(\beta+\phi') + cd\frac{\cos\phi'}{\sin\beta}(1+\frac{s}{w}) - c_a d\frac{\cos(\alpha+\beta+\phi')}{\sin\alpha}]B}{\sin(\alpha+\beta+\delta+\phi')} \qquad (3.7)$$

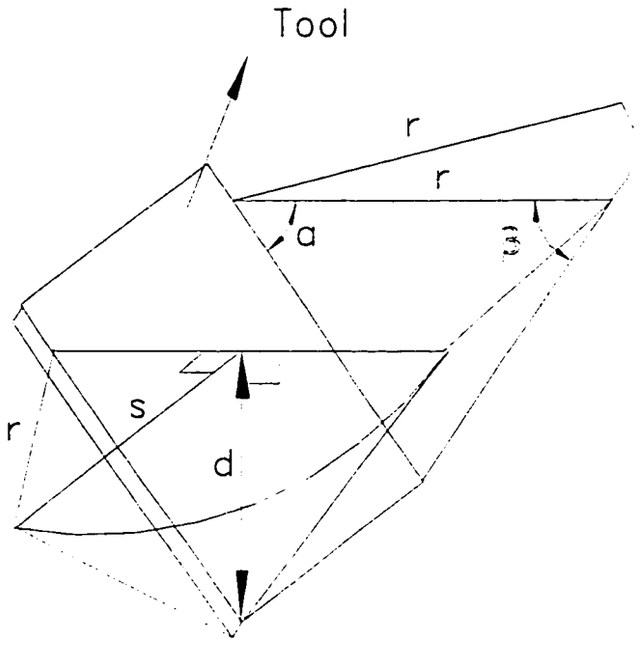

Figure 3.6 Failure pattern of the McKyes-Ali model

This equation falls into the universal earth moving Eq. 3.6.

where:

$$N_\gamma = \frac{\frac{1}{2}(\cot\alpha + \cot\beta)(1 + \frac{2d}{3w}\sqrt{\cot^2\beta + 2\cot\alpha\cot\beta})\sin(\beta + \phi')}{\sin(\alpha + \beta + \delta + \phi')} \tag{3.8}$$

$$N_q = \frac{(\cot\alpha + \cot\beta)(1 + \frac{d}{w}\sqrt{\cot^2\beta' + 2\cot\alpha\cot\beta})\sin(\beta + \phi')}{\sin(\alpha + \beta + \delta + \phi')} \tag{3.9}$$

$$N_c = \frac{\cos\phi'(1 + \frac{d}{w}\sqrt{\cot^2\beta + 2\cot\alpha\cot\beta})}{\sin(\alpha + \beta + \delta + \phi')} \tag{3.10}$$

$$N_{ca} = \frac{-\cos(\alpha + \beta + \phi')}{\sin\alpha\sin(\alpha + \beta + \delta + \phi')} \tag{3.11}$$

$$s = d\sqrt{\cot^2\alpha + 2\cot\alpha\cot\beta} \tag{3.12}$$

$$r = d(\cot\alpha + \cot\beta) \tag{3.13}$$

where:

α = rake angle of the tool from horizontal (degree),

β = angle of soil failure zone (degree),

δ = angle of soil-metal friction (degree), and

ϕ' = internal frictional angle of soil (degree).

The soil resistance can be obtained if the failure angle β can be determined. In the McKyes-Ali model, the failure angle β was obtained by minimizing the gravity term N_γ. A modified model (Zhang and Kushwaha 1995) for predicting soil cutting forces on tillage tools was formulated based on passive earth pressure theory and McKyes and Ali

model. In their modified model, the rupture angle β was identified by minimizing the soil cutting resistance in the passive movement condition instead of minimizing N_γ term.

3.3.2 Two-wedge model

Zhang and Kushwaha (1995) proposed a more accurate approximation by establishing two simple wedges as shown in Fig 3.7 (a) and (b).

The base of the wedge ABC makes an angle of (180-α-β) with the blade surface. β was determined by the original prediction of the simple wedge model mentioned above. The second wedge makes angles of *90*-ϕ′ and β′ with the soil surface. The plane *AC* was treated as an imaginary blade. Therefore, the β′ was obtained by using the simple shape model in the wedge *ACD* for the case of δ=ϕ'. By using the modified model the force *H′* and *V′* on the surface *AC* can be obtained by solving the mechanical equilibrium equation acting on the wedge *ABC*. The depth of the blade *AC* can be estimated from the following equation:

$$d' = \frac{d\sin(\alpha+\beta)\cos\phi'}{\sin\alpha\cos(\beta+\phi')} \tag{3.14}$$

The total force acting on the blade can be resolved as follows:

$$P_t = P'+P_\gamma + P_c + P_{ca} \tag{3.15}$$

In Eq. 3.15 the total force acting on the tool is consisted of the different terms as

$$P' = \frac{V'\sin(\beta+\phi')+H'\cos(\beta+\phi')}{\sin(\alpha+\beta+\delta+\phi')} \tag{3.16}$$

$$P_\gamma = \frac{-dd'w\gamma\sin(\beta+\phi')\cos(\alpha+\phi')}{2\sin\alpha\cos\phi'\sin(\alpha+\beta+\delta+\phi')} \tag{3.17}$$

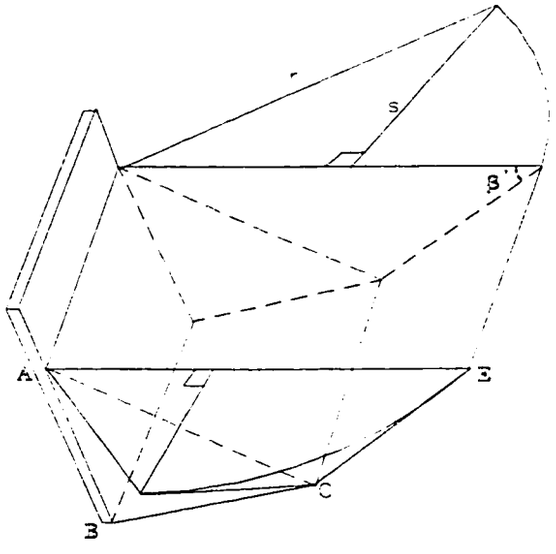

(a) Three-dimensional diagram of the two-wedge model

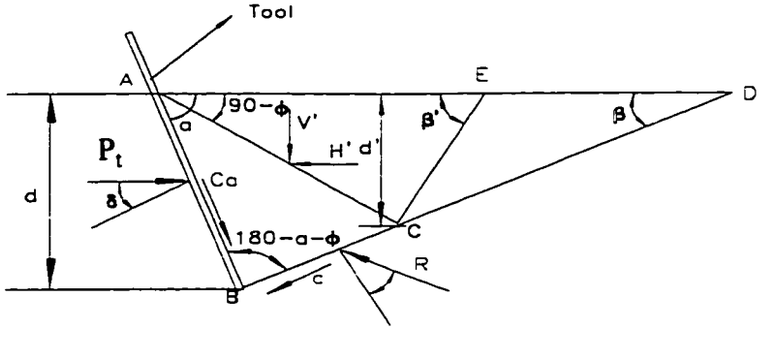

(b) Two-dimensional schematic diagram of soil failure pattern for two-wedge model

Figure 3.7 Failure pattern of the Zhang-Kushwaha model

$$P_c = \frac{cw[(d-d')\frac{\cos\phi'}{\sin\beta} - d'\frac{\sin\beta}{\cos\phi'}]}{\sin(\alpha+\beta+\delta+\phi')} \tag{3.18}$$

$$P_{ca} = \frac{-c_a dw\cos(\alpha+\beta+\phi')}{\sin a\sin(\alpha+\beta+\delta+\phi')} \tag{3.19}$$

where:

P' = force acting on the imaginary blade (kN),

P_γ = force due to gravity term (kN),

P_c = force due to cohesion term (kN),

P_{ca} = force due to adhesion term (kN).

CHAPTER 4

FORCED OSCILLATION OF SOIL CUTTING PROCESS

4.1 Vibratory Soil Cutting

In the vibratory soil cutting process, an implement is considered to travel at constant speed and a tillage tool vibrates relative to the implement.

4.1.1 Vibratory soil cutting model

If a tool is vibrated while cutting soil, the tool responds at a frequency equal to that of the oscillatory forced function. Under ideal operating conditions of forward speed and soil cutting resistance, the tool would experience periodic displacement, velocity, and acceleration. The schematic of the model representing tool force relationship is shown in Fig. 4.1 The diagram represents a Coulomb friction, lightly damped single-degree of freedom oscillatory system. The dynamic system mass, including the oscillator, is connected to the carriage frame through the springs. The carriage moves at speed V_c and the soil resistance *R(t)* acts at the tool tip. The differential equation describing the system is:

$$m\ddot{x} + b\dot{x} + kx = F_0 \sin(\omega t) + R(t) \tag{4.1}$$

where:

m = mass (kg),

b = damping coefficient (Ns/m),

k = spring constant (N/m),

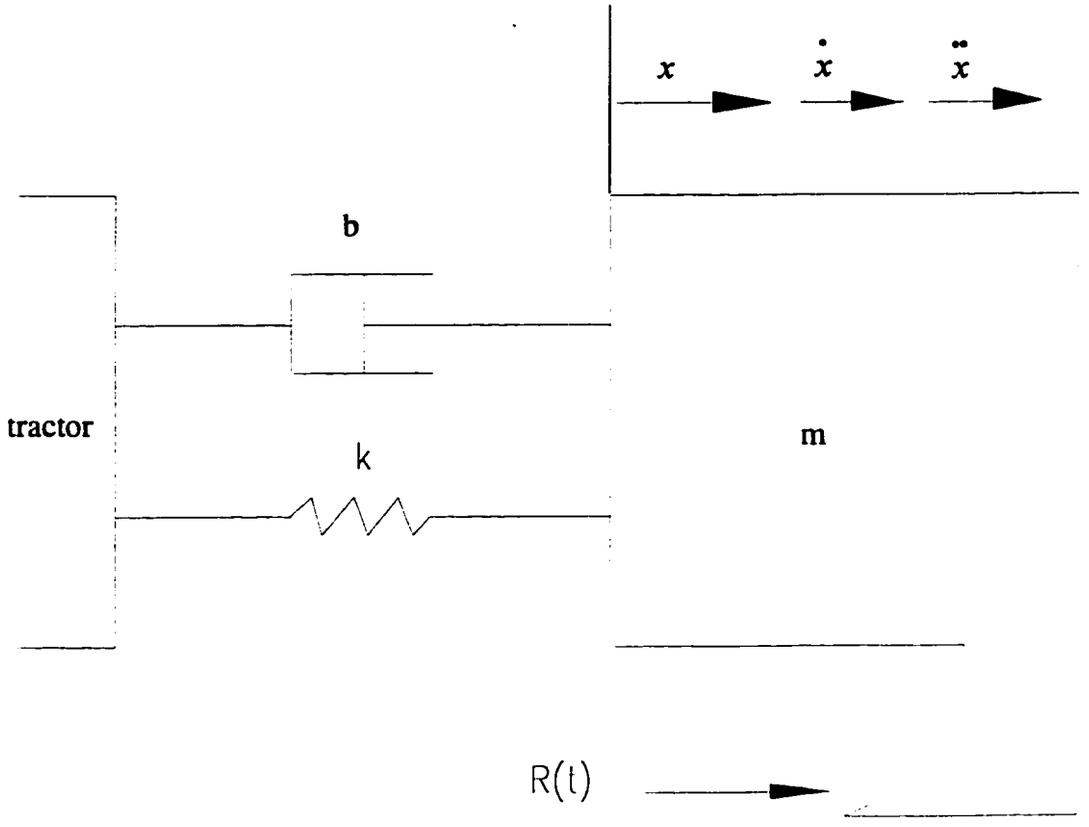

Figure 4.1 Oscillatory model representation

x = displacement of oscillator (m),

R(t) = soil cutting resistance (N),

F_0 = driving force (N),

ω = driving force frequency (rad/s),

t = time (s).

Since the soil cutting resistance is mainly overcome by the drawbar power of the tractor, it is assumed that the driving force $F_0 \sin\omega t$ is responsible for the vibratory motion of the tillage tool relative to the implement. Equation 4.1 can be solved by numerical integration using Runge-Kutta fourth order scheme. The solutions of Eq. 4.1 are shown in Figs. 4.2, 4.3, 4.4, and 4.5. It can be seen that the system reaches the steady state oscillatory movement after the initial transient vibration. The analytical solution of the above equation assumes the steady state response. The oscillatory displacement function can be represented as

$$x(t) = L\sin(\omega t - \phi) \tag{4.2}$$

$$\phi = \tan^{-1}\frac{2\xi\frac{\omega}{\omega_n}}{1-(\frac{\omega}{\omega_n})^2} \tag{4.3}$$

where:

L = oscillation amplitude (m),

ϕ = phase angle (degree),

ξ = damping ratio,

ω_n = undamped natural frequency of the system (rad/s).

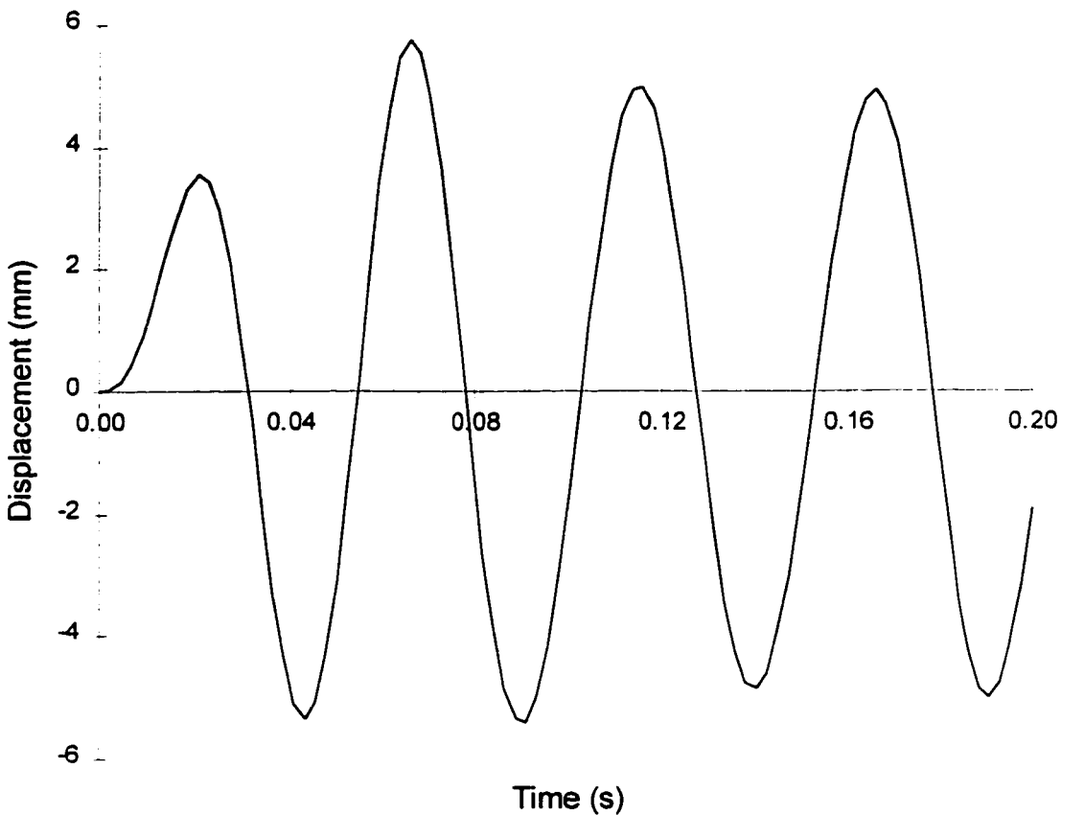

Figure 4.2 Displacement response of vibratory system

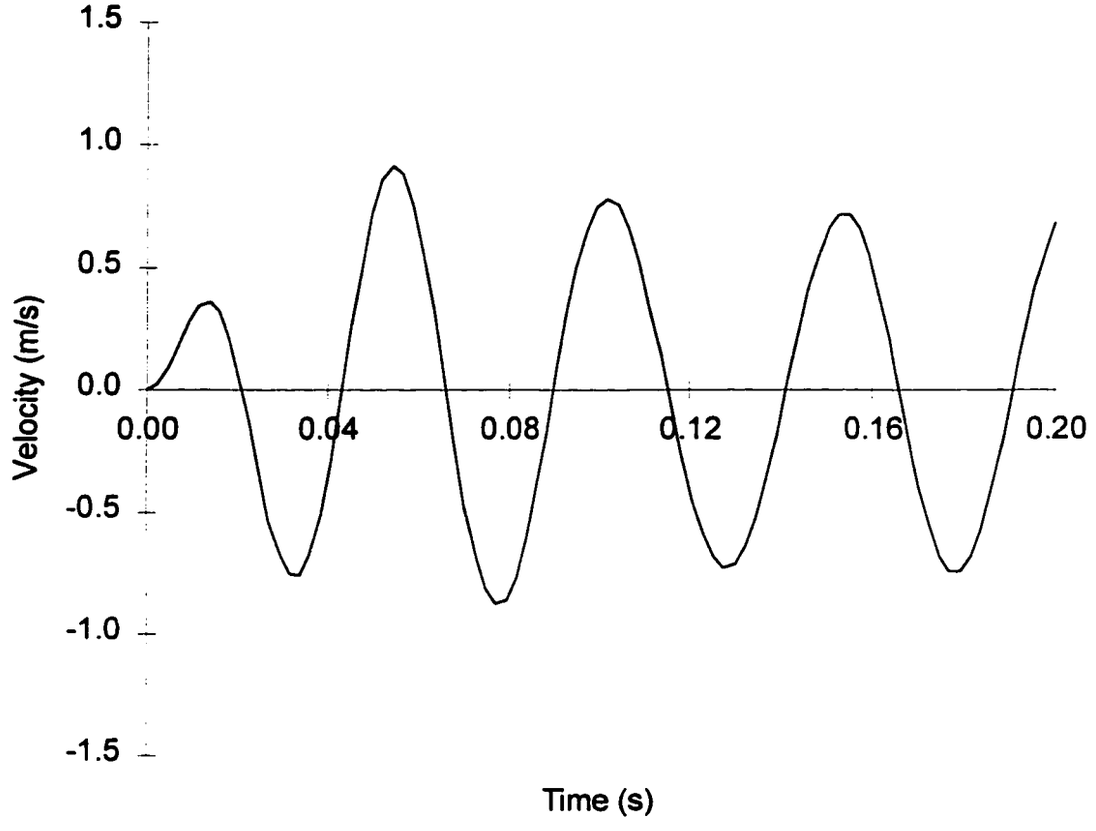

Figure 4.3 Velocity response of vibratory system

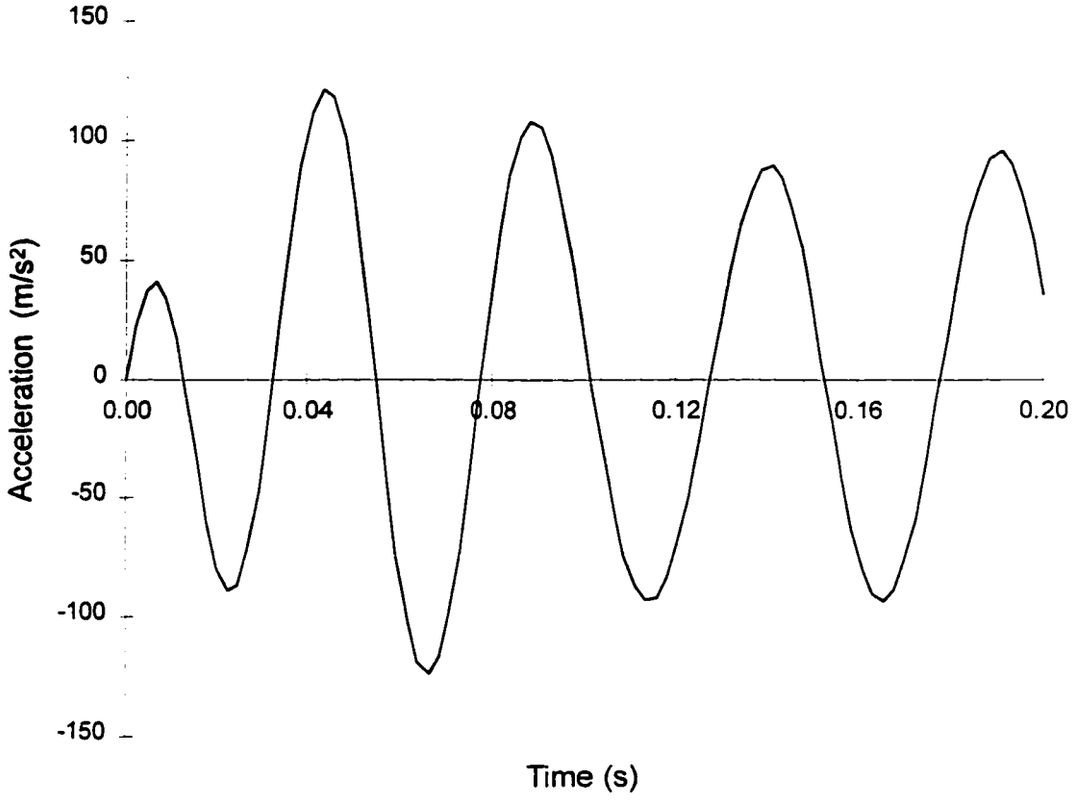

Figure 4.4 Acceleration response of vibratory system

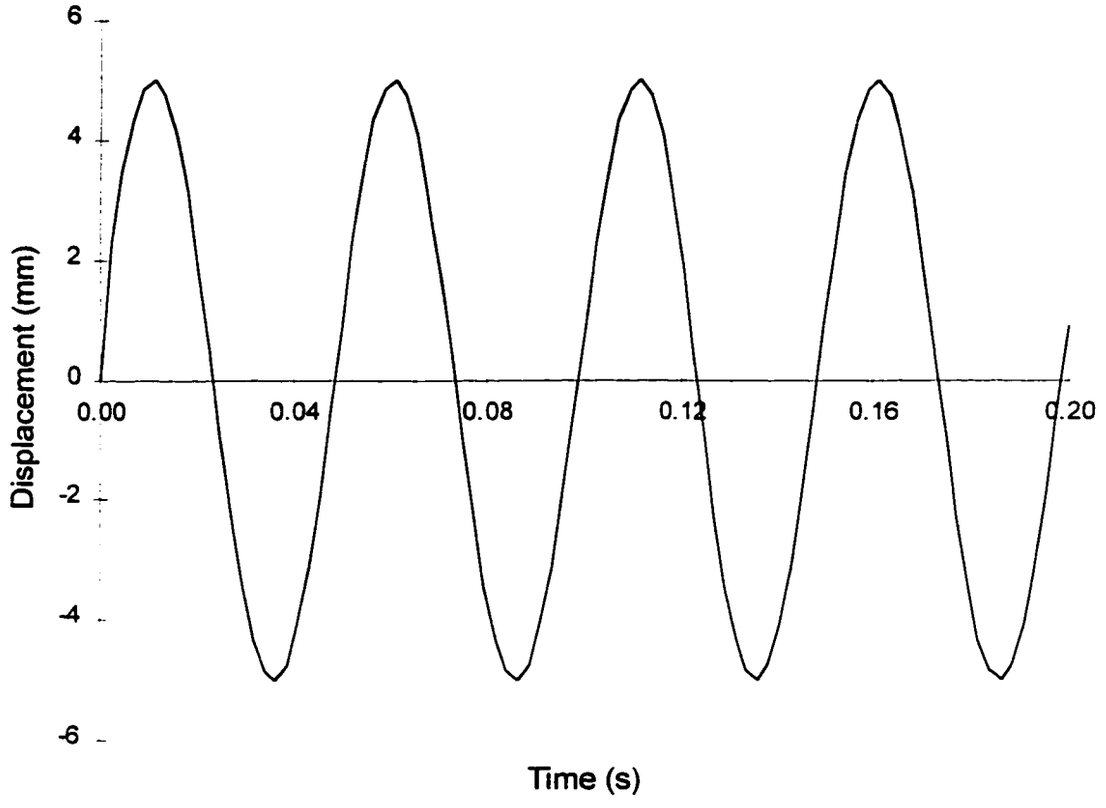

Figure 4.5 Steady state response of vibratory system

All forces acting on the system are balanced. Figure 4.6 shows the phase diagram of each force acting on the system, for different frequency of the driving force.

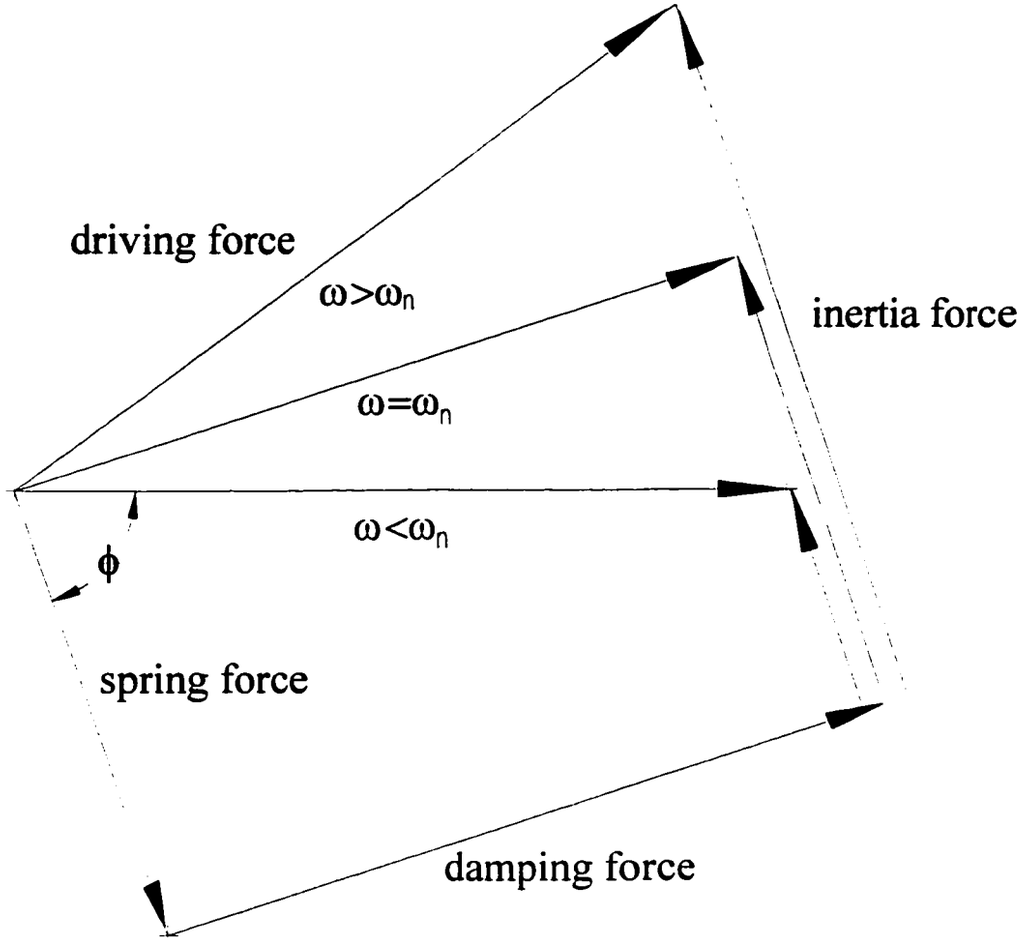

Figure 4.6 Phasor of each force acting on the system for cases: $\omega < \omega_n$, $\omega = \omega_n$, $\omega > \omega_n$.

4.2 Tool Vibratory Movement

It is assumed that a carriage is moving with a constant velocity V_c relative to the ground. A soil cutting tool, mounted on the carriage, executes sinusoidal vibration of amplitude (b) and angular velocity (ω) relative to the carriage and along its line of travel. The velocity ratio (a) is defined as the ratio of the peak vibration (relative to the carriage) to the forward speed of the carriage.

$$a = \frac{L\omega}{V_c} \tag{4.4}$$

Considering the case in which the peak vibration velocity is greater than the forward speed ($a>1$), such that for each vibration cycle, the tools have a chance to move backwards. The cycle is assumed to start at the instant at which the tillage tool begins to move forward through the soil at the end of each retreat phase.

When the oscillator operates, the carriage moves at constant velocity V_c and the oscillator vibrates the tool sinusoidally. The response of the tool related to the ground is given by Eq. 4.5 when it is excited by the driving force $F_0\sin(\omega t)$.

$$x(t) = V_c t + L\sin(\omega t - \phi) \tag{4.5}$$

where:

x(t) = displacement relative to the ground (m).

The instantaneous velocity of the tool relative to the soil, $V(t)$, has a constant component V_c and a fluctuating component $L\omega\cos(\omega t-\phi)$.

$$V(t) = V_c + L\omega\cos(\omega t - \phi) \tag{4.6}$$

where:

V(t) = velocity relative to the ground (m/s).

The absolute displacement of the tool is shown in Fig. 4.7 for different carriage speeds and the given parameters.

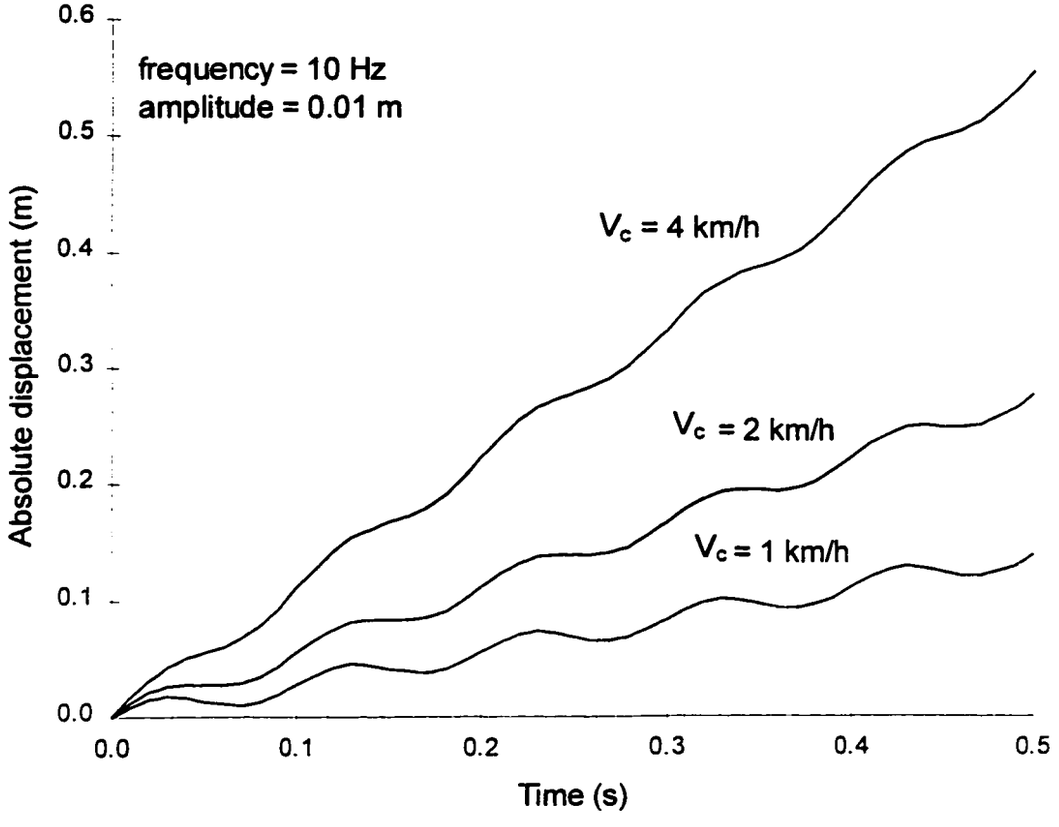

Figure 4.7 Tool motion relative to the ground

4.3 Vibration Cycle

The instantaneous velocity of the tool relative to the ground consists of a constant component V_c and a sinusoidal component $L\omega\cos(\omega t-\phi)$. For a speed ratio less than one, the absolute velocity of the tillage tool relative to the ground is always greater than zero. The tillage tool has no chance to move backward. The tool is always in contact with soil during operation. Figure 4.8 shows the tool velocity with respect to the traveling distance for the speed ratio equal to one. Figure 4.9 gives the shape of motion for the speed ratio greater than one. A negative velocity of the tillage tool indicates that the tool travels backward. The traveling locus suggests that the tool moves through the unfailed soil then it retreats. As the tool repeats the forward routine it first goes through the failed soil then it meets the unfailed soil again.

Figure 4.10 indicates two vibration cycles of the tool movement with respect to time. For $a>1$, the vibration cycle starts at $t= t_0$ with the tool stationary and about to move forward. The tool meets the unfailed soil from t_1 to t_2. It begins to move backward from t_2 to t_3. It can be shown that

$$V(t_0) = V_c + L\omega\cos(\omega t_0 - \phi) = 0$$

Solving above equation the t_0 can be obtained as:

$$t_0 = \frac{2\pi - \theta + \phi}{\omega} \tag{4.7}$$

where:

$$\theta = \cos^{-1}\frac{-V_c}{L\omega} \tag{4.8}$$

$$t_2 = \frac{2\pi + \phi + \theta}{\omega} \tag{4.9}$$

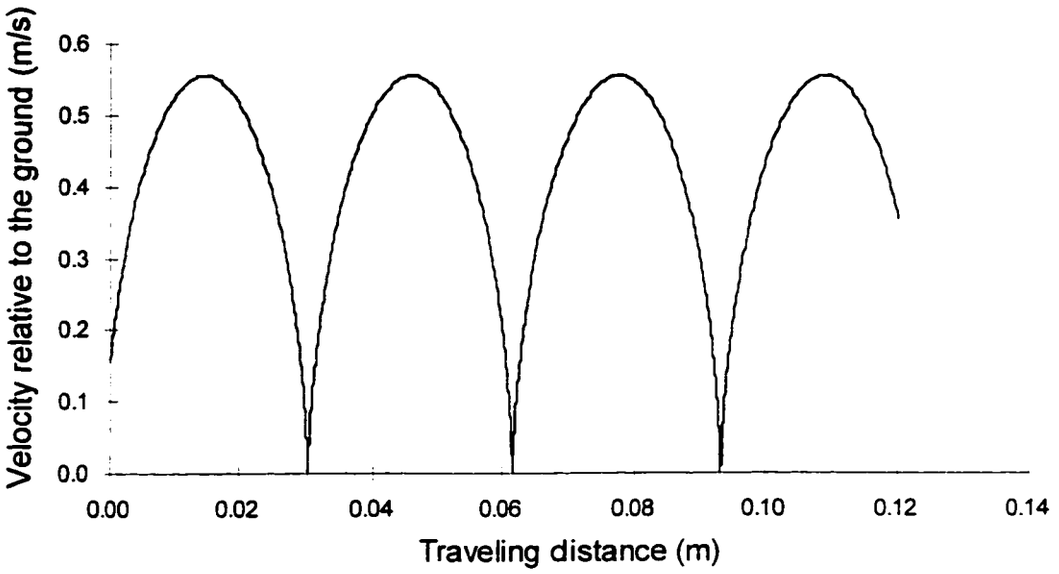

Figure 4.8 Tool velocity with respect to traveling distance for $L\omega=V_c$

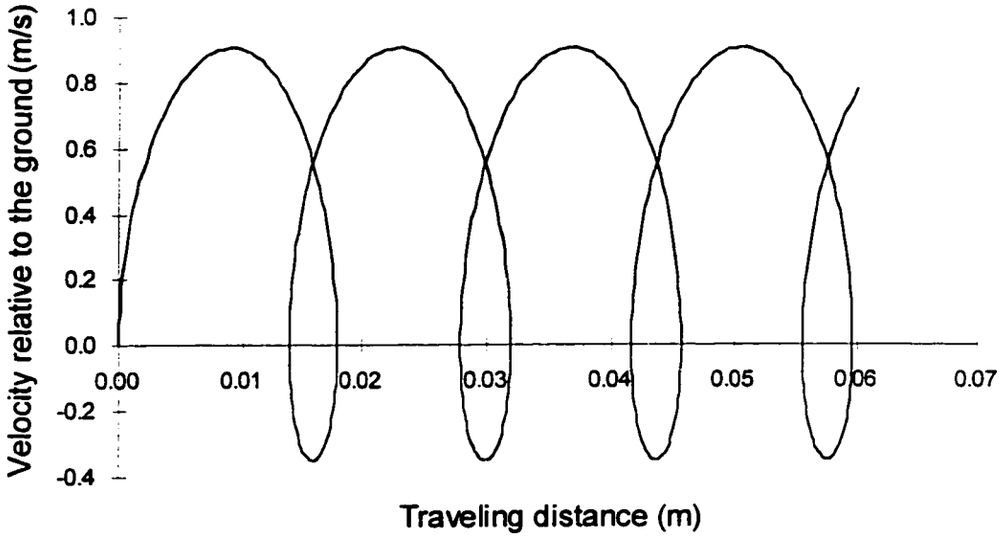

Figure 4.9 Tool velocity with respect to traveling distance for $L\omega > V_c$

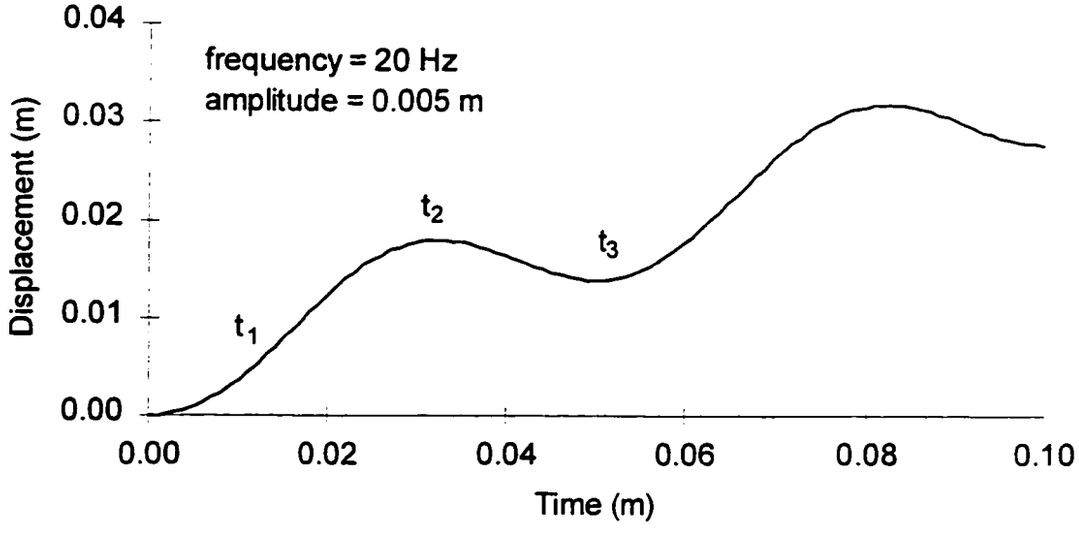

(a)

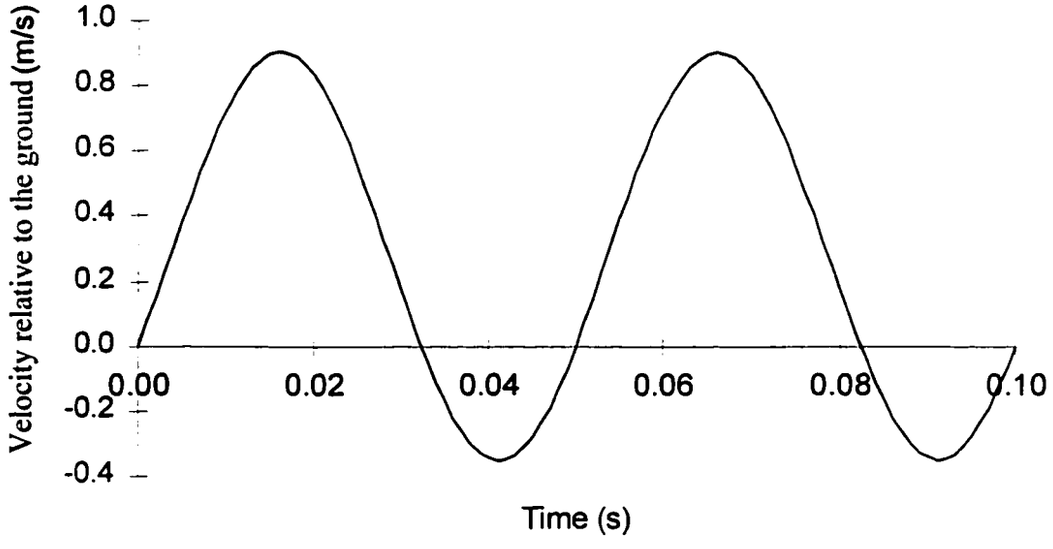

(b)

Figure 4.10 Displacement (a) and velocity (b) with respect to time

$$t_3 = \frac{4\pi - \theta + \phi}{\omega} \tag{4.10}$$

so that

$$x(t_2) = \frac{L}{a}(2\pi + \theta + \phi) + L\sin\theta \tag{4.11}$$

and

$$x(t_3) = \frac{L}{a}(4\pi - \theta + \phi) - L\sin\theta \tag{4.12}$$

where:

t_0 = time the tool begins to move forward (s),

t_2 = time the tool begins to move backward (s),

t_3 = time the tool begins to move forward again (s);

$x(t_2)$ = displacement at the time t_2 (m),

$x(t_3)$ = displacement at the time t_3 (m).

It follows that from t_2 to t_3 the tool has retreated for a distance x_r through soil that has already been failed, where

$$x_r = \frac{L}{a}(2\theta - 2\pi) + 2L\sin\theta \tag{4.13}$$

where:

x_r = retreated distance (m).

At the time t_3 the tool begins to move forward again. It is also the start of a new cycle.

From the start of the cycle, the tool will thus advance through previously failed soil for the same distance x_r until it reaches the interface with unfailed soil. As $x(t_1)$-$x(t_0)=x_r$, time the tool begins to meet untilled soil, t_1 may be obtained by solving

$$\frac{\omega}{a}(t_1 - t_0) + \sin(\omega t_1 - \phi) - \sin(\omega t_0 - \phi) - \frac{2\theta - 2\pi}{a} - 2\sin\theta = 0 \qquad (4.14)$$

where:

t_1 = time the tool begins to meet the untilled soil (s).

If the speed ratio a is less than one, the tool remains in contact with the soil all the time with an average speed V_c. The vibration cycle period is $2\pi/\omega$.

4.4 Soil Cutting Resistance

The draft needed to pull a tillage tool through soil depends upon the dynamics of the tool movement, including the direction of travel and velocity, and on whether it moves through failed or unfailed soil. For a tool moving at a constant low speed V_c through unfailed soil, the draft can be estimated by the non-oscillatory soil cutting model. For the vibration soil cutting process, the tool is in contact with the soil as the tool starts to move forward at time t_0 until it begins to move backwards at time t_2 on each oscillatory cycle. Blekhman's (1954) simple model assumes that the resistance to the motion of a tool is only accounted for all times when it is penetrating unfailed soil. However, when it is penetrating soil that has already been failed the force falls to zero. This means that when the tool is vibrated the instantaneous force is only acting during that part of the vibration cycle from t_1 to t_2, and any draft reduction arises simply because the average force over the whole cycle is therefore lower. The draft of the cutting tool also depends on its forward speed. Gunn and Tramontini (1955) assumed a linear relationship with an intercept R_0 and a gradient $R_0\lambda$.

$$R(t) = R_0(1 + \lambda V(t)) \qquad (4.15)$$

where:

R(t) = soil cutting resistance (N).

The draft thus depends on the instantaneous velocity of the tillage tool and whether it moves through failed or unfailed soil. Figure 4.11 shows the soil resistance ratio during the period of two vibratory cycle. Here, soil resistance ratio is defined as the instantaneous soil cutting resistance over an average value of a non-oscillatory soil cutting resistance with the same speed V_c.

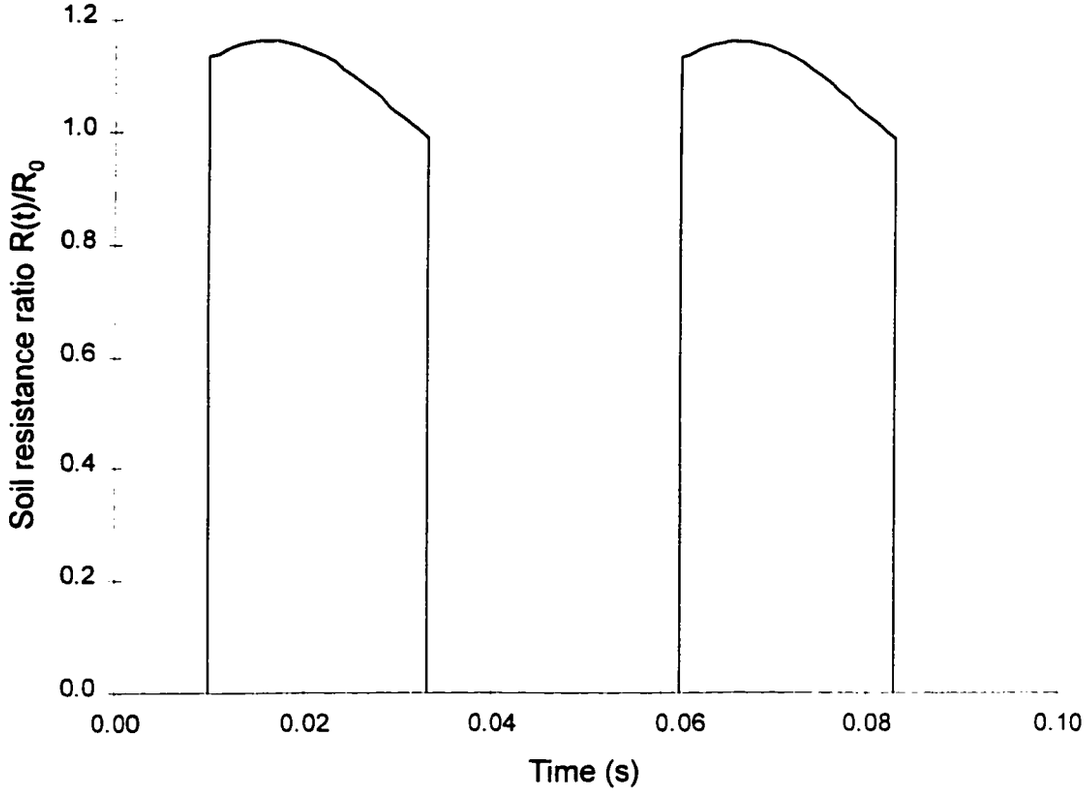

Figure 4.11 Soil resistance ratio with respect to time

4.5 Energy and Power Requirements

Two sources of energy supply provide the required energy to the system, the oscillator driver and the tractor drawbar power. The major part of supplied energy to the oscillator is converted to reduce the soil cutting resistance and the other part is consumed by the oscillator to overcome the frictional energy loss in the oscillator mechanism.

4.5.1 Energy consumption by the oscillator

When a dynamic system vibrates at a frequency ω under the effect of an exciting force $F_0\sin(\omega t)$, this system is balanced by the inertia, elastic and damping forces. From Eq. 4.2, the displacement response of the system is $L\sin(\omega t-\phi)$. The amplitude L is determined by the design of the oscillator. To obtain such an oscillatory response the amplitude F_0 of the driving force is given by

$$F_0 = L\sqrt{(k - m\omega^2)^2 + (b\omega)^2} \tag{4.16}$$

The driving force F_0 has a minimum value when the forced vibration system is in resonant condition. The corresponding frequency is given by

$$\omega_r = \omega_n\sqrt{1 - 2\xi^2}$$

where:

ξ = damping ratio (dimensionless),

ω_r = resonant frequency (rad/s).

The driving force $F(t)$ acts on the displacement $x(t)=L\sin(\omega t-\phi)$ results in energy consumption of the oscillator per cycle, E_{os} as:

$$E_{os} = \oint F(t)dx$$

$$= \int_0^{\tau_c} F_0 \sin(\omega t)\omega L \cos(\omega t - \phi)dt \qquad (4.17)$$

$$= \pi F_0 L \sin\phi$$

where:

E_{os} = energy consumption of oscillator (W),

τ_c = $2\pi/\omega$ (s) (period of the cycle).

Expressing the power as the rate of energy consumption, the required power to run the oscillator is,

$$P_{os} = \frac{E_{os}}{\tau_c} \qquad (4.18)$$

where:

P_{os} = power required to drive oscillator (J).

4.5.2 Energy consumption in soil cutting

Because of value of the force *R(t)* changes through the vibration cycle, an average value is obtained by integration over a cycle and equated to the average drawbar force F_{dr} supplied by the tractor. Soil cutting resistance *R(t)* is a variable of speed and also it is dependent on whether the tool is directly in contact with untilled soil during the vibratory cycle.

$$F_{dr} = \frac{1}{\tau_c}\oint R(t)dt \qquad (4.19)$$

where:

F_{dr} = average drawbar force (N).

And consequently the drawbar power P_{dr} is,

$$P_{dr} = F_{dr}V_c \tag{4.20}$$

where:

P_{dr} = drawbar power (W).

The drawbar energy consumed per cycle E_{dr} is,

$$E_{dr} = F_{dr}V_c\tau_c \tag{4.21}$$

where:

E_{dr} = drawbar energy consumption (J).

A comparison to the non-oscillatory soil cutting would be useful to evaluate the effectiveness of oscillatory cutting process. The energy consumption in a time period equivalent to the oscillatory cycle period and the power required for soil cutting in non-oscillatory process is,

$$E_{st} = R_cV_c\tau_c \tag{4.22}$$

$$P_{st} = R_cV_c \tag{4.23}$$

where:

E_{st} = non-oscillatory energy consumption in a time period (J).

P_{st} = power required for non-oscillatory operation (W).

A comparison between the energy consumed in the cutting process for the oscillator and non-oscillatory case is presented by the energy ratio (E/E_{st}). The energy ratio is shown in Fig. 4.12 and Fig. 4.13 for the different value of frequencies and the amplitudes of the vibration cycle for the cases the speed ratio a is greater than one. A

minimum energy consumption is obtained between the frequency $V_c/L<\omega<\omega_n$. The energy consumed by the oscillator increased as the vibratory frequency increased. The soil cutting energy consumption decreased with the increase in the oscillatory frequency. The energy consumed by the oscillator increased with amplitude while that consumed in soil cutting decreased exponentially. As a result, the total energy ratio has a minimum value at a specified amplitude value.

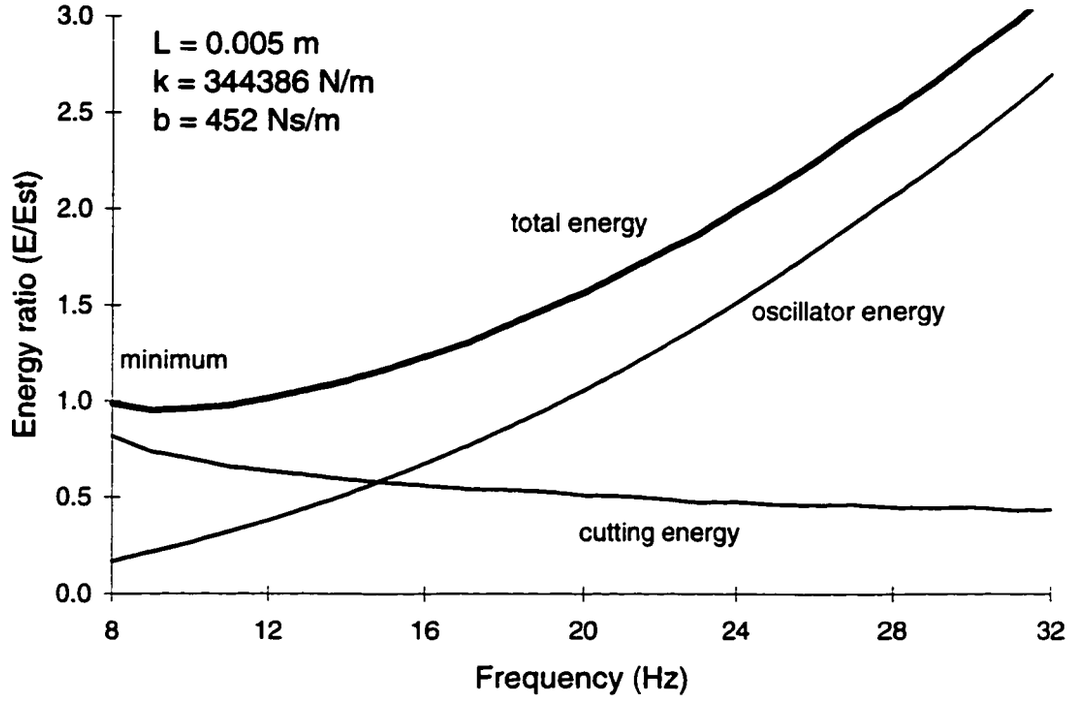

Figure 4.12 Effect of frequency on energy consumption

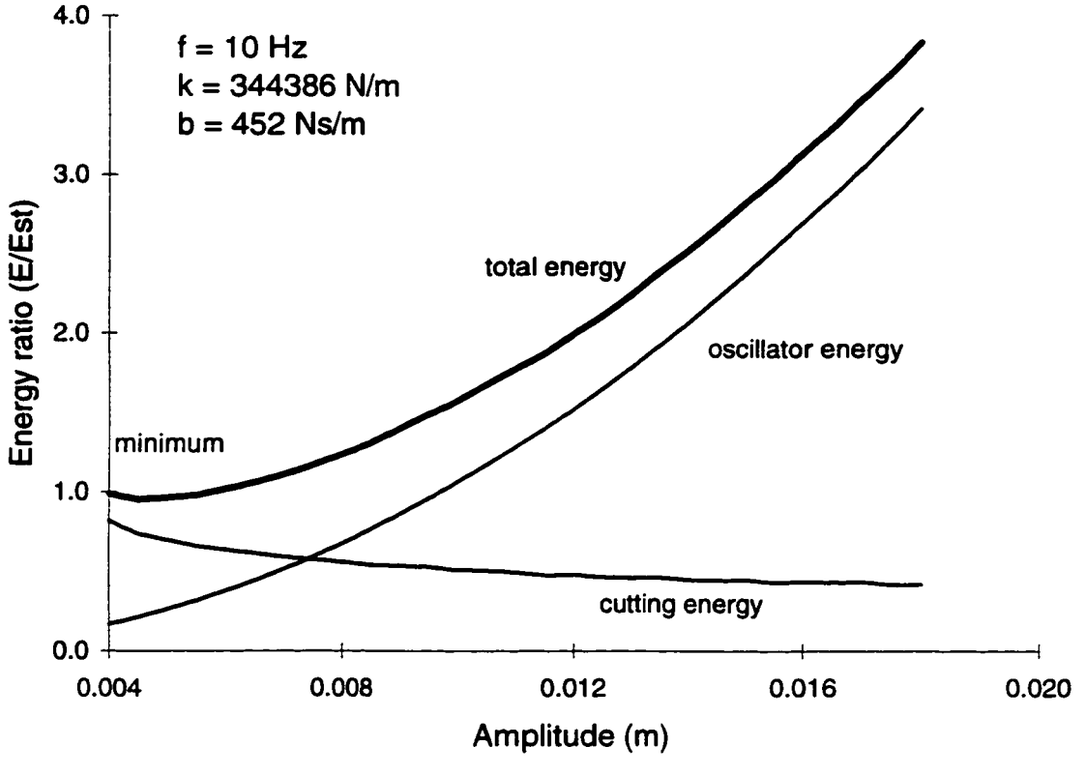

Figure 4. 13 Effect of amplitude on energy consumption

CHAPTER 5

TRANSVERSE VIBRATION OF BEAM

5.1 Equation of Transverse Vibration Beam

When a tillage tool operates in the field, the tool and shank assembly can be considered as a cantilever beam with lumped mass mounted on the bottom. The soil cutting resistance acting on the tool is regarded as the transverse load. The fluctuations of soil resistance will induce the beam to move back and forth. The consequent motion is called the transverse vibration of the beam.

Assume that the beam has a plane of symmetry and that the vibrations occur in that plane. To derive the differential equation of motion for the transverse vibration of beams, consider the forces and moments acting on an element as shown in Fig. 5.1 (Shabana, 1991). *M(x, t)* is the bending moment, *V(x, t)* is the shear force, and *f(x, t)* is the external force per unit length of the beam.

The force equation of motion in the *w* direction gives

$$-(V+dV)+f(x,t)dx+V=\rho A(x)dx\frac{\partial^2 w}{\partial t^2}(x,t) \tag{5.1}$$

where:

ρ = mass density (kg/m^3),

A(x) = cross-sectional area of the beam (m^2).

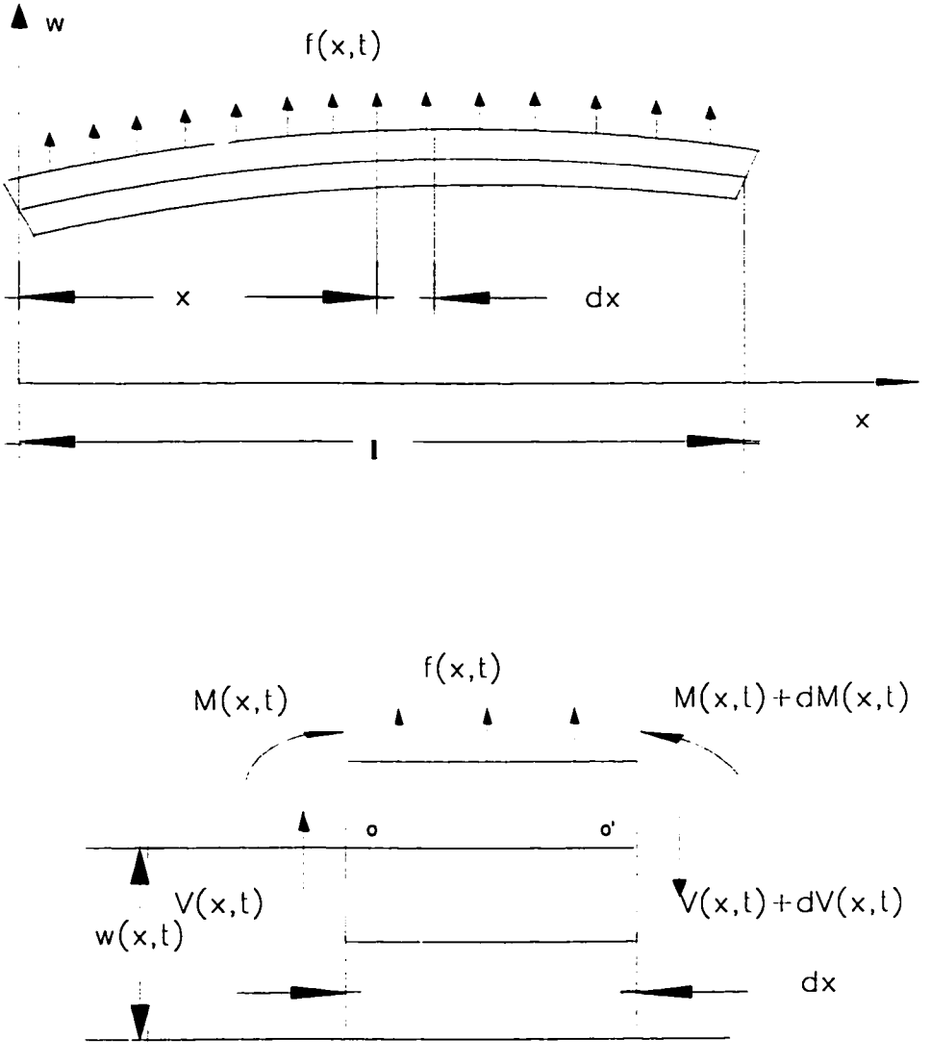

Figure 5.1 A beam in bending

The moment equation of motion passing through the point o in Fig. 5.1 leads to

$$(M+dM)-(V+dV)dx+f(x,t)dx\frac{dx}{2}-M=0 \tag{5.2}$$

Using the theory of bending of beam (also known as the Euler-Bernoulli or thin beam theory), the relation between bending moment and deflection can be expressed as

$$M(x,t)=EI(x)\frac{\partial^2 w}{\partial x^2}(x,t) \tag{5.3}$$

where:

E = Young's modulus (Pa),

I(x) = moment of inertia of the cross section (m^4).

Disgarding terms involving second powers in *dx*, the equation of motion for the forced transverse vibration of a non uniform beam can be obtained as:

$$\frac{\partial^2}{\partial x^2}[EI(x)\frac{\partial^2 w}{\partial x^2}(x,t)]+\rho A(x)\frac{\partial^2 w}{\partial t^2}(x,t)=f(x,t) \tag{5.4}$$

For a uniform beam, Eq. 5.4 reduces to

$$EI(x)\frac{\partial^4 w}{\partial x^4}(x,t)+\rho A(x)\frac{\partial^2 w}{\partial t^2}(x,t)=f(x,t) \tag{5.5}$$

5.2 Free Vibration

For free vibration, $f(x,t)=0$, and so the equation of motion becomes

$$EI(x)\frac{\partial^4 w}{\partial x^4}(x,t)+\rho A(x)\frac{\partial^2 w}{\partial t^2}(x,t)=0 \tag{5.6}$$

The free vibration solution can be found using the method of separation of variables as

$$w(x,t) = W(x)T(t) \tag{5.7}$$

where *W(x)* is a space-dependent function and *T(t)* is a time-dependent function. Substituting Eq. 5.7 into Eq. 5.6 and rearranging leads to

$$\frac{EI}{\rho A W(x)} \frac{d^4 W(x)}{dx^4} = -\frac{1}{T(t)} \frac{d^2 T(t)}{dt^2} \tag{5.8}$$

Since the left-hand side of this equation depends only on the spatial coordinate x and the right-hand side depends only on time, one concludes that Eq. 5.8 is satisfied only if both sides are equal to a constant, that is

$$\frac{EI}{\rho A W(x)} \frac{d^4 W(x)}{dx^4} = -\frac{1}{T(t)} \frac{d^2 T(t)}{dt^2} = \omega_n^2 \tag{5.9}$$

where:

ω_n = natural frequency of the beam (rad/s).

Equation 5.9 can be written as two equations:

$$\frac{d^4 W(x)}{dx^4} - \beta^4 W(x) = 0 \tag{5.10}$$

$$\frac{d^2 T(t)}{dt^2} + \omega_n^2 T(t) = 0 \tag{5.11a}$$

where:

$$\beta 4 = \frac{\rho A \omega_n^2}{EI} \tag{5.11b}$$

The solution of Eq. 5.11 can be expressed as

$T(t) = A\cos\omega_n t + B\sin\omega_n t$

where:

A, B = constants,

They can be found from the initial conditions.

We assume

$W(x) = Ce^{sx}$

The solution of the Eq. 5.10 can be expressed as

$$W(x) = C_1 e^{\beta x} + C_2 e^{-\beta x} + C_3 e^{i\beta x} + C_4 e^{-i\beta x} \tag{5.12}$$

where:

C_1, C_2, C_3, C_4= constants.

Equation 5.12 also can be expressed as

$$W(x) = C_1 \cos\beta x + C_2 \sin\beta x + C_3 \cosh\beta x + C_4 \sinh\beta x \tag{5.13}$$

The constants C_1, C_2, C_3, C_4 can be found from the boundary conditions.

The natural frequencies of the beam are calculated from Eq. 5.11b as

$$\omega_n = \beta^2 \sqrt{\frac{EI}{\rho A}} = (\beta l)^2 \sqrt{\frac{EI}{\rho A l^4}} \tag{5.14}$$

For the tillage shank, the top of the beam is fixed to the frame and the bottom end is free for movement.

The boundary conditions can be stated as

$$W(0)=0 \tag{5.15}$$

$$\frac{\partial W}{\partial x}(0) = 0 \tag{5.16}$$

$$EI \frac{\partial^2 w}{\partial x^2}(l) = 0 \tag{5.17}$$

$$\frac{\partial}{\partial x}(EI\frac{\partial^2 w}{\partial x^2})(l) = 0 \tag{5.18}$$

Substituting the above boundary conditions into Eq. 5.13

condition W(0)=0 leads to

$C_1 + C_3 = 0$

Condition $\frac{\partial W}{\partial x}(0) = 0$ leads to

$\beta(C_2 + C_4) = 0$

Thus Eq. 5.13 becomes

$$W(x) = C_1(\cos\beta x - \cosh\beta x) + C_2(\sin\beta x - \sinh\beta x) \tag{5.19}$$

Applying the condition of Eqs. 5.17 and 5.18 into Eq. 5.19 yields

$$-C_1(\cos\beta l + \cosh\beta l) - C_2(\sin\beta l + \sinh\beta l) = 0 \tag{5.20}$$

$$C_1(\sin\beta l - \sinh\beta l) - C_2(\cos\beta l + \cosh\beta l) = 0 \tag{5.21}$$

For the nontrivial solution of C_1 and C_2 the determinant of their coefficients must be zero. We have

$$\begin{vmatrix} -(\cos\beta l + \cosh\beta l) & -(\sin\beta l + \sinh\beta l) \\ (\sin\beta l - \sinh\beta l) & -(\cos\beta l + \cosh\beta l) \end{vmatrix} = 0 \tag{5.22}$$

Expanding the determinant gives the following relation

$$\cos\beta l \cosh\beta l = -1 \tag{5.23}$$

The following values of βl satisfy Eq. 5.23.

$\beta_1 l = 1.875104$

$\beta_2 l = 4.694091$

$\beta_3 l = 7.854757$

$\beta_4 l = 10.995541$

The roots of Eq. 5.23, $\beta_n l$, give the natural frequencies of vibration:

$$\omega_n = (\beta_n l)^2 \sqrt{\frac{EI}{\rho A l^4}}, \qquad \text{n=1,2,3,4...} \tag{5.24}$$

If the value of C_1 corresponding to β_n is denoted as C_{1n}, C_{2n} can be expressed in terms of C_{1n} from Eq. 5.20.

$$C_{2n} = -C_{1n} \frac{\cos\beta l + \cosh\beta l}{\sin\beta l + \sinh\beta l} \tag{5.25}$$

Hence the Eq. 5.19 can be written as

$$W_n(x) = C_{1n}[(\cos\beta_n x - \cosh\beta_n x) - (\frac{\cos\beta_n l + \cosh\beta_n l}{\sin\beta_n l + \sinh\beta_n l})(\sin\beta_n x - \sinh\beta_n x)] \tag{5.26}$$

The normal modes of vibration can be obtained by the use of Eq. 5.7:

$$w_n(x,t) = W_n(x)(A\cos\omega_n t + B\sin\omega_n t) \tag{5.27}$$

The general solution of the vibratory beam can be expressed by the sum of the normal modes:

$$w(x,t) = \sum_{n=1}^{\infty} w_n(x,t) \tag{5.28}$$

5.3 Mode Shapes

Mode shapes are the eigenvectors associated with each characteristic value of natural frequencies of vibrating system. The first three mode shapes of beam vibration, in the case in which one end is fixed and other is free, are shown in Fig. 5.2.

5.4 Effect of Axial Force

When an axial tensile or compressive load acts on a beam, the natural frequencies are different from those for the same beam without such load. To find the effect of an axial force *P(x,t)* on the bending vibrations of a beam, consider the equation of motion of an element, as shown in Fig. 5.3. For the vertical motion, we have

$$-(V + dV) + fdx + V + (P + dP)\sin(\theta + d\theta) - P\sin\theta = \rho A dx \frac{\partial^2 w}{\partial t^2} \tag{5.29}$$

and for the rotational motion about o,

$$(M + dM) - (V + dV)dx + fdx\frac{dx}{2} - M = 0 \tag{5.30}$$

for small deflection,

$$\sin(\theta + d\theta) \approx \theta + d\theta = \theta + \frac{\partial \theta}{\partial x}dx = \frac{\partial w}{\partial x} + \frac{\partial^2 w}{\partial x^2}dx \tag{5.31}$$

Equations 5.29, 5.30, and 5.31 can be combined to obtain a single differential equation of motion:

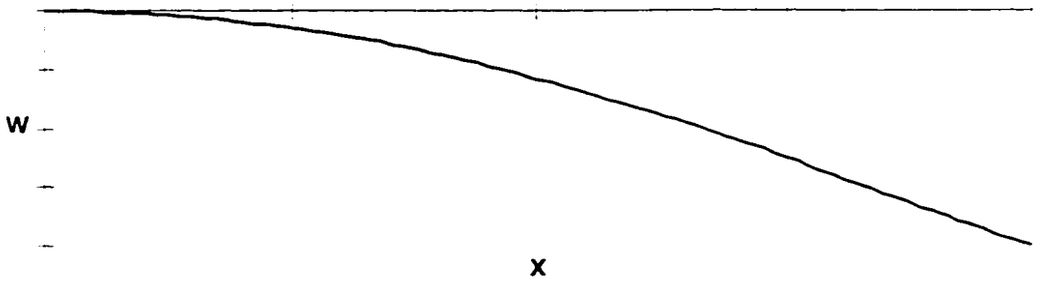

First mode

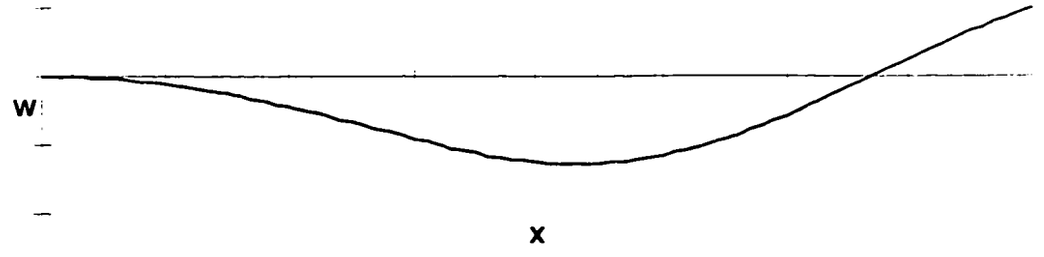

Second mode

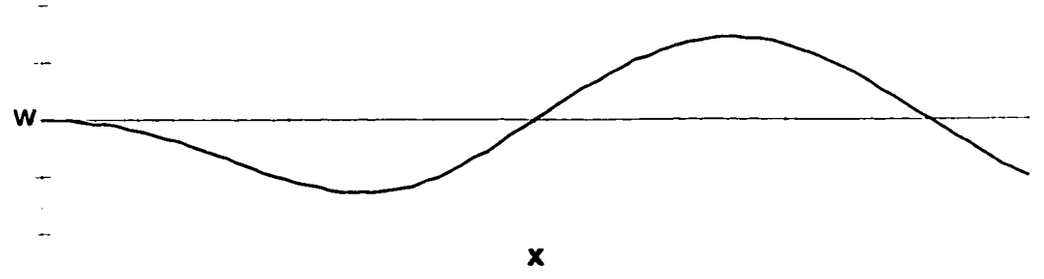

Third mode

Figure 5.2. First three mode shapes of a cantilever beam

$$\frac{\partial^2}{\partial x^2}[EI\frac{\partial^2 w}{\partial x^2}] + \rho A\frac{\partial^2 w}{\partial t^2} - P\frac{\partial^2 w}{\partial x^2} = f(x,t) \tag{5.32}$$

For the vibration of a uniform beam, Eq. 5.32 reduces to

$$EI\frac{\partial^4 w}{\partial x^4} + \rho A\frac{\partial^2 w}{\partial t^2} - P\frac{\partial^2 w}{\partial x^2} = f(x,t) \tag{5.33}$$

For the free vibration of a uniform beam, Eq. 5.33 reduces to

$$EI\frac{\partial^4 w}{\partial x^4} + \rho A\frac{\partial^2 w}{\partial t^2} - P\frac{\partial^2 w}{\partial x^2} = 0 \tag{5.34}$$

The solution of Eq. 5.34 can be obtained using the method of separation of variables as

$$w(x,t) = W(x)(A\cos\omega_n t + B\sin\omega_n t)$$

(5.35)

Substitution of Eq. 5.35 into Eq. 5.34 gives

$$EI\frac{d^4 W}{dx^4} - P\frac{d^2 W}{dx^2} - \rho A\omega_n{}^2 W = 0 \tag{5.36}$$

By assuming the solution W(x) to be

$$W(x) = Ce^{sx} \tag{5.37}$$

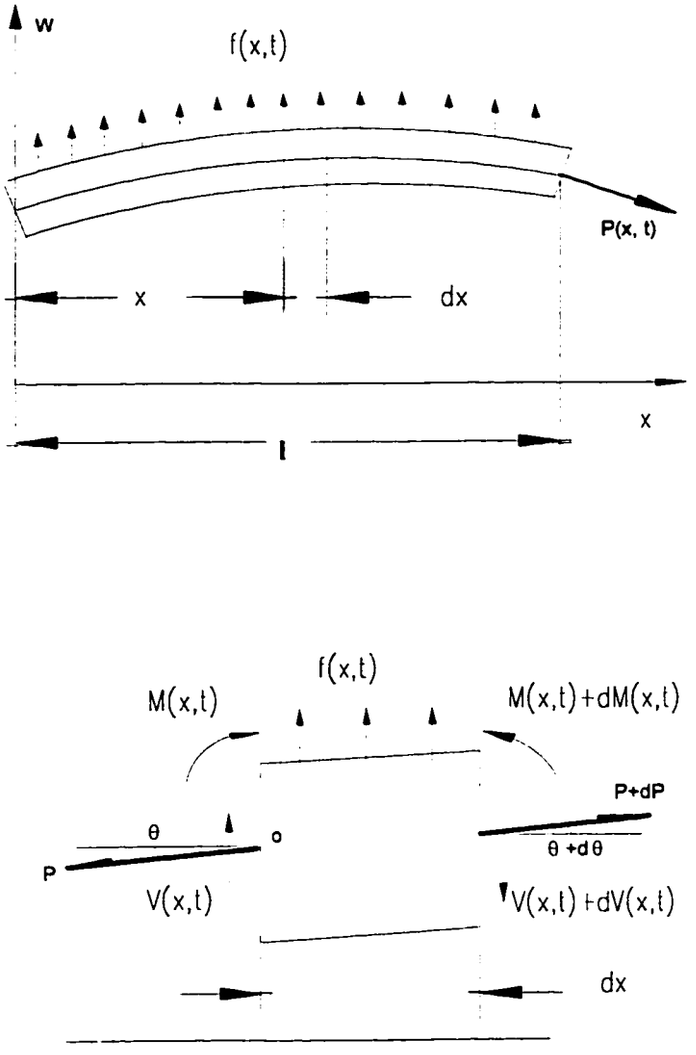

Figure 5.3 A beam under axial load

The auxiliary equation can be obtained:

$$s^4 - \frac{P}{EI}s^2 - \frac{\rho A \omega^2}{EI} = 0 \tag{5.38}$$

The roots of Eq. 5.38 are

$$s_1^2, s_2^2 = \frac{P}{2EI} \pm \sqrt{\frac{P^2}{4E^2I^2} + \frac{\rho A \omega^2}{EI}} \tag{5.39}$$

The solution can be expressed as

$$W(x) = C_1 \cos s_1 x + C_2 \sin s_1 x + C_3 \cosh s_2 x + C_4 \sinh s_2 x \tag{5.40}$$

By applying boundary conditions to the Eq. 5.40 and getting rid of the constant, the equation becomes

$$s_1^4 + s_2^4 + (s_1 s_2^3 - s_1^3 s_2)\sinh(s_1 l)\sin(s_2 l) + 2s_1^2 s_2^2 \cosh(s_1 l)\cos(s_2 l) = 0$$

(5.41)

By solving Eqs. 5.39 and 5.41, we can find the natural frequencies of vibration beam subjected to an axial force.

Equation 5.41 can only be solved numerically. Figure 5.4 shows the fundamental natural frequency of the vibratory beam with respect to the axial force.

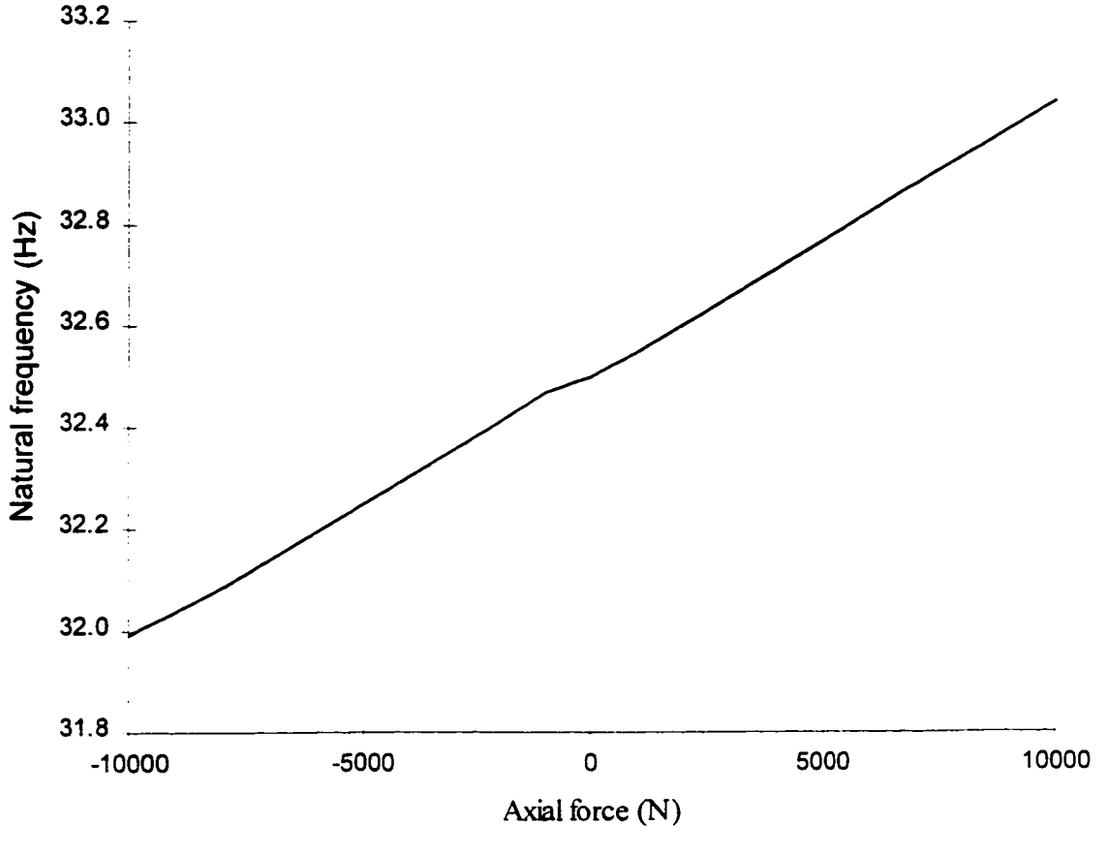

Figure 5.4 Natural frequency affected by the axial force

5.5 Effects of Rotary Inertia and Shear Deformation

If the cross-sectional dimensions are not small compared to the length of the beam, the effects of rotary inertia and shear deformation should be considered. The procedure, first presented by Timoshenko (1921), is known as the Timoshenko beam theory and the vibrating beam is called a Timoshenko beam. The free-body diagram and the geometry for the beam element are shown in Fig. 5.5. If the shear deformation is zero, the center line of the beam element will coincide with a line perpendicular to the face of the cross section. Due to shear, the rectangular element tends to go into a diamond shape without rotation of the face, and the slope of the center line is diminished by the shear angle (ψ-*dw/dx*). Equation 5.42 then can be obtained:

$$\gamma' = \psi - \frac{dw}{dx} \tag{5.42}$$

where ψ denotes the slope of the deflection curve due to bending deformation alone. *dw/dx* is the slope of the center line of the beam. γ' is the loss of slope which is equal to the shear angle.

There are two elastic equations for the beam:

$$M = EI\frac{d\psi}{dx} \tag{5.43}$$

$$V = k_T AG\gamma' = kAG(\psi - \frac{dw}{dx}) \tag{5.44}$$

where G denotes the shear modulus, k_T is a constant, also known as Timoshenko's shear coefficient, which depends on the shape of the cross section. For a rectangular section the value of k is 5/6; for a circular section it is 9/10 (Cowper, 1966).

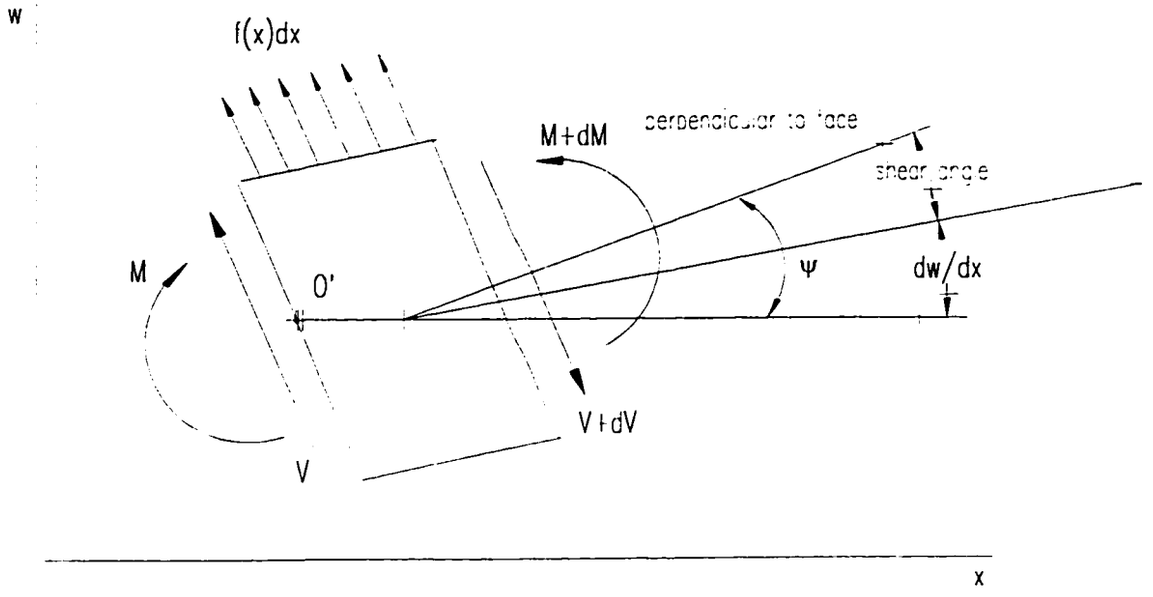

Figure 5.5 Effect of shear deformation

The equations of motion for the element shown in Fig. 5.5 can be derived as

$$-[V(x,t)+dV(x,t)]+f(x,t)dx+V(x,t)=\rho A(x)dx\frac{d^2w}{dt^2}(x,t) \tag{5.45}$$

For the rotation about a line passing through point O':

$$[M(x,t)+dM(x,t)]-[V(x,t)+dV(x,t)]dx+f(x,t)\frac{dx}{2}-M(x,t)=\rho I(x)dx\frac{d^2w}{dt^2} \tag{5.46}$$

along with Eqs. 5.43 and 5.44 and disgarding terms involving second powers in dx, Eqs. 5.45 and 5.46 can be expressed as

$$-k_TAG(\frac{d\psi}{dx}-\frac{d^2w}{dx^2})+f(x,t)=\rho A\frac{d^2w}{dt^2} \tag{5.47}$$

$$EI\frac{d^2\psi}{dx^2}-k_TAG(\psi-\frac{dw}{dx})=\rho I\frac{d^2\psi}{dt^2} \tag{5.48}$$

By solving Eq. 5.47 for $d\psi/dx$ and substituting the result in Eq. 5.48 the desired equation of motion for the forced vibration of a uniform beam can be obtained as:

$$EI\frac{\partial^4w}{\partial x^4}+\rho A\frac{\partial^2w}{\partial t^2}-\rho I(1+\frac{E}{k_TG})\frac{\partial^4w}{\partial x^2\partial t^2}+\frac{\rho^2I}{k_TG}\frac{\partial^4w}{\partial t^4}+\frac{EI}{k_TAG}\frac{\partial^2f}{\partial x^2}-\frac{\rho I}{k_TAG}\frac{\partial^2f}{\partial t^2}=f \tag{5.49}$$

CHAPTER 6

VIBRATORY ANALYSIS OF TILLAGE SHANK MOVEMENT

When a tillage tool operates in the field, it carries transverse loads that induce bending of the tillage shank. The soil resistance acting on the shank of the tillage tool becomes stored by the mechanism of deformation known as strain or elastic energy through the entire stressed volume. The stored energy is released as soon as the soil resistance begins to decrease. The released energy causes the shank of the tillage tool to move forward relative to the implement. Soil cutting is a discrete process which is dependent upon the soil clods forming and the dynamic system of the implements. Generally, the soil resistance fluctuates during the tillage operation. The soil resistance fluctuation induces the shank of the tillage tool to move back and forward relative to the tool implement corresponding to the dynamic characteristics of the system. This phenomenon dictates that the actual tillage tool operation be an oscillatory process in practice.

6.1 System Equation

When a tillage implement operates in the field, the soil cutting resistance acting on the tillage tool is conveyed to the shank. The soil resistance can be regarded as a point transverse load acting on the end of shank. Thus, the shank of the implement can be considered as a cantilever beam subjected to the point transverse load on the end of the beam. Figure 6.1 shows the free body diagram of the shank of a tillage tool subjected to a transverse soil resistance.

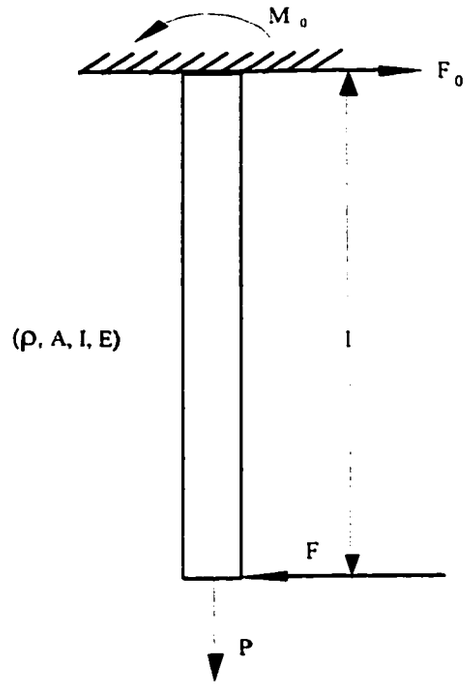

Figure 6.1 Shank of tillage tool subject to transverse soil resistance

The general differential equation of motion for the transverse vibration of a beam has been discussed in Chapter 5. Assuming the tractor as well as the implement travels at a constant speed V_c the general differential Eq. 5.35 can be used to describe the motion of the shank of the tillage tool relative to the implement. It has the form:

$$\frac{\partial^2}{\partial x^2}[EI(x)\frac{\partial^2 w}{\partial x^2}(x,t)]+\rho A(x)\frac{\partial^2 w}{\partial t^2}(x,t)-P\frac{\partial^2 w}{\partial x^2}(x,t)=f(x,t) \tag{5.32}$$

where $f(x, t)$, given function of x and t, denotes the transversely distributed load. P is the axial force, and w is the transverse deflection of the beam.

For a uniform beam, Eq. 5.32 can be reduced to

$$EI(x)\frac{\partial^4 w}{\partial x^4}(x,t)+\rho A(x)\frac{\partial^2 w}{\partial t^2}(x,t)-P\frac{\partial^2 w}{\partial x^2}(x,t)=f(x,t) \tag{5.33}$$

The governing differential equation contains fourth order derivatives and a second order time dependent problem. The analytical solution of w in the Eq. 5.32 does not exist as the beam is not uniform and/or the transverse load is discontinuous. However, the finite element method can be employed to solve this problem by using the variational method to reduce the continuity requirement of the solution. The soil resistance is concentrated on the free end of beam and is a discrete variable with respect to time.

6.2 Finite Element Formulation

The semidiscrete variational formulation of the general Eq. 5.32 can be constructed as follows (Reddy 1984).

(1) Multiplying by a test function $v(x)$ and integrating the domain of the problem and setting the integral to zero.

$$\int_0^l v[\frac{\partial^2}{\partial x^2} EI(x)\frac{\partial^2 w}{\partial x^2} + \rho A\frac{\partial^2 w}{\partial t^2} - P\frac{\partial^2 w}{\partial x^2} - f]dx = 0 \tag{6.1}$$

(2) Integrating by parts yields

$$\int_0^l [-\frac{\partial v}{\partial x}\frac{\partial}{\partial x} EI\frac{\partial^2 w}{\partial x^2} + \rho Av\frac{\partial^2 w}{\partial t^2} + P\frac{\partial v}{\partial x}\frac{\partial w}{\partial x} - vf]dx + [v\frac{\partial}{\partial x} EI\frac{\partial^2 w}{\partial x^2} - vP\frac{\partial w}{\partial x}]_0^l = 0 \tag{6.2}$$

Since the equation contains a fourth order derivative, it is necessary to integrate it twice to distribute the derivatives equally between the dependent variable w and the test function v:

$$\int_0^l [\frac{\partial^2 v}{\partial x^2} EI\frac{\partial^2 w}{\partial x^2} + v\rho A\frac{\partial^2 w}{\partial t^2} + P\frac{\partial v}{\partial x}\frac{\partial w}{\partial x} - vf]dx + [v\frac{\partial}{\partial x} EI\frac{\partial^2 w}{\partial x^2} - vP\frac{\partial w}{\partial x} - \frac{\partial v}{\partial x} EI\frac{\partial^2 w}{\partial x^2}]_0^l = 0 \tag{6.3}$$

the following notations are defind

$$Q_1 = [-P\frac{\partial w}{\partial x} + \frac{\partial}{\partial x} EI \frac{\partial^2 w}{\partial x^2}]_{x=0} \tag{6.4}$$

$$Q_2 = [EI \frac{\partial^2 w}{\partial x^2}]_{x=0} \tag{6.5}$$

$$Q_3 = [-P\frac{\partial w}{\partial x} + \frac{\partial}{\partial x} EI \frac{\partial^2 w}{\partial x^2}]_{x=l} \tag{6.6}$$

$$Q_4 = [EI \frac{\partial^2 w}{\partial x^2}]_{x=l} \tag{6.7}$$

With these notations, the variational form becomes.

$$\int_0^l [\frac{\partial^2 v}{\partial x^2} EI \frac{\partial^2 w}{\partial x^2} + P\frac{\partial v}{\partial x}\frac{\partial w}{\partial x} + v\rho A \frac{\partial^2 w}{\partial t^2} - vf]dx - Q_1 v(0) + Q_3 v(l) + Q_2 \frac{\partial v(0)}{\partial x} - Q_4 \frac{\partial v(l)}{\partial x}] = 0 \tag{6.8}$$

The test function v is twice differentiable and satisfies the boundary conditions. It is regarded as a variation in w, consistent with the boundary conditions. By formulating the problem variationally, the continuity requirement of the solution is reduced. Now *w* needs to be differentiable only twice.

6.2.1 Boundary conditions

Considering the boundary conditions for the beam, at the top end, the beam is fixed. As the essential boundary condition it gives:

w=0	deflection equal zero
$\frac{\partial w}{\partial x} = 0$	slope equal zero

$$Q_1 = [\frac{\partial}{\partial x} EI \frac{\partial^2 w}{\partial x^2}]_{x=0} = F_0 \tag{6.9}$$

$$Q_2 = [EI \frac{\partial^2 w}{\partial x^2}]_{x=0} = M_0 \tag{6.10}$$

At the bottom end, it is subjected to the point load F and axial force P.

$F = [\frac{\partial}{\partial x} EI \frac{\partial^2 w}{\partial x^2}]_{x=l}$ soil resistance acting as point load

$Q_3 = [P \frac{\partial w}{\partial x} + F]_{x=l}$

$Q_4 = [EI \frac{\partial^2 w}{\partial x^2}]_{x=l} = 0$ bending moment equal zero

The beam is subjected to a point load F_0 and a moment M_0 at the fixed end; (Fig. 6.1)

Using the method of variable separation, w is interpolated by an expression of the form

$$w = \sum_{j=1}^{n} U_j(t)\Phi_j(x) \tag{6.11}$$

Where $U_j(t)$ is the value of w at time t, at the jth node of the element. $\Phi_j(t)$ is the shape function at jth node of element.

Equation 6.11 implies that at any arbitrarily fixed time t>0, the function w can be approximated by a linear combination of Φ_j and U_j. By substituting $v = \Phi_i(x)$ into Eq. 6.8 it becomes

$$0 = \int_0^l [EI \frac{\partial^2 \Phi}{\partial x^2} \sum_{j=1}^{n} U_j \frac{\partial^2 \Phi}{\partial x^2} + P \frac{\partial \Phi}{\partial x} \sum_{j=1}^{n} U_j \frac{\partial \Phi}{\partial x} + \rho A \Phi_i \frac{\partial^2 U}{\partial t^2} \Phi_j - f \Phi_i] dx - F_0 \Phi(0) + M_0 \frac{\partial \Phi(0)}{\partial x} - Q_3 \Phi(l) \tag{6.12}$$

It can also be written in matrix form

$$[M][\ddot{U}]+[K][U]=[F] \tag{6.13}$$

where:

$$[M]=\int_0^l \rho A\Phi_i\Phi_j dx \tag{6.14}$$

$$[K]=\int_0^l EI\frac{\partial^2\Phi_i}{\partial x^2}\frac{\partial^2\Phi_j}{\partial x^2}dx+\int_0^l P\frac{\partial\Phi_i}{\partial x}\frac{\partial\Phi_j}{\partial x}dx \tag{6.15}$$

$$[F]=\int_0^l \Phi_i f dx+Q_1\Phi(0)-Q_2\frac{\partial\Phi(0)}{\partial x}+Q_3\Phi(l) \tag{6.16}$$

where Φ is a test function that should be differentiable twice with respect to x. The essential boundary conditions involve the specification of w and dw/dx, and the natural boundary conditions contain the specification of Q_3 and Q_4 at the endpoint of the element.

The variational form requires that the interpolating functions be continuous with continuous derivatives up to order three, so that the boundary condition exists. In the effort to satisfy the end conditions, the continuity conditions are automatically satisfied

Since there is a total of four boundary conditions in an element, a four-parameter polynomial must be selected for w:

$$w(x)=C_1+C_2x+C_3x^2+C_4x^3 \tag{6.17}$$

The continuity conditions are automatically met since $C_4 \neq 0$.

The interpolating form is given by

$$w(x) = \Phi_1 U_1 + \Phi_2 U_2 + \Phi_3 U_3 + \Phi_4 U_4 \tag{6.18}$$

where:

$$U_1 = w_1$$

$$U_2 = -\frac{dw}{dx} = \theta_1$$

$$U_3 = w_2$$

$$U_4 = -\frac{dw}{dx} = \theta_2$$

The shape functions are given by

$$\Phi_1 = 1 - 3(\frac{x}{h})^2 + 2(\frac{x}{h})^3 \tag{6.19}$$

$$\Phi_2 = -x(1 - \frac{x}{h})^2 \tag{6.20}$$

$$\Phi_3 = 3(\frac{x}{h})^2 - 2(\frac{x}{h})^3 \tag{6.21}$$

$$\Phi_4 = -x[(\frac{x}{h})^2 - \frac{x}{h}] \tag{6.22}$$

at x =0, $\Phi_1 = 1$, $-\frac{d\Phi_2}{dx} = 1$, other values are zero.

at x=h, $\Phi_3 = 1$, $-\frac{d\Phi_4}{dx} = 1$, other values are zero.

For the given parameters, the three components of the element matrix can been obtained as:

The mass matrix can be written as

$$[M]=\frac{\rho Ah}{420}\begin{vmatrix} 156 & -22h & 54 & 13h \\ -22h & 4h^2 & -13h & -3h^2 \\ 54 & -13 & 156 & 22h \\ 13h & -3h^2 & 22h & 4h^2 \end{vmatrix} \tag{6.23}$$

The stiffness matrix is given by

$$[K]=\frac{2EI}{h^3}\begin{vmatrix} 6 & -3h & -6 & -3h \\ -3h & 2h^2 & 3h & h^2 \\ -6 & 3h & 6 & 3h \\ -3h & h^2 & 3h & 2h^2 \end{vmatrix}+P\begin{vmatrix} \frac{16}{15h} & \frac{-1}{10} & \frac{-16}{15h} & \frac{-1}{10} \\ \frac{-1}{10} & \frac{2h}{15} & \frac{1}{10} & \frac{-h}{30} \\ \frac{-16}{15h} & \frac{1}{10} & \frac{16}{15h} & \frac{1}{10} \\ \frac{-1}{10} & \frac{-h}{30} & \frac{1}{10} & \frac{2h}{15} \end{vmatrix} \tag{6.24}$$

The force matrix can be given as

$$[F]=\frac{fh}{12}\begin{vmatrix} 6 \\ -h \\ 6 \\ h \end{vmatrix}+\begin{vmatrix} Q_1 \\ Q_2 \\ Q_3 \\ Q_4 \end{vmatrix} \tag{6.25}$$

6.3 Assembly of Element Equations

In a continuum problem, the variable possesses infinitely many values because it is a function of each generic point in the whole region. Consequently, the problem is one with an infinite number of unknowns. The finite element discretization procedures reduce the problem to one of a finite number of unknowns by dividing the solution region

into elements and by expressing the unknowns in terms of assumed an approximating function within each element. The nodal values of the field variable and the test function for the elements completely define the behavior of the represented problem within the element. At the nodes where elements are connected, the values of the unknown nodes are the same for all the elements joining at that node.

Figure 6.2 indicates the one dimensional element. Each element has two nodes. The domain of the problem, (Ω=*0, L*) is divided into eight elements of equal length h. Although an increase in the number of elements generally means more accurate results, for the problem at hand, the accuracy could not be improved significantly as the element number increased to six. Since these elements are connected at each local node and U is continuous, the values of *U* for the connected nodes should be the same. The correspondence between the local nodes and the global nodes can be expressed through the connectivity matrix. A concentrated force, representing the soil resistance, is considered to act on the right side of the last element.

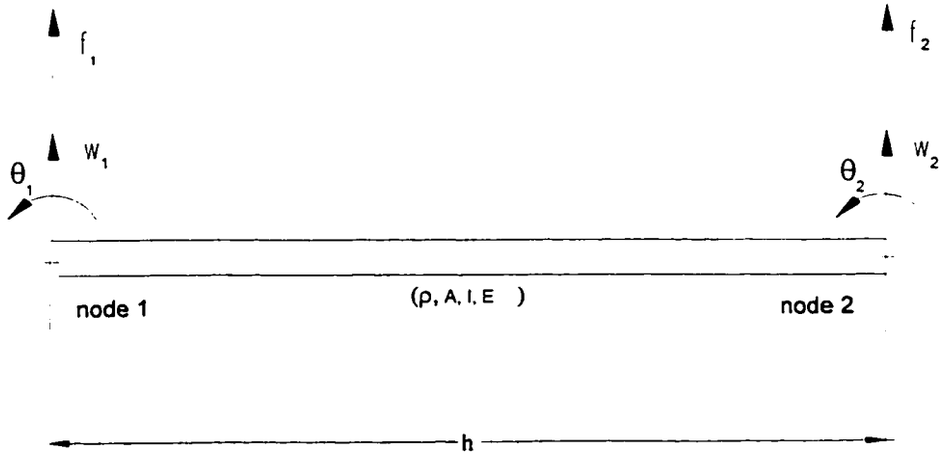

Figure 6.2 Shape of element

So far a uniform beam has been considered. When the tillage tool operates in the field a sweep or other soil cutting tool is attached at the bottom of the shank. Figure 6.3 shows the assembly where the tillage tool is represented by a lumped mass attached to the end of the beam. The properties of the tillage shank are given in Table 6.1.

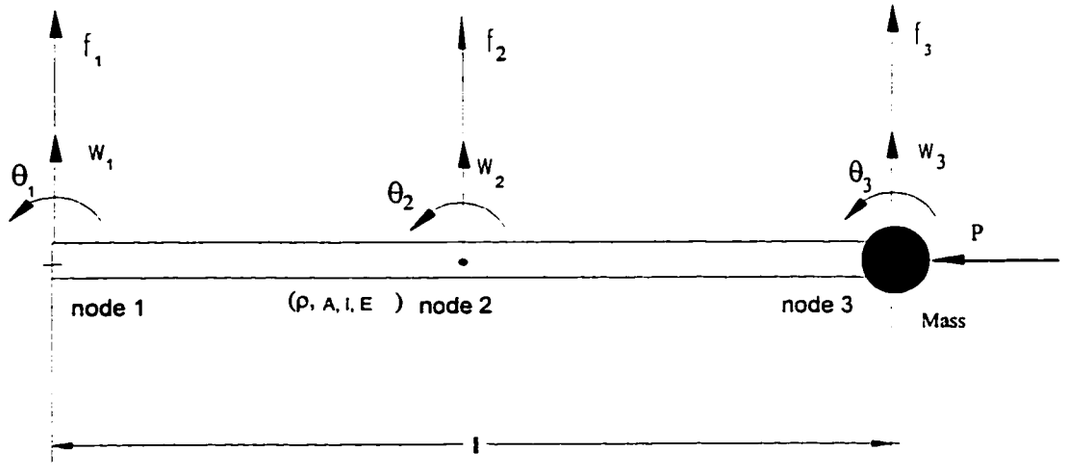

Figure 6.3 Assembly of the beam elements

Table 6.1 Physical properties of tillage shank

Terms	Value
density (ρ)	7800 kg/m^3
Young's modulus (E)	210 GPa
moment of inertia of the cross section (I)	69.37×10^{-9} m^4
length of shank (L)	0.65 m
cross section area of the beam (A)	0.00129 m^2
lumped mass (m)	4.5 kg

6.4 Transient Solution of Finite Element Analysis

The sequential solution of the differential equation of motion can be obtained by using the Newmark method (Newmark 1959). The Newmark direct integration method identities are written as:

$$\dot{U}_{j+1} = \dot{U}_j + \Delta t[(1-\gamma)\ddot{U}_j + \gamma \ddot{U}_{j+1}] \tag{6.26}$$

$$U_{j+1} = U_j + \Delta t \dot{U}_j + (\Delta t)^2[(\frac{1}{2}-\beta)\ddot{U}_j + \beta \ddot{U}_{j+1}] \tag{6.27}$$

The Newmark integration method is based on the assumption that the acceleration varies linearly between two instants of time. The parameters γ and β indicate how much the acceleration at the end of the interval enters the velocity and displacement equations at the end of the interval Δt. By using this method, it is not intended to satisfy the governing differential equation at all times, but only at discrete time intervals Δt apart. A suitable type of variation of the displacement U, velocity $\dot{U}$, and acceleration $\ddot{U}$ is assumed within each time interval Δt.

Equation 6.13 is valid at times t_{j+1}, t_j and t_{j-1}, thus give

$$M\ddot{U}_{j+1} + KU_{j+1} = F_{j+1} \tag{6.28}$$

$$M\ddot{U}_j + KU_j = F_j \tag{6.29}$$

$$M\ddot{U}_{j-1} + KU_{j-1} = F_{j-1} \tag{6.30}$$

The Newmark integration method identities can also be written as

$$\dot{U}_j = \dot{U}_{j-1} + \Delta t[(1-\gamma)\ddot{U}_{j-1} + \gamma\ddot{U}_j] \tag{6.31}$$

$$U_j = U_{j-1} + \Delta t\dot{U}_{j-1} + (\Delta t)^2[(\frac{1}{2}-\beta)\ddot{U}_{j-1} + \beta\ddot{U}_j] \tag{6.32}$$

In Eqs 6.26 to 6.32, the unknowns are the three displacements, three velocities and three accelerations at the time t_{j-1}, t_j and t_{j+1} respectively. From the initial conditions the values of U_0 and $\dot{U}_0$ are known, leaving seven equations and seven unknowns. Solving the above equations (Eq. 6.26 to Eq. 6.32) the expression of U_{j+1} in terms of U_j and U_{j-1} can be obtained at each time step Δt as follows:

$$AU_{j+1} = BU_j + CU_{j-1} + \bar{F} \tag{6.33}$$

where:

$$A = M + \beta(\Delta t^2)K$$

$$B = 2M - (\Delta t^2)(\frac{1}{2} - 2\beta + \gamma)K$$

$$C = -M - (\Delta t^2)(\frac{1}{2} + \beta - \gamma)K$$

$$\bar{F} = (\Delta t^2)[\beta F_{j+1} + (\frac{1}{2} - 2\beta + \gamma)F_j + (\frac{1}{2} + \beta - \gamma)F_{j-1}]$$

where γ and β are parameters that can be determined depending on the desired accuracy and stability. Newmark suggested a value of γ=1/2 to avoid artificial damping. The value of β depends on the way in which the acceleration is assumed to vary during the time interval t and t+Δt.

6.4.1 Initial conditions

Equation 6.33 requires a special starting procedure to obtain the displacement U_1 at time Δt based on the initial value U_0 and $\dot{U}_0$. The displacement U_1 at time t_1 is obtained from the Eqs 6.34, 6.35, 6.36.

$$M\ddot{U}_0 + KU_0 = F_0 \tag{6.34}$$

$$M\ddot{U}_1 + KU_1 = F_1 \tag{6.35}$$

$$U_1 = U_0 + \Delta t\,\dot{U}_0 + (\Delta t)^2[(\frac{1}{2} - \beta)\ddot{U}_0 + \beta\ddot{U}_1] \tag{6.36}$$

Substituting for $\ddot{U}_0$ and $\ddot{U}_1$ in Eq. 6.36 from Eqs. 6.34 and 6.35 gives

$$[M + \beta(\Delta t)^2 K]U_1 = [M - (\frac{1}{2} - \beta)(\Delta t)^2 K]U_0 + M\Delta t\,\dot{U}_0 + (\Delta t)^2[\frac{1}{2} - \beta]F_0 + \beta(\Delta t)^2 F_1 \tag{6.37}$$

For the problem at hand the initial conditions are

$U_0 = 0$

$\dot{U}_0 = 0$

Solving the Eq. 6.37, the expression of U_1 in terms of the initial condition U_0 and $\dot{U}_0$ can be obtained. As the value of U_0 and U_1 is known the displacement solution at other time sequences can be obtained by using Eq. 6.33 iteratively.

Acceleration of the system equation can be solved by using Eq. 6.28 at different time intervals for the given value of the displacement. The velocity of the system equation can be obtained by using Eq. 6.31 after acquiring the acceleration term at the time sequence.

6.5 Stability of Finite Element Calculation

When the stability is examed, it is sufficient to consider the homogenous form of the equation of motion obtained by taking the external force equal to zero. The idea is that if a solution procedure is stable with no external loading, then it will also be stable if an external force is non zero but bounded.

The maximum value of Δt for which the solution is numerically stable can be obtained by applying Eq. 6.33 to free vibration of an undamped system. This gives

$$[M+\beta(\Delta t)^2 K]U_{j+1}+[(\frac{1}{2}-2\beta-\gamma)(\Delta t)^2 K-2M]U_j+[M+(\frac{1}{2}+\beta-\gamma)(\Delta t)^2 K]U_{j-1}=0 \qquad (6.38)$$

Dividing by M and rearranging the terms gives

$$[1+\beta(\omega_0\Delta t)^2]U_{j+1}+[(\frac{1}{2}-2\beta-\gamma)(\omega_0\Delta t)^2-2]U_j+[1+(\frac{1}{2}+\beta-\gamma)(\omega_0\Delta t)^2]U_{j-1}=0 \qquad (6.39)$$

Assuming the solution of Eq. 6.39 is of the form

$U_{j+1}=\lambda U_j$ and

$U_j=\lambda U_{j-1}$

Dividing by U_{j-1} Eq. 6.39 can be written as

$$[1+\beta(\omega_0\Delta t)^2]\lambda^2+[(\frac{1}{2}-2\beta-\gamma)(\omega_0\Delta t)^2-2]\lambda+[1+(\frac{1}{2}+\beta-\gamma)(\omega_0\Delta t)^2]=0 \qquad (6.40)$$

Equation 6.40 is a quadratic equation in λ, the solution of which is

$$\lambda_{1,2}=\frac{-(\frac{1}{2}-2\beta+\gamma)(\omega_0\Delta t)^2+2\pm\sqrt{[(\frac{1}{2}-2\beta+\gamma)(\omega_0\Delta t)^2-2]^2-4(1+\beta(\omega_0\Delta t)^2)[1+(\frac{1}{2}+\beta-\gamma)(\omega_0\Delta t)^2]}}{2[1+\beta(\omega_0\Delta t)^2]} \qquad (6.41)$$

The general solution of Eq. 6.38 is of the form

$$U_j=C_1\lambda_1^j+C_2\lambda_2^j \qquad (6.42)$$

where:

$$\lambda_1=e^{\mu_1\Delta t} \quad \text{and} \quad \lambda_2=e^{\mu_2\Delta t} \qquad (6.43)$$

in which μ_1 and μ_2 (and hence λ_1 and λ_2) are generally complex numbers. Constants C_1 and C_2 can be determined from initial conditions.

Equation 6.42 will represent an oscillation motion provided λ_1 and λ_2 are complex conjugates. This will be the case if

$$[(\frac{1}{2}-2\beta+\gamma)(\omega_0\Delta t)^2-2]^2-4[1+\beta(\omega_0\Delta t)^2][1+(\frac{1}{2}+\beta-\lambda)(\omega_0\Delta t)^2]<0 \qquad (6.44)$$

By simplifying, Eq 6.45 can be obtained

$$\gamma^2+\gamma+\frac{1}{4}-4\beta<(\frac{2}{\omega_0\Delta t})^2 \qquad (6.45)$$

The solution is unconditionally stable provided

$$\beta \geq \frac{1}{4}(\frac{1}{2}+\gamma)^2 \quad \text{and} \quad \gamma \geq \frac{1}{2} \tag{6.46}$$

The method is unstable for $\gamma < \frac{1}{2}$, where there is an artificial spurious negative damping introduced. This means that oscillations will increase in amplitude. If $\gamma > \frac{1}{2}$, a positive damping is introduced. This reduces the magnitude of response even without real damping in the problem. It also reduces the accuracy of Newmark method to first order (Newmark 1959).

The solution is conditionally stable when

$$\Delta t \leq \frac{2\sqrt{(\frac{1}{2}+\gamma)^2 - 4\beta}}{\omega_{max}[(\frac{1}{2}+\gamma)^2 - 4\beta]}, \quad \gamma \geq \frac{1}{2} \quad \text{and} \quad \beta < \frac{1}{4}(\frac{1}{2}+\gamma)^2 \tag{6.47}$$

6.6 Finite Element Results and Discussions

In the dynamic system of the finite element analysis, the tillage assembly was considered as a uniform cantilever beam affixed by a lumped mass on the bottom. The response of the vibratory system was obtained from the finite element analysis considering a transverse load acting on the end of the beam. The solution includes the deflection, slope, velocity and acceleration of the shank with respect to time at each node relative to the implement frame. Soil resistance acting on the sweep was considered as a point transverse load on the end of the shank.

6.6.1 Tillage tool subjected to constant load

A constant transverse load is first considered acting on the tillage tool although the soil cutting resistance fluctuates during the tillage operation. A concentrated constant load of 500 N was assumed at the first step of the finite element analysis. The finite element analysis calculated the responses at each node of the shank assuming a constant transverse load is suddenly supplied to the shank. Figure 6.4 shows the finite element solution of deflection with respect to length of shank at a specific time t=1.0 second. The value at the end node of the shank was equivalent to the movement of sweep. Hence, the values at the end of the shank were employed throughout the chapter in the discussion.

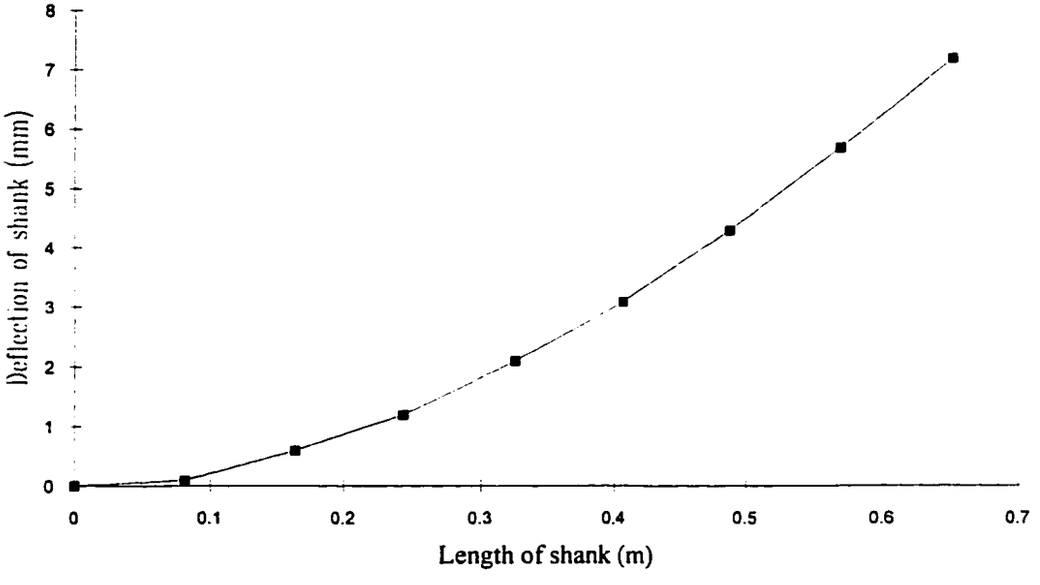

Figure 6.4 Deflection of shank
with respect to length at specific time t=1 s

Figures 6.5 indicates the transient response in deflection of the shank with respect to time relative to the implement. Figures 6.6 and 6.7 give the transient response in velocity and acceleration of the shank with respect to time relative to the carriage. It can be seen that a fundamental frequency of 14 Hz was associated with the movement of the tillage shank with the properties of Table 6.1.

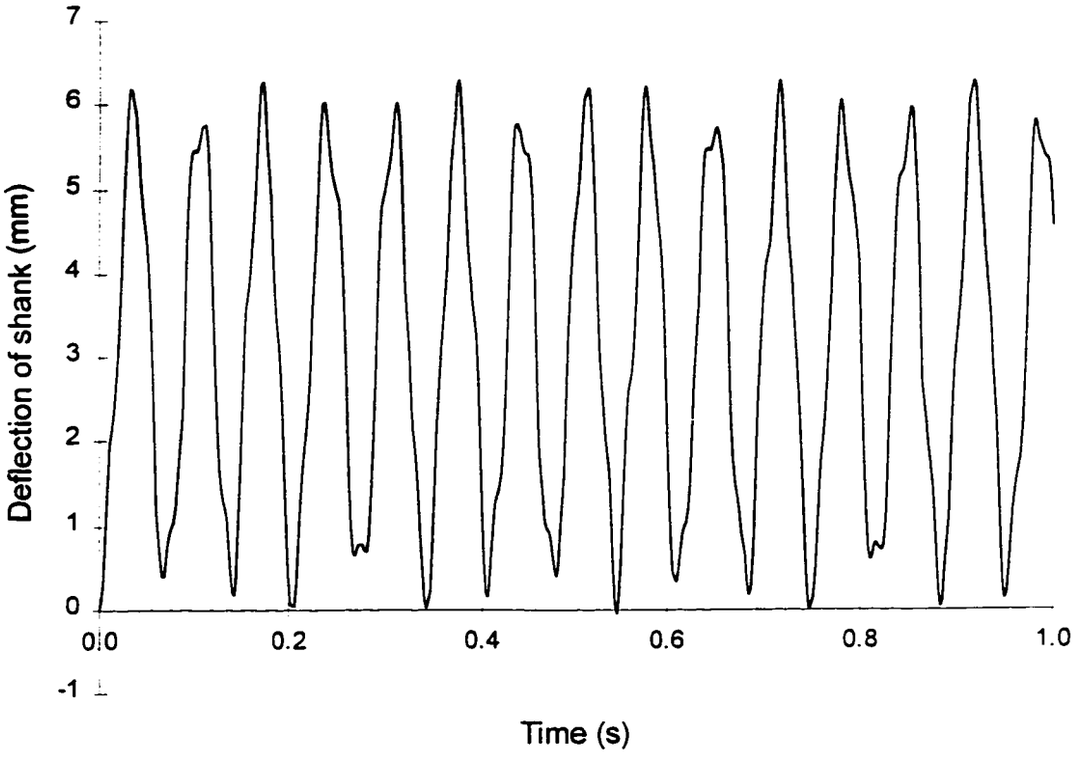

Figure 6.5 Transient deflection response of shank under constant transverse load

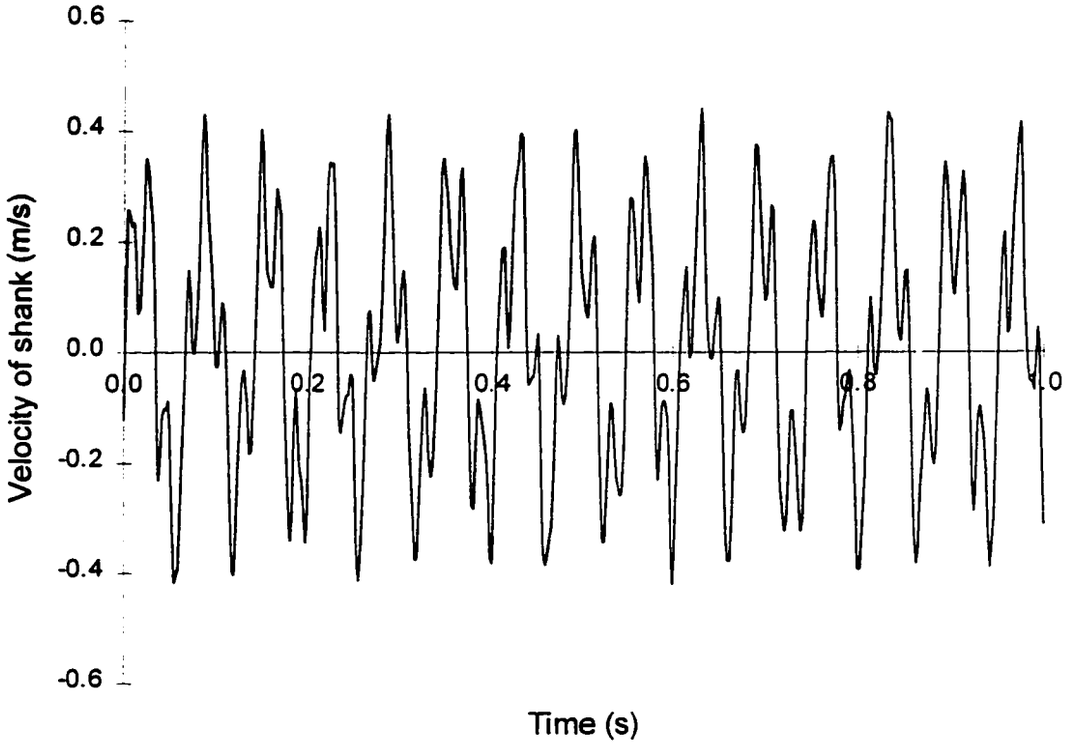

Figure 6.6 Transient velocity response of shank under constant transverse load

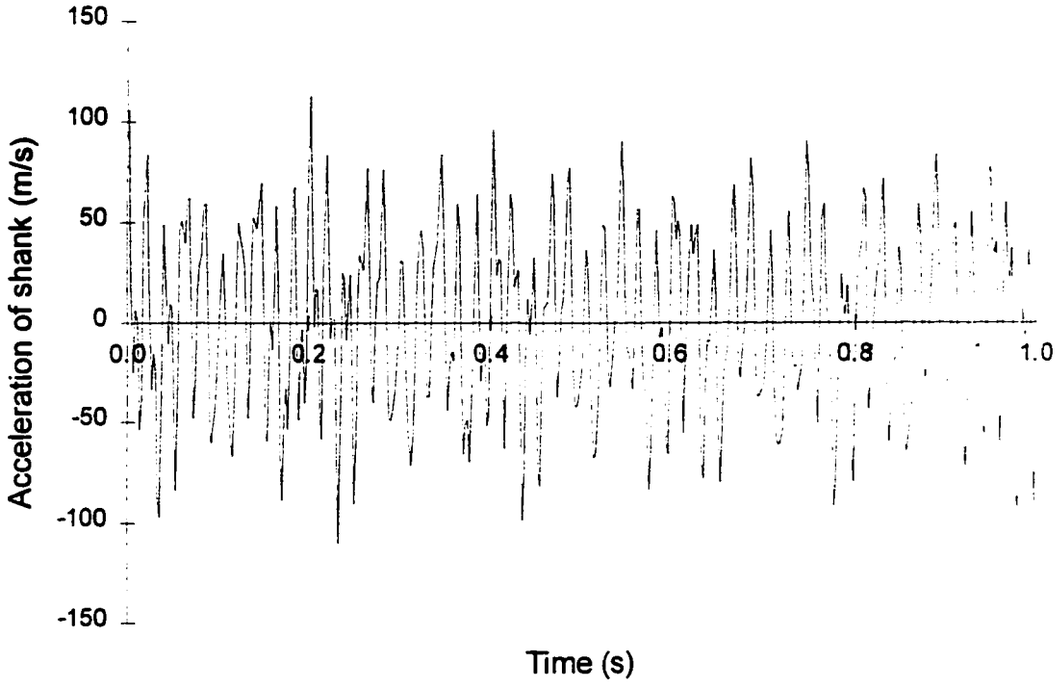

Figure 6.7 Transient acceleration response of shank under constant transverse load

6.6.2 Tillage tool subjected to a sinusoidal load

The soil cutting resistance fluctuated during the tillage operation. The cutting resistance depends upon the properties of the soil, tool shape and the manner of traveling. It was a time dependent variable. A primary test has been conducted to measure the soil cutting force variations on a sweep operated in a soil bin. The Fast Fourier transform analysis technique was used to analyze the soil bin test results of the cutting resistance. It was found that the dominant frequency of the soil cutting resistance was approximately one Hz with the average value of 500 N. Hence, a concentrated harmonic load, $500(1+\sin\omega t)$, which represented the soil resistance, was considered as the transverse load acting on the bottom of shank.

Finite element method was used to calculate the corresponding movement of the shank. The sweep was considered as a lumped mass attached on the bottom. Figures 6.8 and 6.9 indicate the displacement and slope at the end of shank for the time intervals. Figures 6.10 and 6.11 give the velocity and acceleration of the shank related to the implement with respect to time. It can be seen that two dominated frequencies were associated with the curves of deflection, slope, velocity and acceleration. One was the frequency of the applied soil resistance, and other was the natural frequency of the system. The complete motion was expressed as the sum of the harmonic curves of the different frequency. When the forcing frequency ω is smaller than the natural frequency the high frequency curve is added to the low frequencies curve.

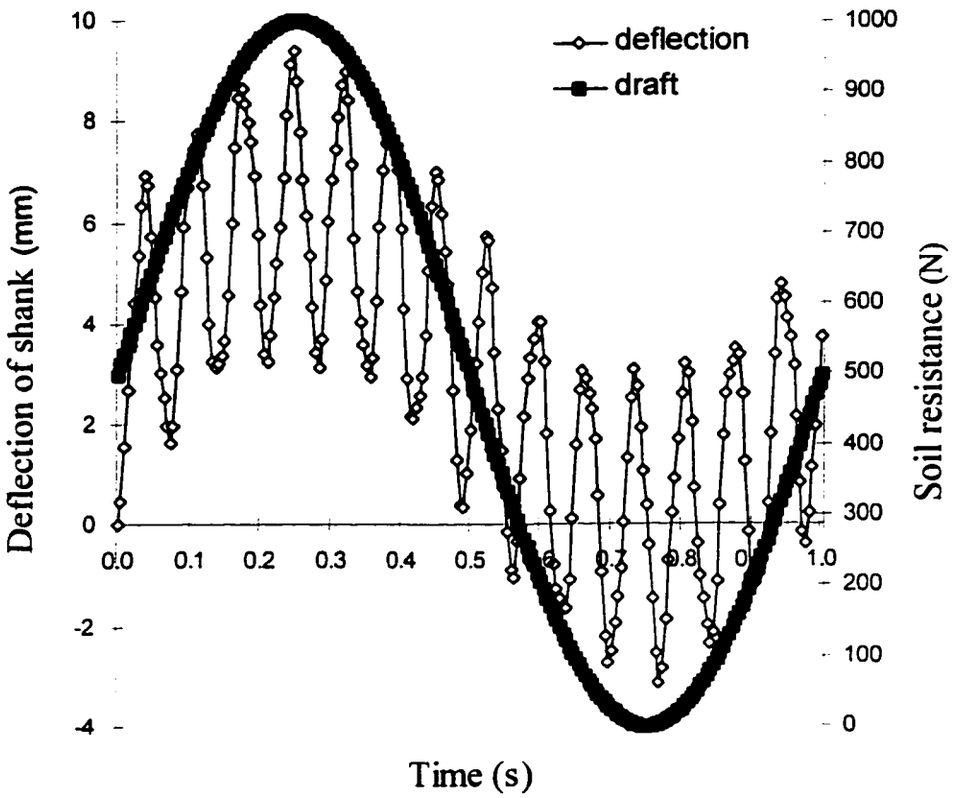

Figure 6.8 Deflection of shank under 1 Hz sinusoidal transverse load

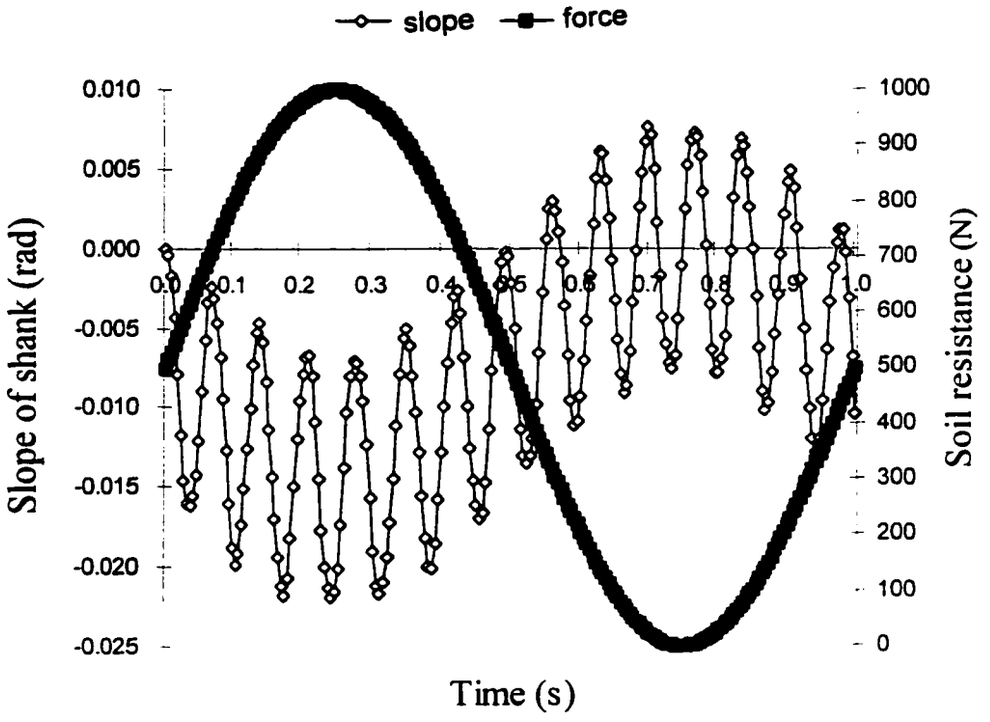

Figure 6.9 Slope of shank under 1 Hz sinusoidal transverse load

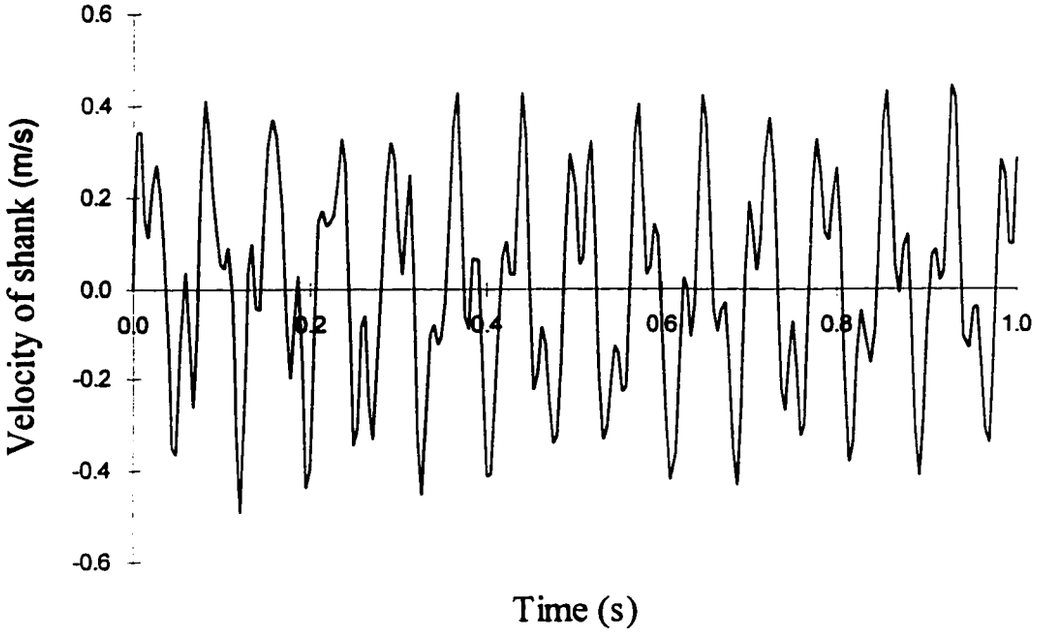

Figure 6.10 Velocity of shank under 1 Hz sinusoidal transverse load

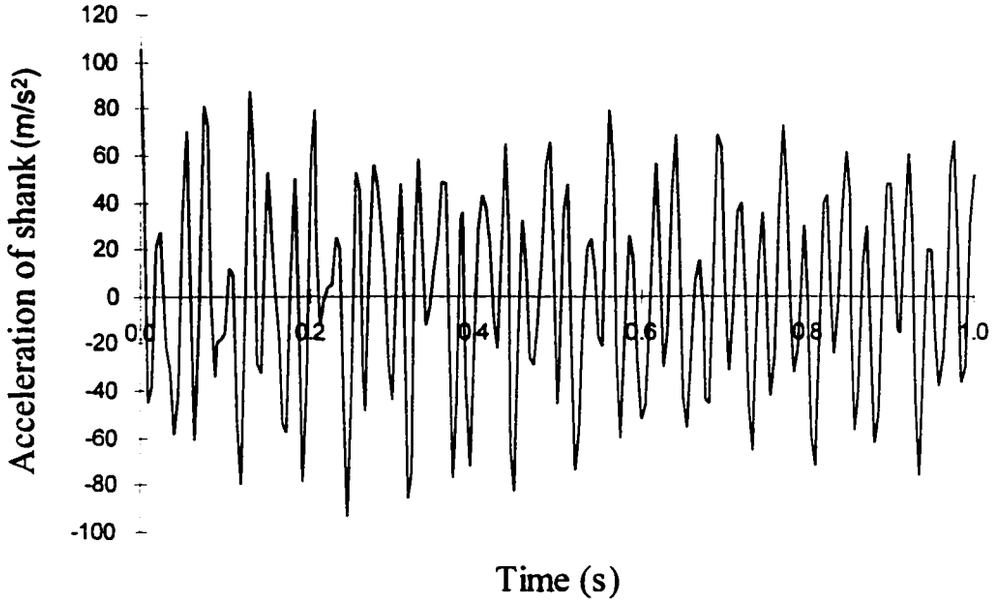

Figure 6.11 Acceleration of shank under 1 Hz sinusoidal transverse load

If only the shank of tillage tool was considered, no lumped mass added on the bottom of the shank, the solution of the displacement, velocity and acceleration related to the implement was obtained by using finite element analysis while the tillage tool was excited by the harmonic soil resistance. Figure 6.12 shows the deflection of the tillage tool with respect to time when the mass of tillage tool is not added. It can be seen that the displacement curve has a high frequency and almost the same amplitude when compared with the system with the tillage tool mass added. It is obvious that the dynamic response of the shank under the action of the soil cutting resistance is associated with some frequencies that are dependent on the characteristics of the tool implement and the soil cutting resistance. The Fourier transform theory can be used for the frequency domain analysis.

6.6.3 Effect of the axial force

When an axial tensile or compressive load adds on the tillage shank the rigidity of the beam will be changed. Hence the response of the beam will be affected although the axial force does not directly cause the bending of the shank. As it is discussed in Chapter 6, the fundamental frequency of the shank increases with an increase of the tensile load while the compressive load reduces the natural frequency of the vibrating system.

Figure 6.13 shows the deflection of the shank for different axial forces. It can be seen that the tensile axial force tends to decrease the amplitude of the deflection and to increase the oscillatory frequency of the system, vice verse for the compressive axial load. The effect of the axial load on the motion of the vibrating system is very small comparing the values of the axial force of 10000 N and the transverse load of 500 N.

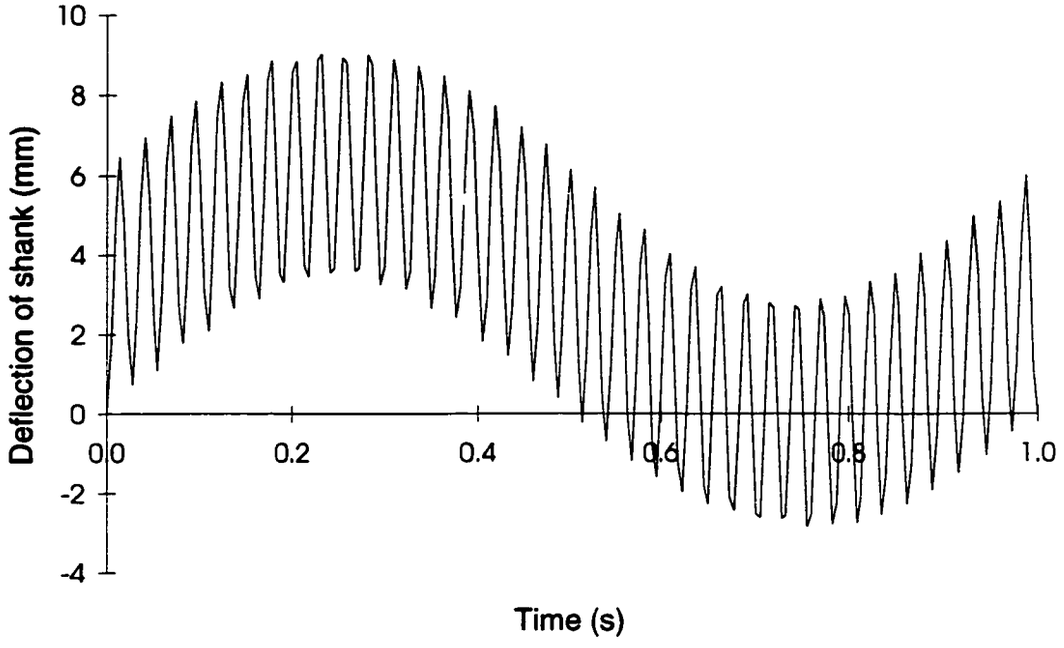

Figure 6.12. Deflection of shank under 1 Hz sinusoidal transverse load for the shank no sweep attached

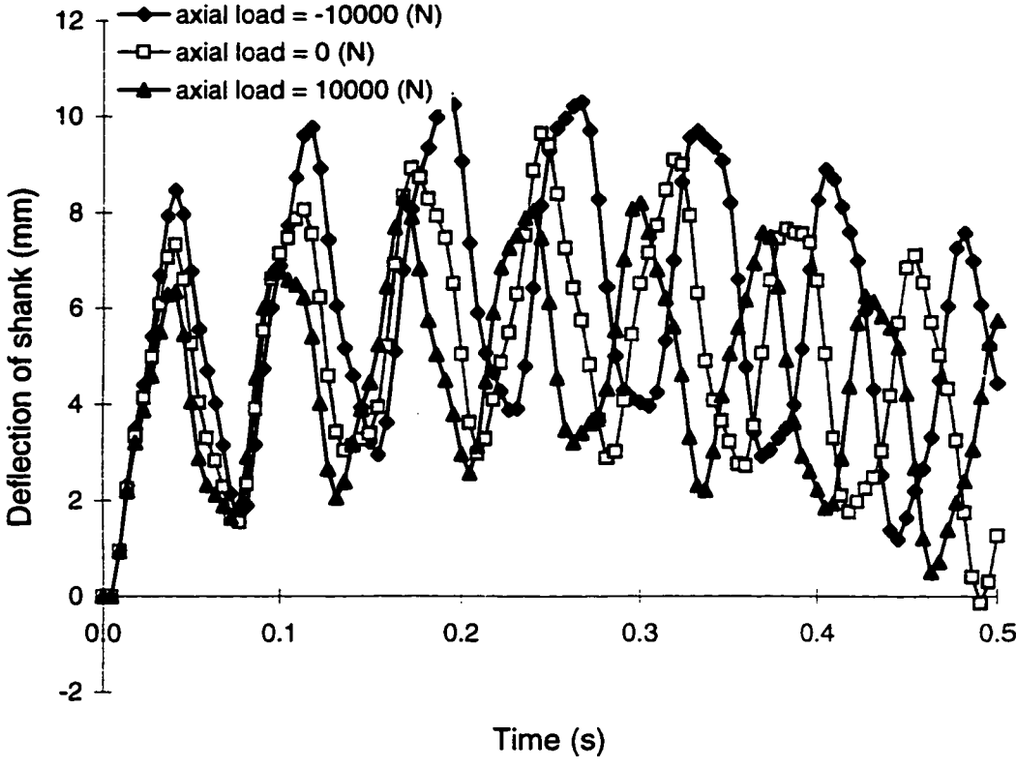

Figure 6.13 Deflection of the shank under different axial loads

6.6.4 Fourier transfer analysis of finite element results

Fourier's theorem states that any single valued periodic function can be represented by an infinite series of sine and cosine that are harmonics of the fundamental repetition interval. The discrete Fourier transform was used to approximate the Fourier transform of a discrete signal. The discrete Fourier transform (DFT) is defined as

$$x(f) = \sum_{k=0}^{N-1} x(k) e^{\frac{-j2\pi nk}{N}} \tag{6.48}$$

The expression is used to transfer a time series of samples to a series of frequency domain samples. The finite element results and experimental data were analyzed using a Fast Fourier Transform (FFT) technique to locate the dominant frequency. This information was used to fit the data into a Fourier series using a harmonic analysis technique. The regression equation had the following form:

$$x(t) = A_0 + \sum_{n=1}^{N} [A_n \cos(2\pi nft) + B_n \sin(2\pi nft)] \tag{6.49}$$

Figure 6.14 shows FFT analysis of deflection output in the frequency domain. The FFT analysis of acceleration and velocity output in frequency domain are presented in Figs. 6.15 and 6.16. The fundamental frequency of the dynamic system is about 14.20 Hz. In Fig 6.14 the two peak amplitudes correspond to the frequency of applied transverse load of 1 Hz and the natural frequency of the system of 14.20 Hz. Note that the amplitudes increase in the high frequencies for the velocity and acceleration output since their output are proportional to the ω and ω^2 respectively. The frequency was high for the shank without lumped mass attached.

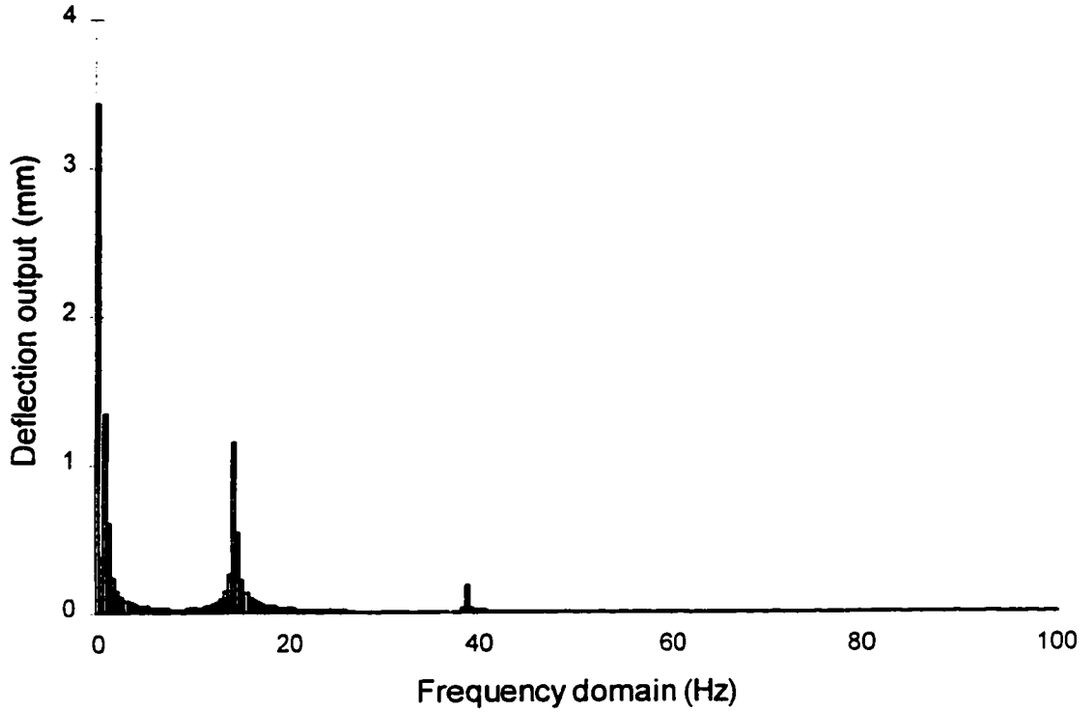

Figure 6.14 FFT analysis of deflection under 1 Hz sinusoidal transverse load

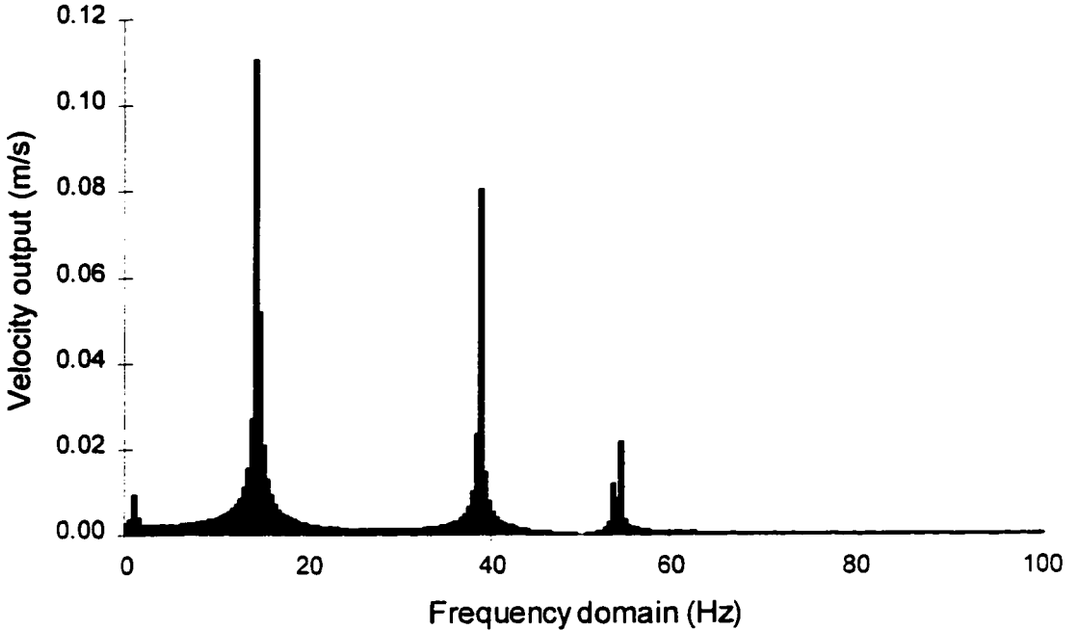

Figure 6.15 FFT analysis of velocity under 1 Hz sinusoidal transverse load

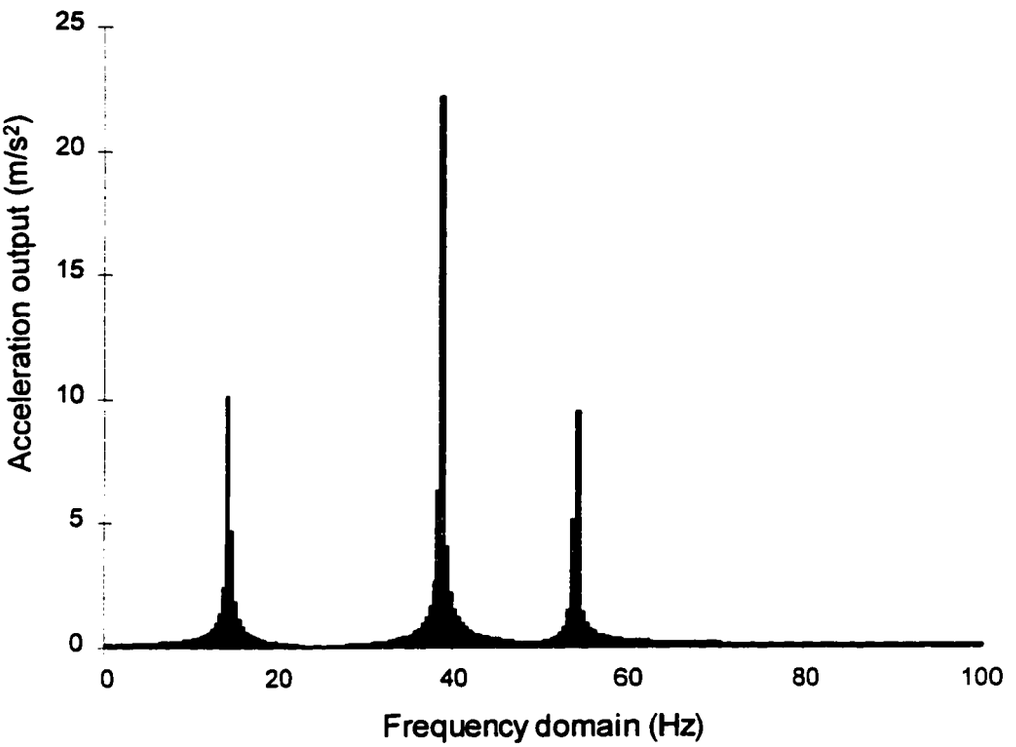

Figure 6.16 FFT analysis of acceleration under 1 Hz sinusoidal transverse load

6.6.4 Resonant vibration of tillage tool

The natural frequency is depended upon the characteristics of the implement. By changing the parameters of the beam, such as material, rotary inertia, and length, the natural frequency of the implement can be changed. The frequency of the transverse load represents the variation of the soil resistance. The frequency of the soil resistance could be decided through the field test although we assumed one Hz for the preliminary investigation by the finite element analysis.

It is possible to turn the tillage tool so that its resonant frequency is synchronized to the pattern of the soil cutting resistance. The vibration of the tool at its resonant frequency may result in large amplitudes. To simulate this condition, a soil cutting resistance with frequency of 14 Hz was assumed for the vibratory system. The responses of the dynamic system were obtained by using the finite element model. Figure 6.17 gives the deflection of the sweep assembly with respect to time under the action of 14 Hz transverse load. Similar curves for the velocity and acceleration can be obtained. This condition may induce the resonance vibration causing damage to the implement.

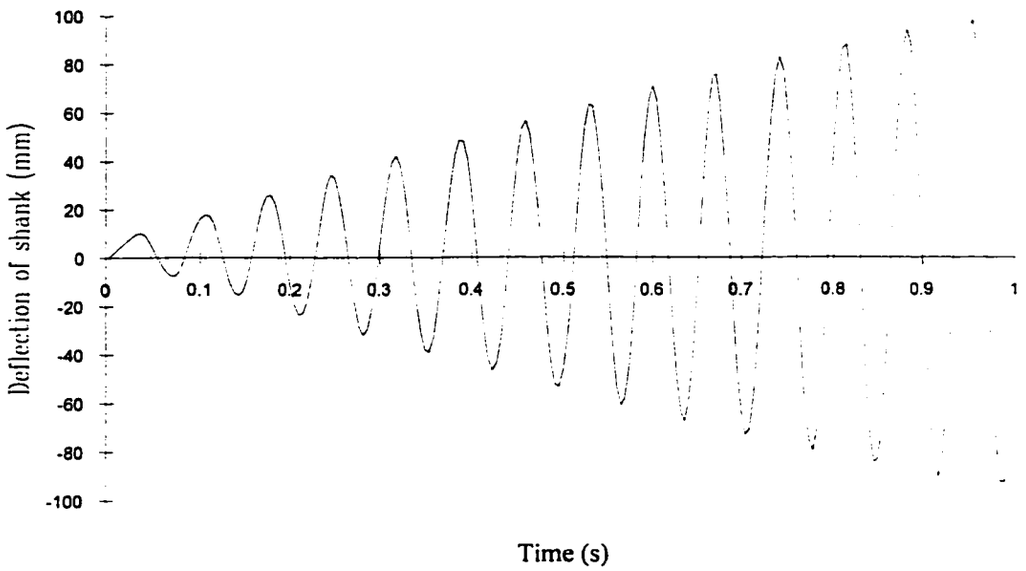

Figure 6.17 Deflection of shank under 14 Hz sinusoidal transverse load

6.7 Parametric Sensitivity Analysis

In general, the dynamic behavior of a tillage tool is influenced by a number of factors, such as the material characteristics, length of shank, soil resistance pattern, etc. A better understanding of these factors is achieved through a parametric study of the model. The parametric study results indicate a trend in the effect of various parameters on the response and provide a basis for selecting the parameters that yield optimal operation.

The responses of the dynamic system varied corresponding to the applied transverse load and its characteristics during operation. The output varied in the positive and negative region for different intervals. The peak value of the output was used to compare the results for the different parameters. Figure 6.18 indicates the peak values of deflection and velocity for the different length of shank under the action of the same soil cutting resistance. It can be seen that the peak values of deflection and velocity were proportional to the length of shank. Figure 6.19 shows the peak values of acceleration for the different shank lengths. Contrary to the deflection and velocity curves the acceleration generally has a tendency to decrease as the length of shank increases although the difference in the acceleration value is not very great. In other words, the values of acceleration are not very sensitive to the length of shank. The results obtained from the finite element analysis are discrete curves for the time intervals. The results of the calculation also depend on the time step that has been used in the model. This is why there is a little inconsistency for some points in the curve in Fig. 6.19. For the various materials, the elasticity modulus are different. The moment of inertia could be different although the cross section is the same. The product of elasticity modulus and the moment of inertia is known as the flexural rigidity that plays a key role in determining the motion of the dynamic system. Figure 6.20 gives the peak values of deflection and velocity as the flexural rigidity changes. The corresponding deflection and velocity of the beam

decrease with an increase of flexural rigidity of the shank. There is no apparent variation in the acceleration as the flexural rigidity changes.

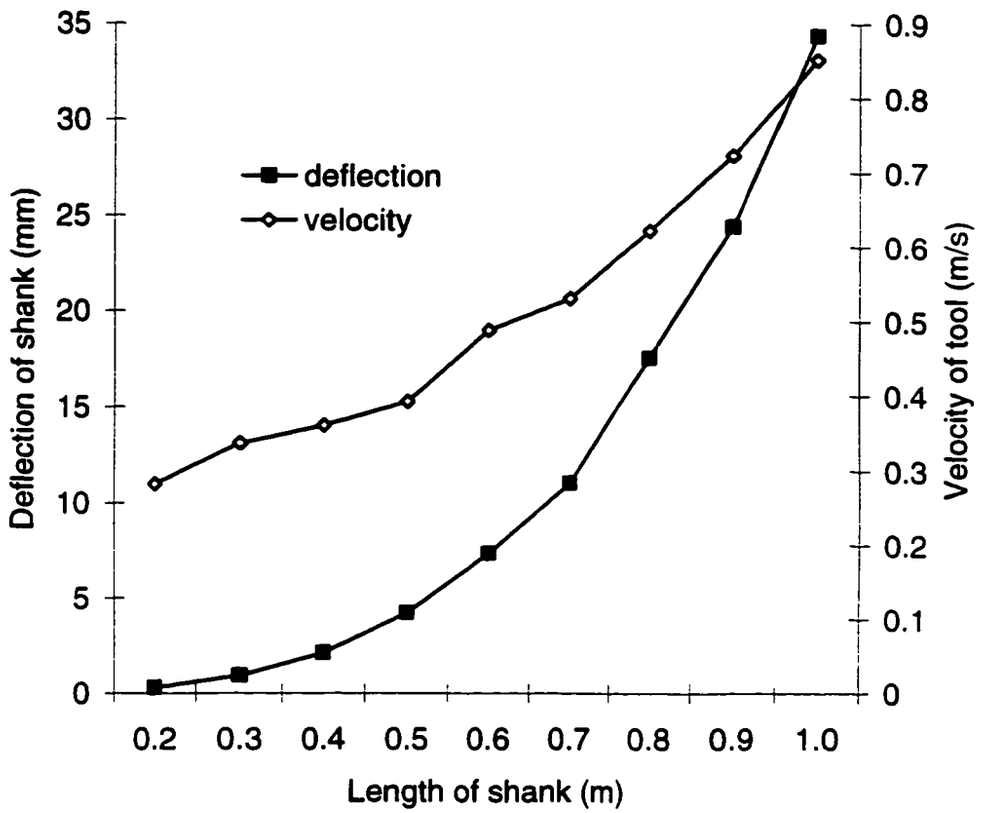

Figure 6.18 Peak values of deflection and velocity for the different length of shank

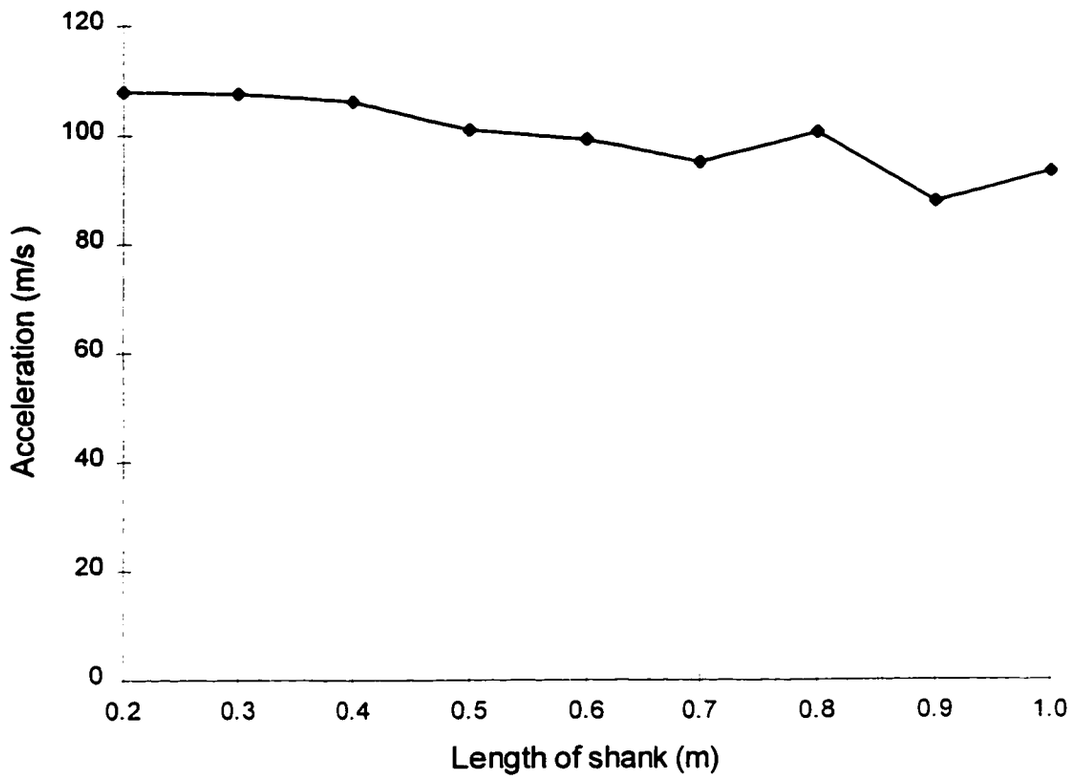

Figure 6.19 Peak values of acceleration for the different length of shank

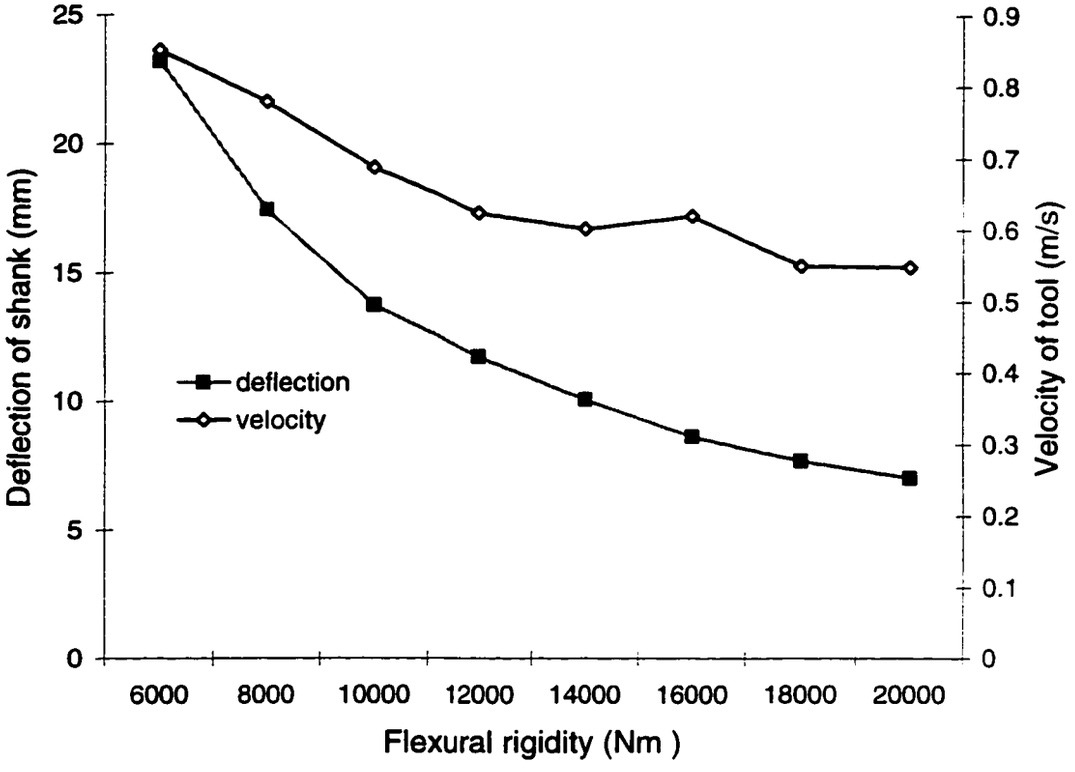

Figure 6.20 Deflection and velocity vs. flexural rigidity of shank

6.8 Soil Resistance Fluctuation Prediction

Soil cutting resistance depends upon tool geometry, soil properties and traveling manner. During tillage operation, the soil resistance generally fluctuates since the soil is consisted of discrete clods. If a tool is excited to vibrate by the soil cutting resistance, the tool will respond corresponding to the fluctuating soil resistance function. Under ideal operating conditions of forward speed, the tool would experience periodic displacement, velocity, acceleration, and force characteristics. It was decided that a linear regression of static soil cutting resistance and forward speed would give a suitable working model for the soil-tool interaction (Gunn and Tramontini 1955). This equation is given as

$$R(t) = R_0(1 + \lambda V(t)) \tag{4.15}$$

For the dynamic system of vibratory soil cutting

$V(t) = V_c + V_t$

where:

V_c = constant forward speed of vehicle (m/s),

V_t = velocity of tool relative to the vehicle (m/s).

The static soil cutting resistance could be obtained through field test or by using the soil cutting prediction model. The dynamic soil resistance thus can be obtained if the absolute traveling velocity of the tool can be determined. Considering the tillage implement traveling at a constant speed of 1.6 km/h, the relationship between the soil cutting resistance and the motion of the dynamic system can be obtained by applying the soil resistance, which is a function of the speed, into the system equation, Eq. 6.13, as the transverse load acting on the beam. The soil resistance is a function of speed $V(t)$. The velocity of the tool relative to the implement is also dependent upon the soil resistance

acting on the vibratory system. By applying these conditions to the Eq 6.13, a new expression of the system equation can be obtained as:

$$[M][\ddot{U}] + [K][U] = [F_0] + \lambda[\dot{U}][F_0] \tag{6.50}$$

The solution of the system equation should meet the requirement of the relationship of the soil cutting force and traveling velocity. The soil resistance and appropriate velocity of the tool was determined by using the intensive search method. Figure 6.21 presents the soil resistance for the time intervals assuming the soil resistance is dependent on the forward speed. If the velocity relative to the ground $V(t) < 0$, the soil resistance will be zero since there is no soil tool interaction. However, while the absolute velocity is close to zero, the soil cutting resistance will decrease accordingly, in turn the potential energy will be released to move the tool forward until a new equilibrium state is reached. According to the calculation the velocity relative to the ground is always greater than zero and no zero soil resistance is found although the soil resistance is very small when it is in the critical state. It would also explain the sudden reduction of the soil resistance as shown in Fig. 6.21. Figure 6.22 shows the deflection of the tool related to the implement with respect to time. Figures 6.23 and 6.24 give the velocity and acceleration curves of the tool relative to the implement with respect to time, assuming the homogeneous soil and cutting resistance is linearly proportional to velocity. It can be seen from the figures that the motion of the system gradually stabilizes as the homogeneous material tends to restrict the motion of the tool. However, the stable motion of the dynamic system is realized under the assumption that soil is a homogenous material and the cutting resistance is linearly dependent upon the velocity. In reality, soil cutting resistance fluctuates due to the nonhomogenous characteristics of the soil. The sudden change of the soil cutting resistance will cause the vibration to be an inevitable phenomenon associated with the soil cutting operation.

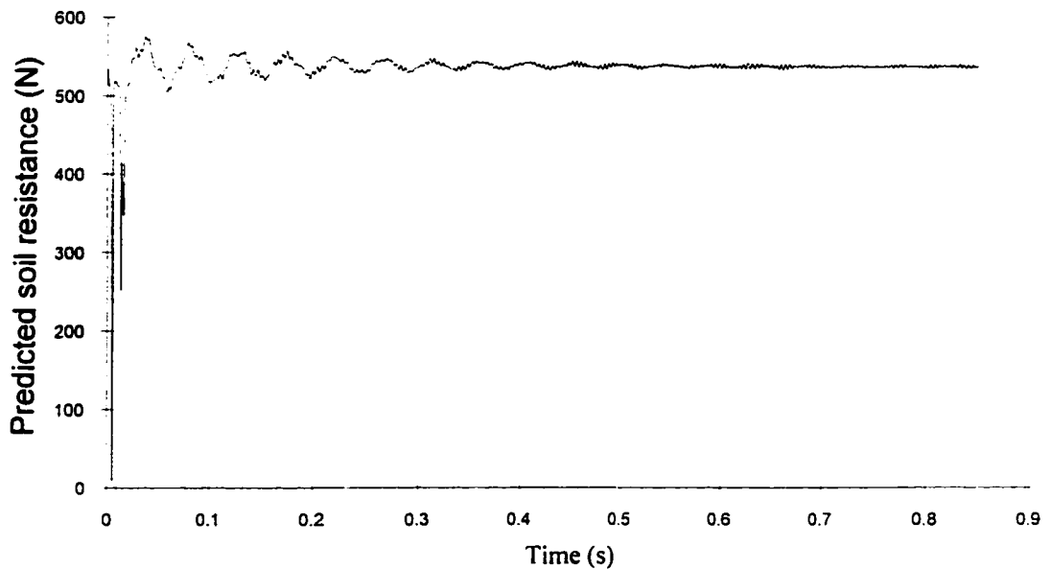

Figure 6.21 Predicted tillage resistance

assuming soil is homogeneous and draft is linearly dependent on velocity

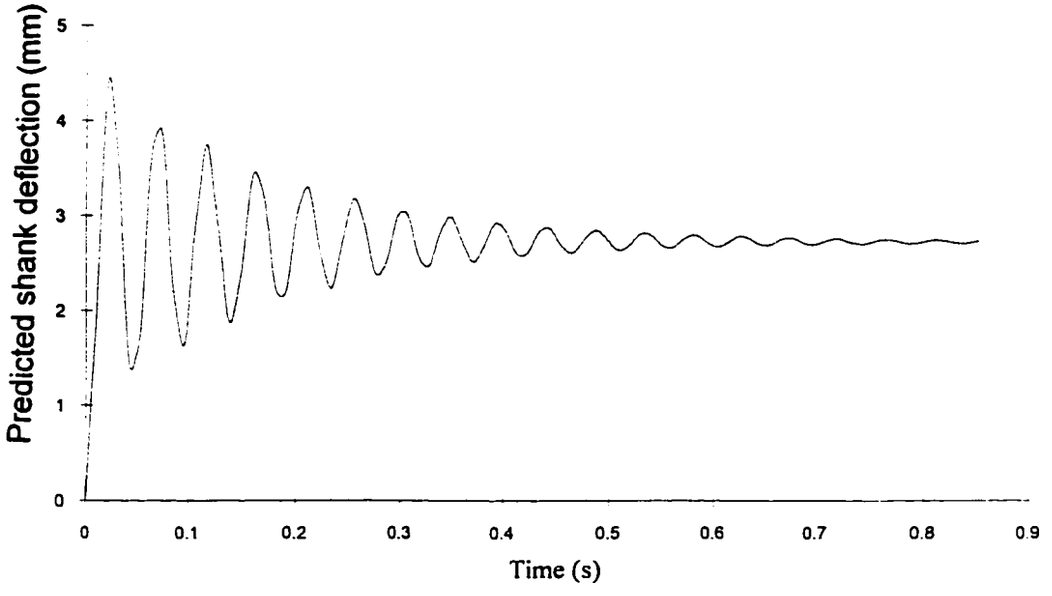

Figure 6.22 Predicted deflection of shank relative to the implement assuming soil is homogenous and draft is linearly dependent on velocity

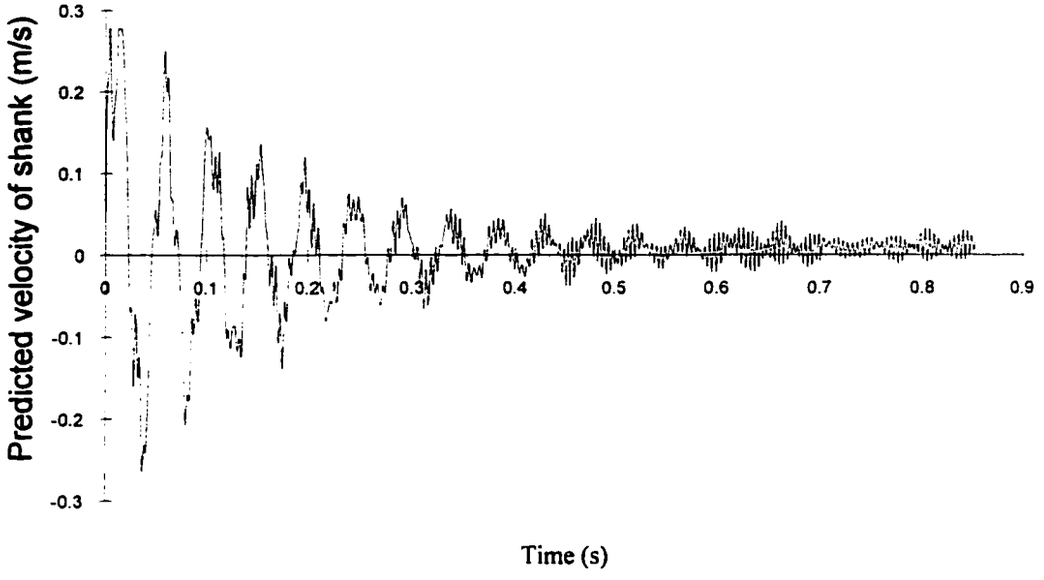

Figure 6.23 Predicted velocity of shank relative to the implement assuming soil is homogenous and draft is linearly dependent on velocity

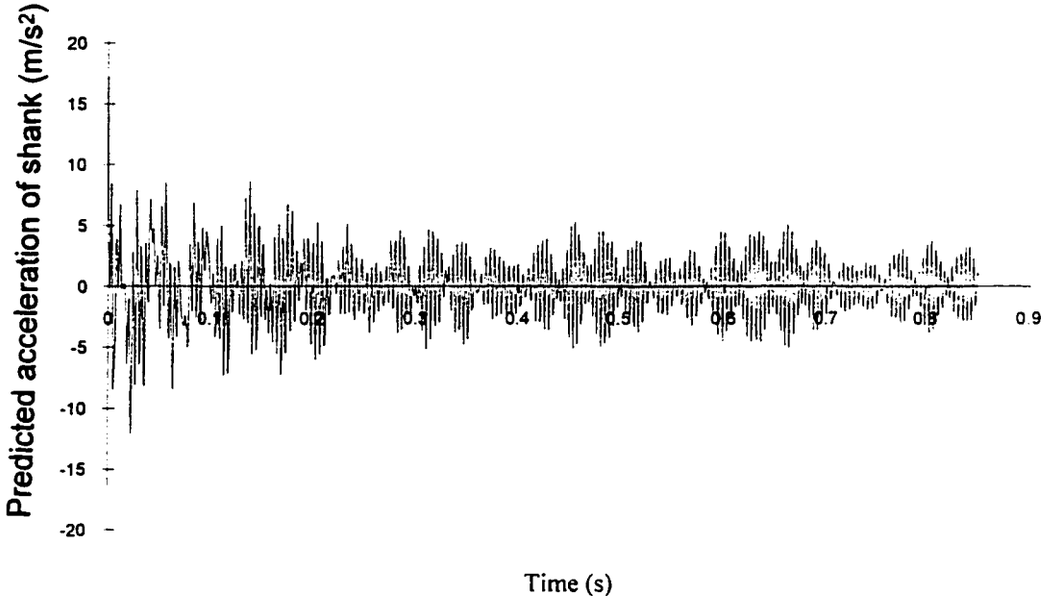

Figure 6.24 Predicted acceleration of shank relative to the implement assuming soil is homogenous and draft is linearly dependent on velocity

CHAPTER 7
SOIL BIN TEST VERIFICATION AND DISCUSSIONS

Laboratory tests were conducted to compare the results of the finite element analysis with experimental test results. Tests were carried out in an indoor soil bin for a shank and sweep assembly at travel speeds of 1.6 km/h and 3.2 km/h. Figure 7.1 shows the shank and sweep assembly mounted on the carriage tool-bar. Tests were conducted to measure the draft and acceleration of tillage tool related to the carriage frame.

The soil used in the soil bin is a clay loam. The average moisture content of the soil was 12% in the soil bin during the test runs. The physical properties of soil are given in Table 7.1. The soil conditions were carefully controlled during the tests to provide relatively uniform conditions throughout all test runs.

7.1 Soil Bin Test Procedure

At the beginning of the soil preparation, water was sprayed uniformly on the soil. Then the soil was covered with a plastic sheet for 18 hours to allow the moisture to infiltrate from the soil surface down to the sub-surface. The soil was then rototilled into fine particles (Fig. 7.2), leveled and packed. Two different packers were used to compress the soil. The soil was first packed with a sheep-foot packer (Fig. 7.3), five times forward and back, which compacted the sub-surface soil. Finally a smooth roller (Fig. 7.4) was used to pack the surface soil twice forward and back. Figure 7.5 shows a prepared soil bin site.

Table 7.1 Engineering classification of soil (Adams 1996)

Parameter	Value
Particle analysis	
Sand	48.1%
Silt	23.6%
Clay	28.3%
Specific gravity	2.65
Atterberg consistency limits	
Liquid limit, water content	32.9%
Plastic limit, water content	18.8%
Plasticity index	14.1%
Optimum compaction state	
Water content	18%
Dry bulk density (Mg/m^3)	1.65

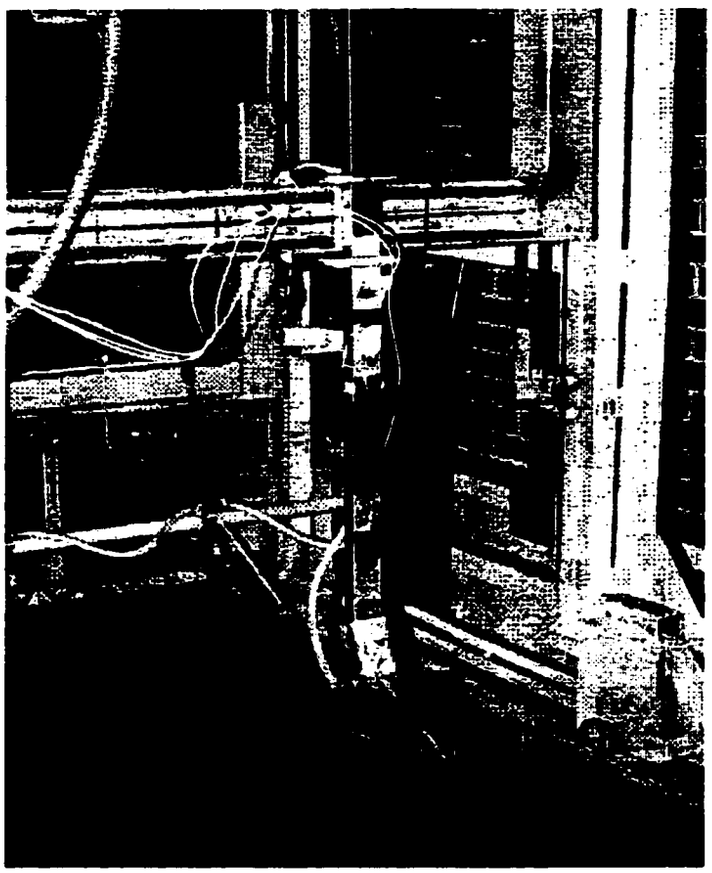

Figure 7.1 Tillage shank mounted on the carriage frame

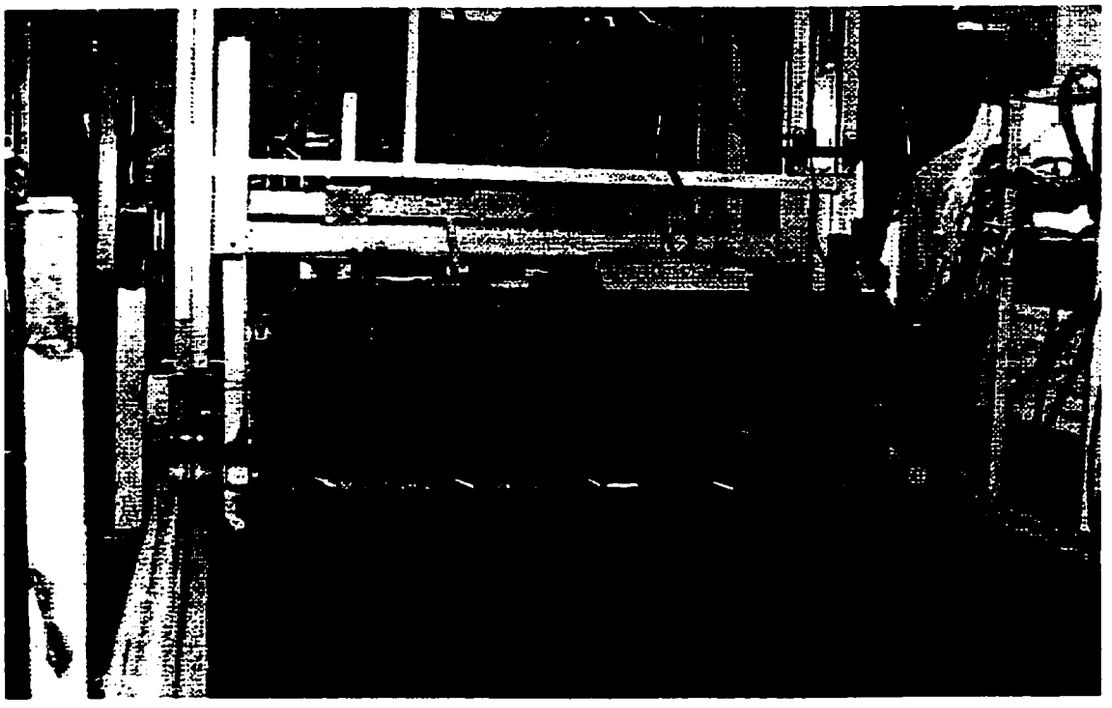

Figure 7.2 Rotortilling operation of soil bin

Figure 7.3 Sheep foot packer

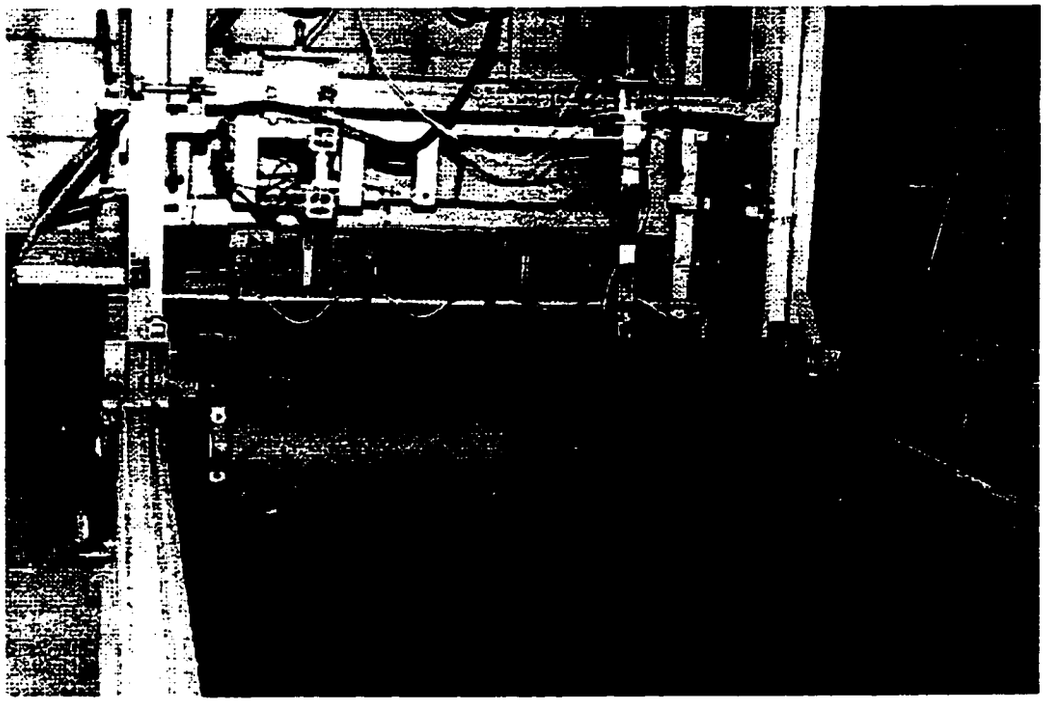

Figure 7.4 Surface packer

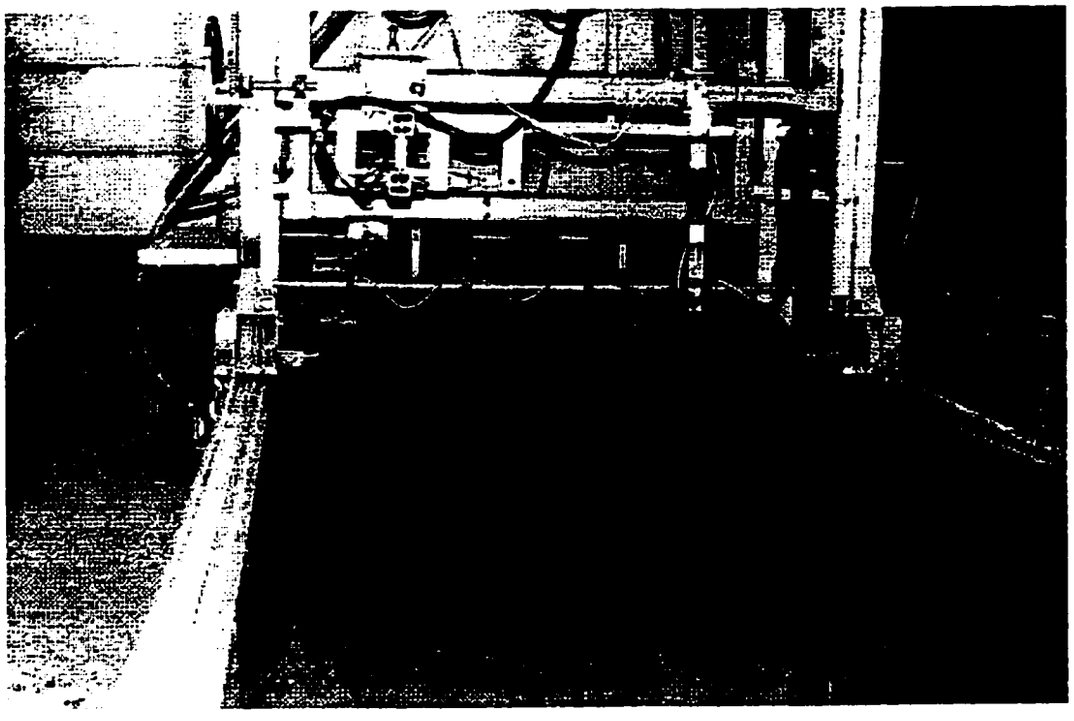

Figure 7.5 Prepared soil bin

7.2 Acceleration of Tillage Shank and Tool

Two accelerometers, model JTF/3629-05 (Sensotec), were used for acceleration measurements. One was mounted on the bottom of the shank to measure the acceleration of tillage tool. Another was mounted on the traveling frame to check the significance of background acceleration. The accelerometers had good sensitivity characteristics and a wide useful frequency ranges up to 350 Hz. With a small size and light weight, the accelerometers were able to measure the vibration of the dynamic system without loading the shank. The accelerometer generated a voltage output signal that was proportional to the acceleration of the vibrating system by using a low impedance strain gauge bridge.

The cable of the accelerometer was taped to the vibrating shank, and the other end of the cable, which was connected to the amplifier, was kept away from the vibrating shank. This procedure was done to eliminate or at least minimize cable noise caused by dynamic bending, compression, or tension in the cable.

The background noise was checked by comparing the relative magnitudes of the acceleration of the frame and the vibrating shank. Figure 7.6 indicates the acceleration magnitudes of the vibrating shank and carriage frame with respect to time. The induced vibration caused by the background noise was less than one-third of the value obtained on the vibrating system under test as suggested by Irwin and Graf (1979) for reasonably accurate results.

The differences in acceleration values between the tillage tool and frame were considered as the measured data since the frame was regarded as the reference of the dynamic system. The motion of the dynamic system was relative to the frame.

A low pass filter with cut off frequency 200 Hz was used in the data acquisition system to eliminate high frequency noise.

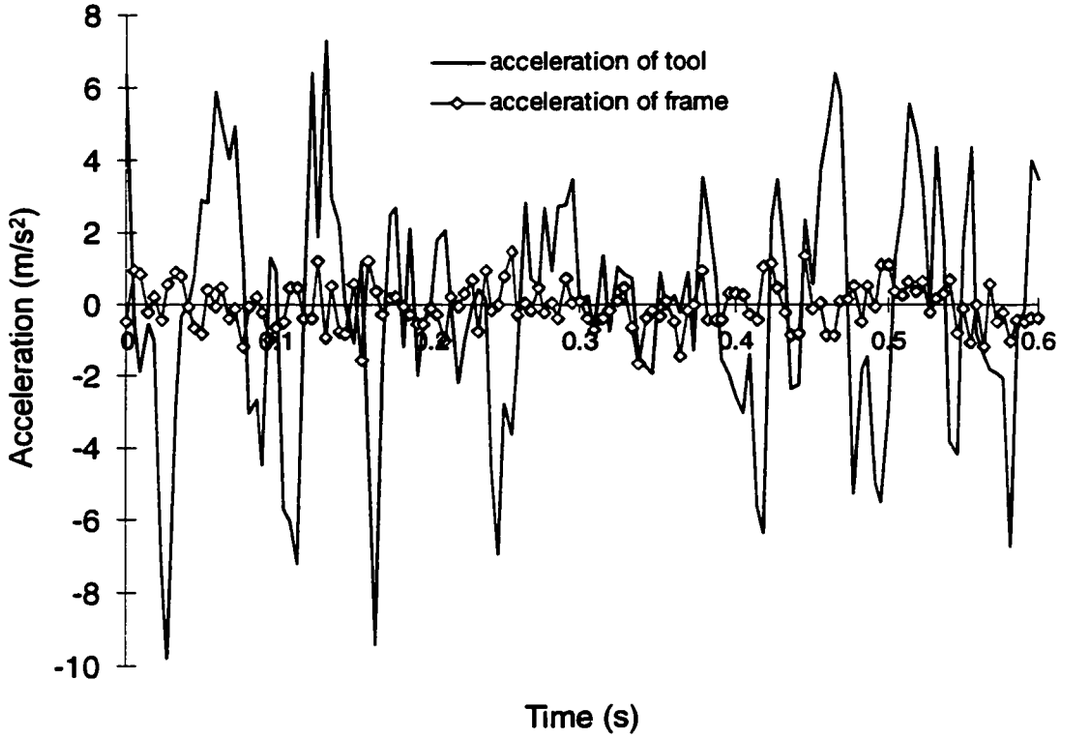

Figure 7.6 Measured acceleration with respect to time at speed 1.6 km/h

7.3 Draft of Tillage Tool

The draft of the tillage tool was obtained by measuring the strain change on the shank of the sweep. The shank of the tillage tool operating in the soil bin was rigidly clamped to the horizontal beam of the carriage frame. The sweep was bolted at the end of the shank. The soil resistance acting on the sweep could be represented as a transverse force acting on a vertical cantilever beam. A four arm bridge circuit transducer, with two tension arms and two compression arms on opposite sides, was used to measure the draft of the tillage tool. To increase the sensitivity of measurement, the transducer was installed on the top part of the shank with h=500 mm from the acting point of the soil resistance to the transducer. Four 350 Ω (KFC-5-350-c1-11) strain gauges were used in the bridge circuit. The gauges were mounted on the shank of the tillage tool according to the direction of the strain gauge installation. After the adhesive was cured, M coating and then plastic sponge was applied to the surface to protect the strain gauge.

The strain gauge transducer mounted on the shank was sensitive to the stress change of the beam. The stress is directly related to the bending moment generated as.

$$\varepsilon = \frac{\sigma}{E} \tag{7.1}$$

$$\sigma = \frac{Mc}{I} \tag{7.2}$$

where:

ε = strain (mm/mm),

σ = stress (Pa),

M = bending moment applied on the strain gauge (Nm),

I = moment of inertia of the beam (m^4),

c = half thickness of shank (m).

For the static problem, the bending moment is caused by the transverse load on the beam. The transverse load on the beam can be obtained by the proper calibration through the measurement of strain. However, for the dynamic system, the acceleration of the mass also adds a bending moment on the beam which affects the strain of the measurement. Figure 7.7 shows the free body diagram of the dynamic system.

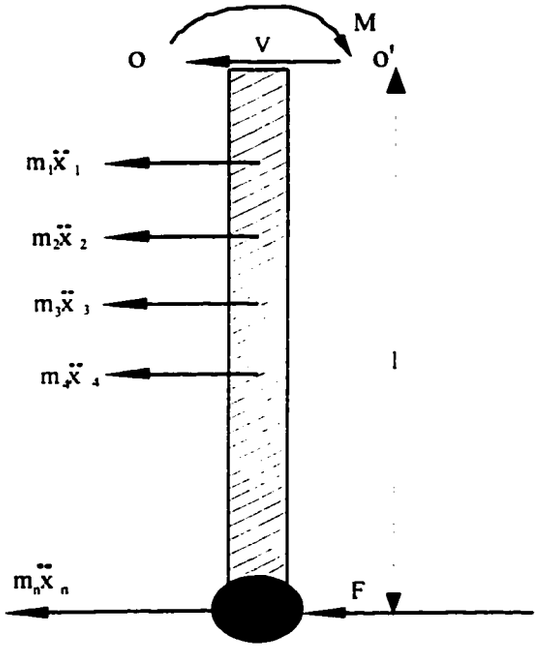

Figure 7.7 Free body diagram of tillage assembly

The bending moment of the beam is mainly caused by the transverse load F and $m_n \ddot{x}_n$ term. If the inertia term at the other point of the beam is not considered, the component force acting on point n can be obtained by reading the strain at the point o-o' of the transducer.

Let $P = F + m_n \ddot{x}_n$

The deflection and the slope of beam at each point x, can then be obtained as:

$$U_n = \frac{P}{6EI}(3Lx_n^2 - x_n^3) \qquad n = 1,3,5,\ldots \tag{7.3}$$

where:

U_n = deflection of beam at node n (m),

P = component load acting on the end of shank (N),

L = length of shank (m).

$$U_n = \frac{P}{2EI}(x_n^2 - 2Lx_n) \qquad n = 2,4,6,\ldots \tag{7.4}$$

where:

U_n = slope of bending beam at node n (rad).

The differential equation of motion for the lateral vibration of beam can be represented in matrix form by using the finite difference method:

$$[M][\ddot{U}] + [K][U] = [F] \tag{6.13}$$

In Eq. 6.13, [U] is known at each point. $[\ddot{U}_{n-1}]$ is the acceleration at the end point of the beam which was measured by the accelerometer.

For the force matrix, there is only one point load F acting on the beam. We have:

$$[F]=\begin{vmatrix}0\\0\\\cdot\\\cdot\\F\\0\end{vmatrix} \tag{7.5}$$

Substituting [U], $[\ddot{U}_{n-1}]$, and [F] into Eq. 7.13, we obtain

$$\begin{aligned}
&m_{11}\ddot{U}_1+m_{12}\ddot{U}_2+\ldots+m_{1n-1}\ddot{U}_{n-1}+m_{1n}\ddot{U}_n=-k_{11}U_1-k_{12}U_2-\ldots-k_{1n-1}U_{n-1}-k_{1n}U_n\\
&m_{21}\ddot{U}_1+m_{22}\ddot{U}_2+\ldots+m_{2n-1}\ddot{U}_{n-1}+m_{2n}\ddot{U}_n=-k_{21}U_1-k_{22}U_2-\ldots-k_{2n-1}U_{n-1}-k_{2n}U_n\\
&\qquad\qquad\qquad\qquad\cdot\cdot\\
&\qquad\qquad\qquad\qquad\cdot\cdot\\
&m_{n-11}\ddot{U}_1+m_{n-12}\ddot{U}_2+\ldots+m_{n-1n-1}\ddot{U}_{n-1}+m_{n-1n}\ddot{U}_n=F-k_{n-11}U_1-k_{n-12}U_2-\ldots-k_{n-1n-1}U_{n-1}-k_{n-1n}U_n\\
&m_{n11}\ddot{U}_1+m_{n2}\ddot{U}_2+\ldots+m_{nn-1}\ddot{U}_{n-1}+m_{nn}\ddot{U}_n=-k_{n1}U_1-k_{n2}U_2-\ldots-k_{nn-1}U_{n-1}-k_{nn}U_n
\end{aligned} \tag{7.6}$$

Rearranging the matrix equation, substituting the [F] for $[\ddot{U}_{n-1}]$ we get:

$$\begin{bmatrix}
m_{11} & m_{12} & \cdot\cdot & 0 & m_{1n}\\
m_{21} & m_{22} & \cdot\cdot & 0 & m_{2n}\\
 & & \cdot\cdot & & \\
 & & \cdot\cdot & & \\
m_{n-11} & m_{n-12} & \cdot\cdot & -1 & m_{n-1n}\\
m_{n1} & m_{n2} & \cdot\cdot & 0 & m_{nn}
\end{bmatrix}\begin{bmatrix}\ddot{U}_1\\\ddot{U}_2\\\cdot\\\cdot\\F\\\ddot{U}_n\end{bmatrix}=\begin{bmatrix}
-k_{11}U_1-k_{12}U_2-\ldots-k_{1n-1}U_{n-1}-k_{1n}U_n-m_{1n-1}\ddot{U}_{n-1}\\
-k_{21}U_1-k_{22}U_2-\ldots-k_{2n-1}U_{n-1}-k_{2n}U_n-m_{2n-1}\ddot{U}_{n-1}\\
\cdot\\
\cdot\\
-k_{n-11}U_1-k_{n-12}U_2-\ldots-k_{n-1n-1}U_{n-1}-k_{n-1n}U_n-m_{n-1n-1}\ddot{U}_{n-1}\\
-k_{n1}U_1-k_{n2}U_2-\ldots-k_{nn-1}U_{n-1}-k_{nn}U_n-m_{nn-1}\ddot{U}_{n-1}
\end{bmatrix} \tag{7.7}$$

By solving Eq. 7.7, the transverse soil cutting resistance F acting on the point n-1 and the acceleration value at the other points on the shank can be obtained. Thus, by

measuring the strain change of the beam, the soil cutting resistance can be obtained at each time interval. Figure 7.8 shows the soil cutting resistance with respect to time.

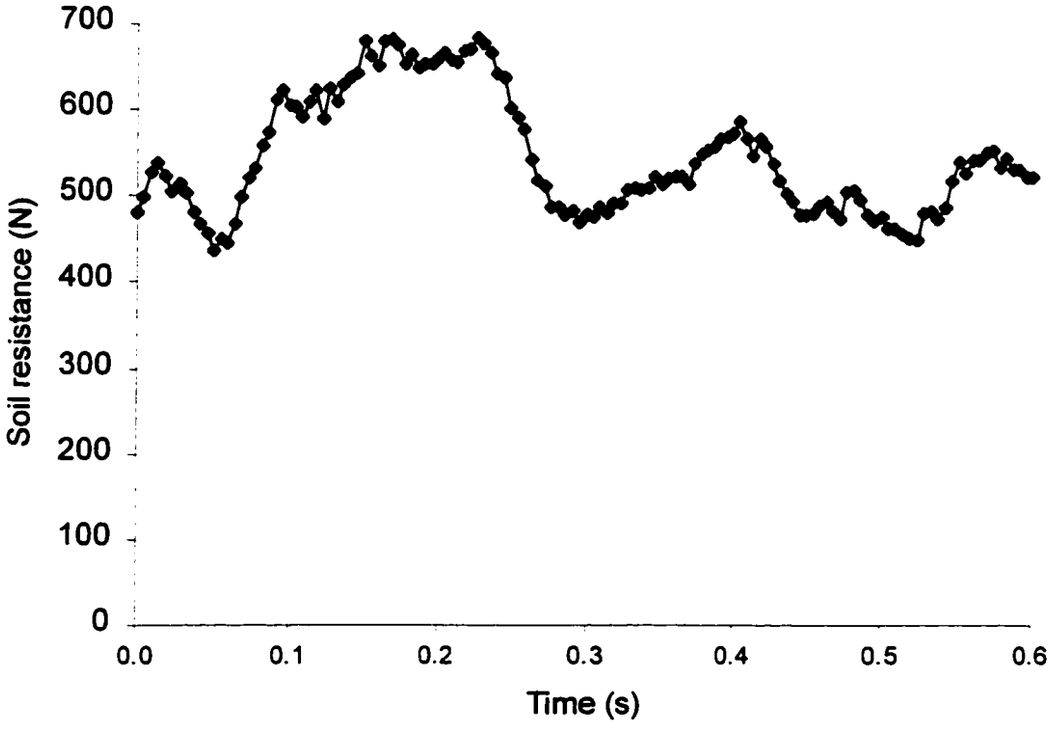

Figure 7.8 Measured soil cutting resistance at 1.6 km/h speed

7.4 Model Verification and Discussion

Theoretical analysis of the shank vibration has been given in Chapter 6 by using the finite element model to simulate the motion of the shank under the assumed harmonic soil cutting resistance. The parameters that affected the vibration of the shank also have been analyzed. However, the measured draft was different from the harmonic assumption. The draft is not an independent parameter as the previous analysis suggested. It is dependent upon the soil properties, tool geometry and the relative movement between the sweep and soil. The soil resistance applied on the blades arises from the relative motion between the blade and the soil. The soil bin tests were carried out for the purpose of verifying the finite element model.

The soil cutting resistance was obtained by solving the dynamic equations governing the lateral motion of the beam through the measurement of the strain change on the beam. By doing so, the inertial effect on the bending of the shank was eliminated. Then, the soil cutting resistance acting on the shank thus obtained, was applied in the finite element analysis. The soil cutting resistance was measured after the tillage tool traveled some distance in the soil bin. The soil resistance applied on the blade tended to produce restrained deflection and velocity. With restrained deflection and velocity, after a sufficiently large number of impacts and force cycles, both the soil cutting force and the rebound velocity are close to their values at some previous impact time as detected experimentally. From this time on, the motion was more likely as the practical operation. Thus, the measured value of deflection of the beam at that time was introduced as the initial condition of the finite element model. The sampling rate was 220 Hz for the test at the traveling speed of 1.6 km/h.

Figure 7.9 shows the finite element solution of deflection of the shank under the action of the measured soil cutting resistance at the traveling speed of 1.6 km/h. Figure

7.10 illustrates the finite element solution for the acceleration of the shank under the action of the measured soil cutting resistance. Figure 7. 11 gives the finite element solution of the velocity of the shank for the carriage speed of 1.6 km/h.

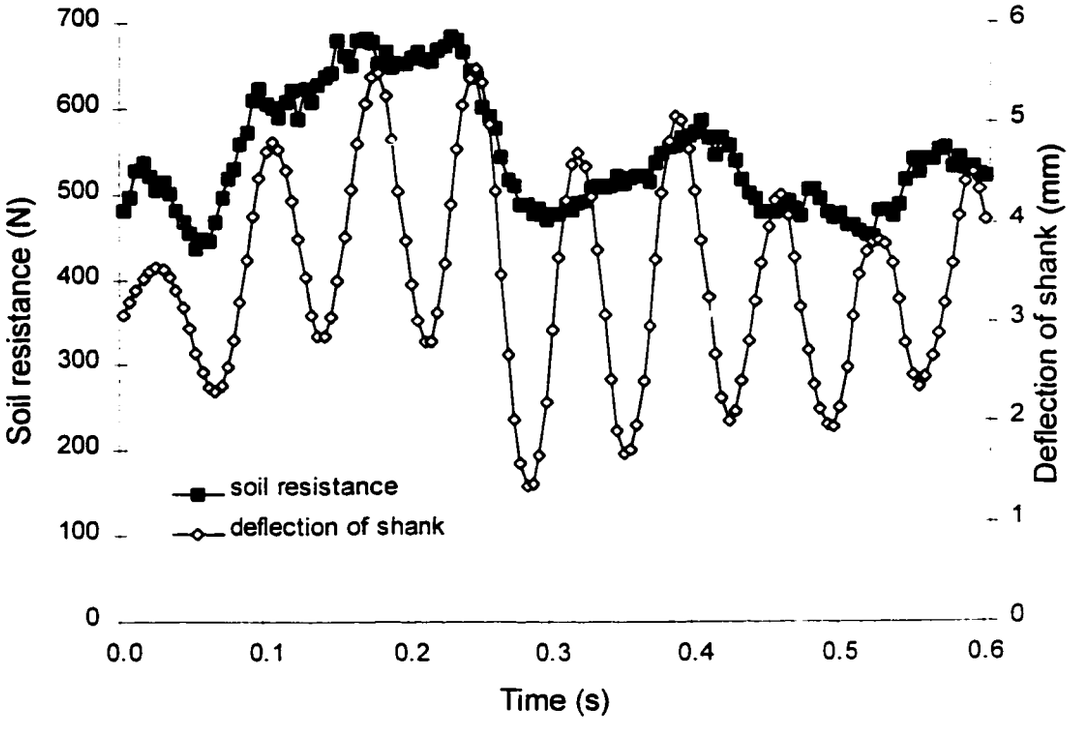

Figure 7.9 Finite element solution of the deflection of shank under measured soil resistance at speed 1.6 km/h

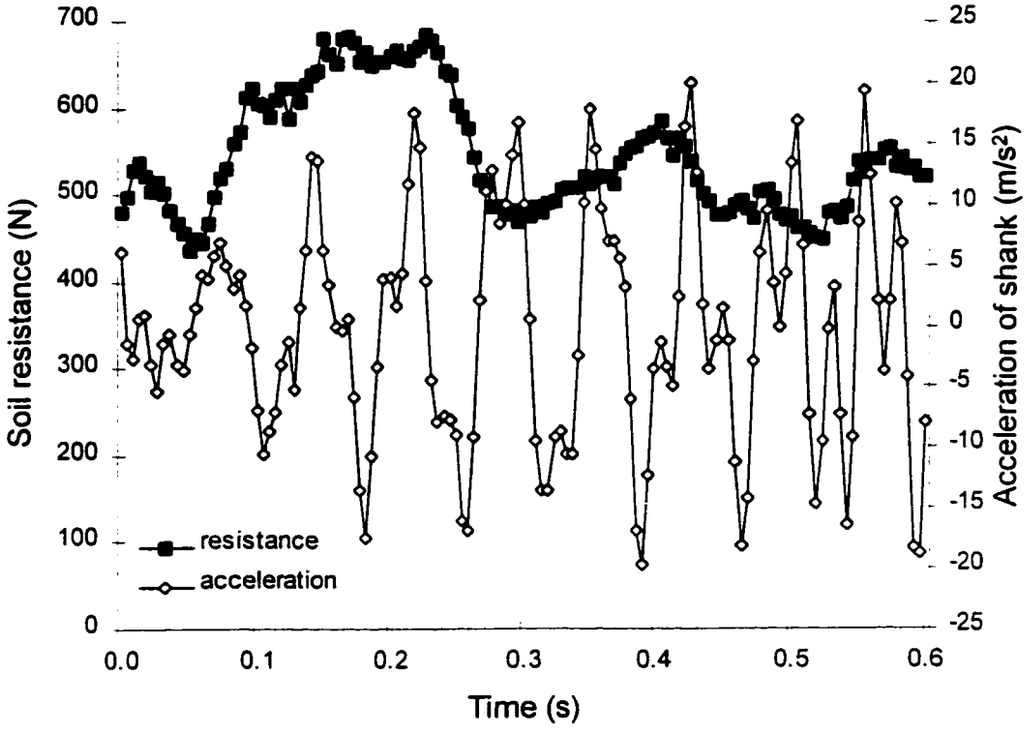

Figure 7.10 Finite element solution of the acceleration of shank under measured soil resistance at speed 1.6 km/h

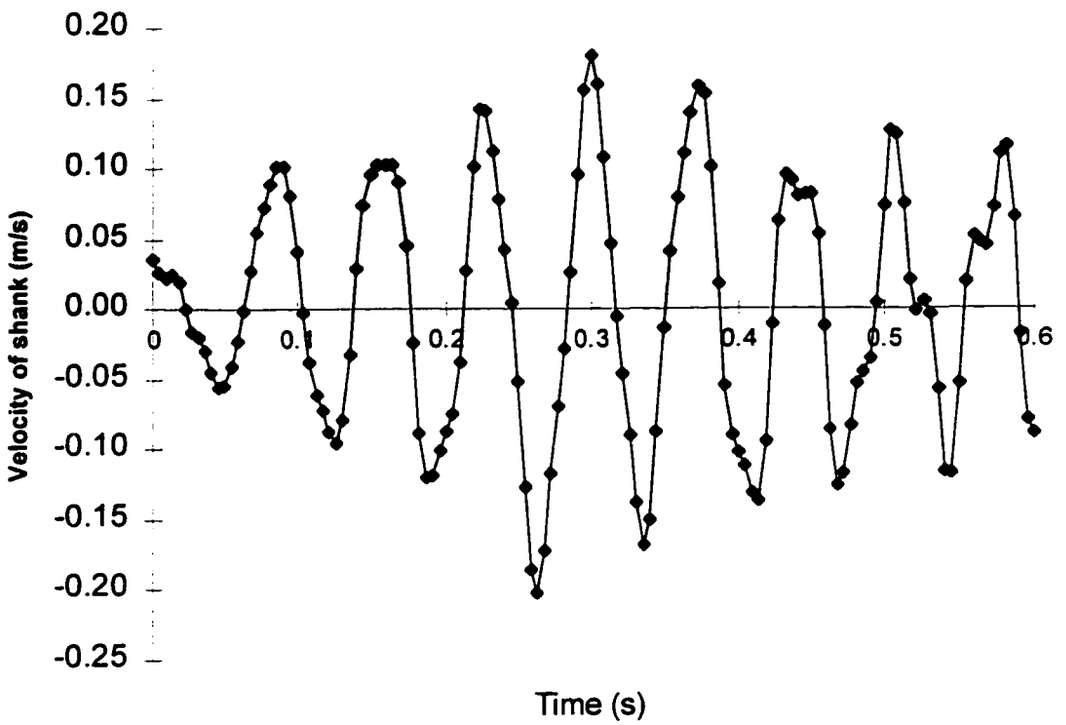

Figure 7.11 Finite element solution of the velocity of shank under measured soil resistance at speed 1.6 km/h

The solutions of the finite element model were compared with the data from the soil bin test. Figure 7.12 presents the direct comparison between static solution and simulated deflection traces for the test implement at traveling speed of 1.6 km/h, at the different time intervals. Figure 7.13 shows the comparison between the measured and predicted acceleration response. It can be seen that there is a correlation between predicted and measured data. The comparison exhibits generally good agreement in terms of the deflection and acceleration at the first few points. Beyond the first few data points, the predicted data have a higher fluctuation.

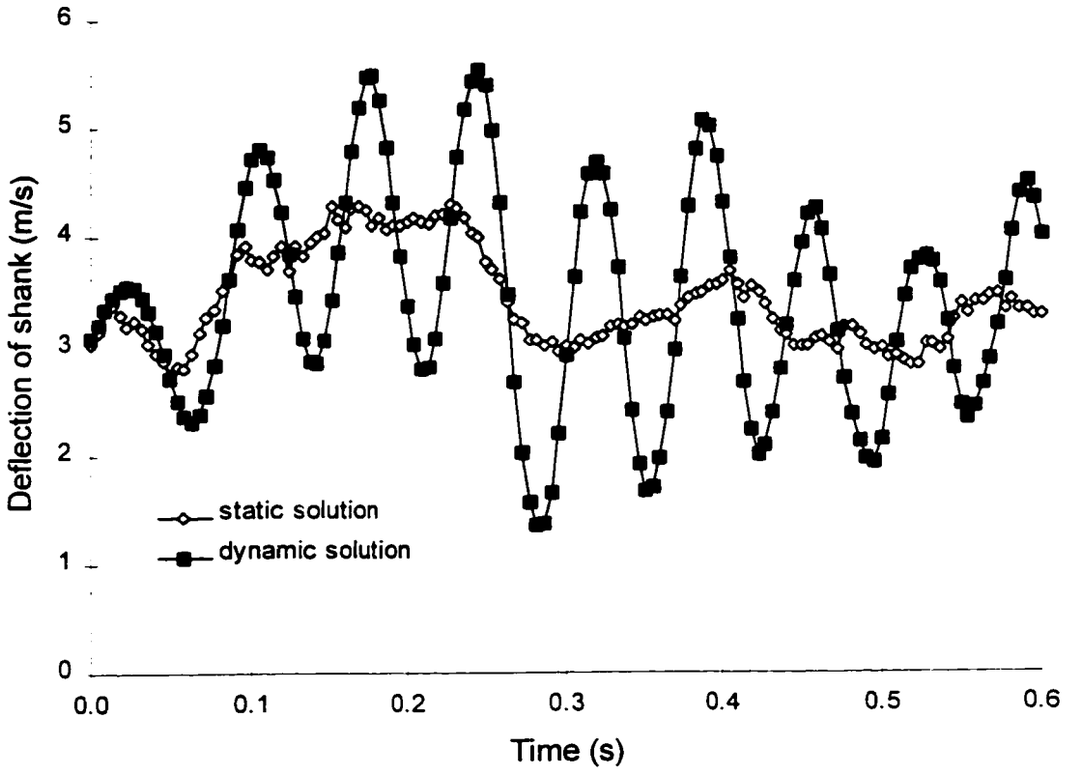

Figure 7.12 Comparison of the finite element solution of deflection with the static solution under measured soil resistance at speed 1.6 km/h

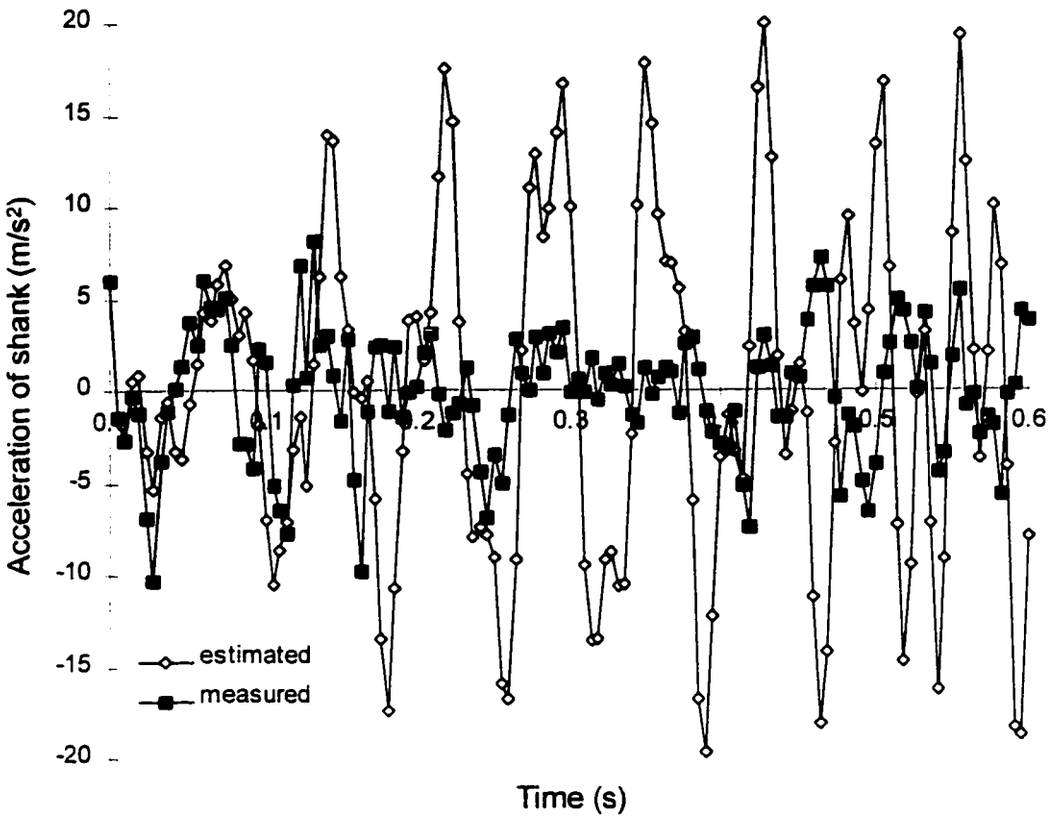

Figure 7.13 Comparison of the finite element solution of acceleration with the measured value under soil bin resistance at speed 1.6 km/h

The soil bin test also was conducted for a carriage speed of 3.2 km/h. The soil cutting resistance and the acceleration of the shank was measured at the sampling rate of 440 Hz. The measured soil cutting resistance was applied to the finite element model to simulate the response motion of the shank at each time interval. Figure 7.14 shows the finite element solution of deflection of the shank under the action of the measured soil cutting resistance at the traveling speed 3.2 km/h. Figure 7.15 illustrates the finite element solution of acceleration of the shank under the action of the measured soil cutting resistance. Figure 7.16 gives the finite element solution of the velocity while the measured soil resistance was applied to the model. The solutions of the finite element model were compared with the data from the soil bin test. Figure 7.17 shows the direct comparison between the static solution and the simulated deflection traces for the test implement at traveling speed 3.2 km/h with respect to time. Figure 7.18 shows the comparison between the measured and predicted acceleration curves. Comparing the finite element solution for different speeds, the estimated acceleration at speed 3.2 km/h was closer to the measured value. The high sampling rate might have contributed to the better simulation results since at a high sampling rate, a smaller Δt was used in the finite element analysis.

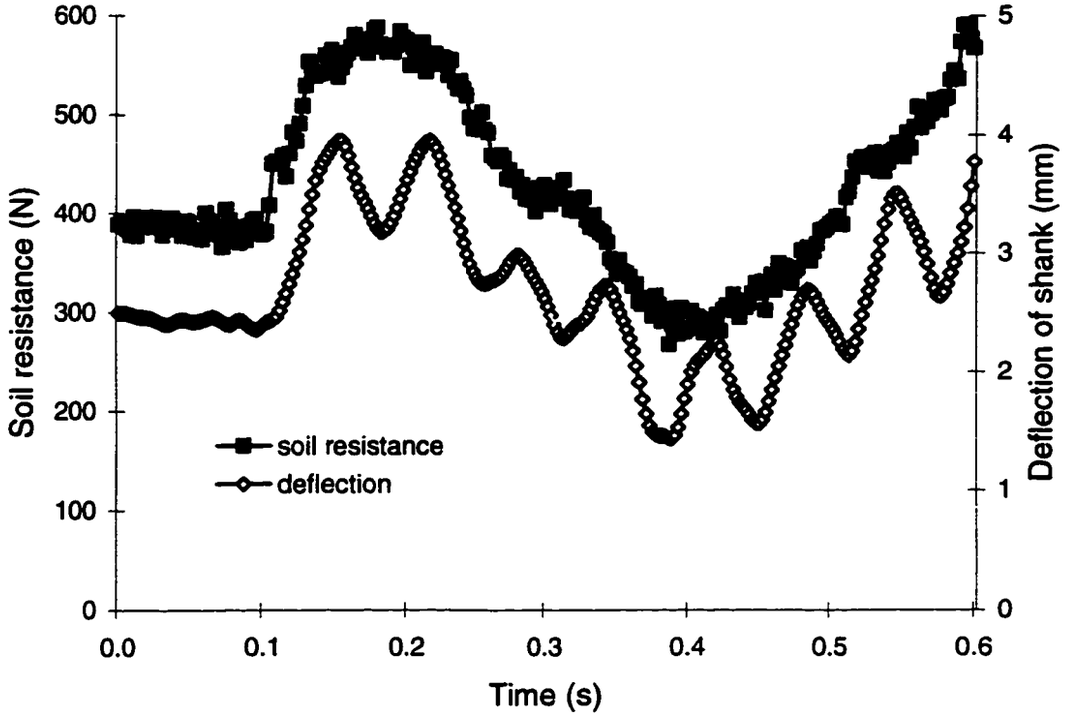

Figure 7.14 Finite element solution of deflection

under soil bin cutting resistance at speed 3.2 km/h

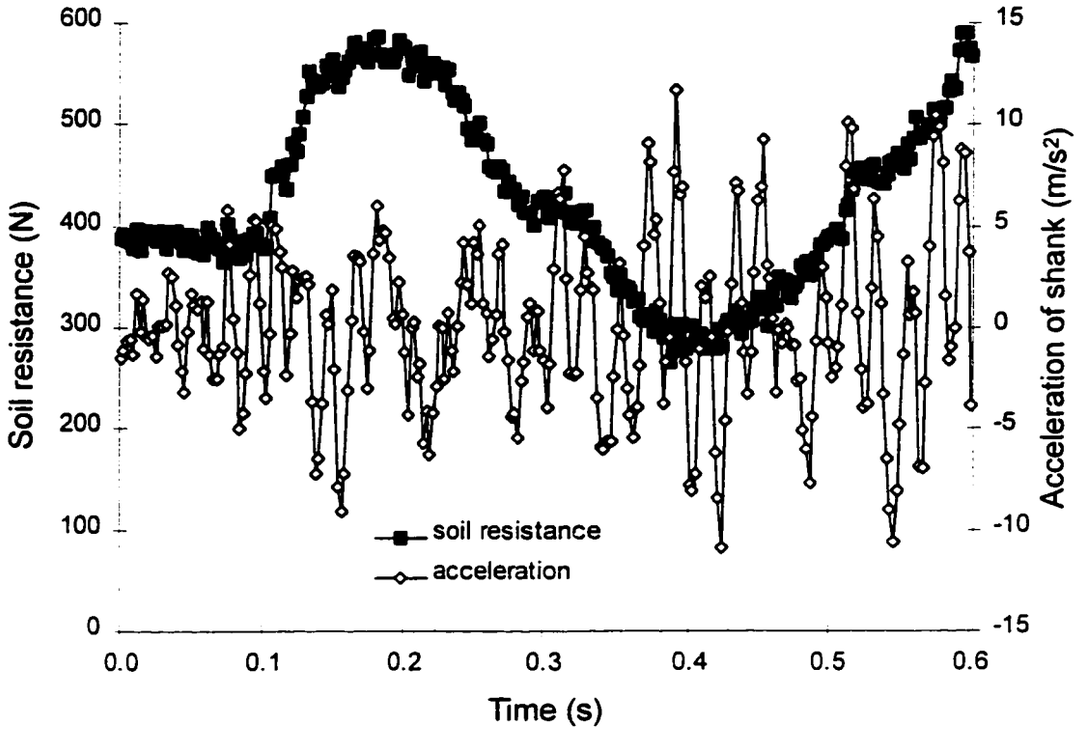

Figure 7.15 Finite element solution of acceleration under soil bin cutting resistance at speed 3.2 km/h

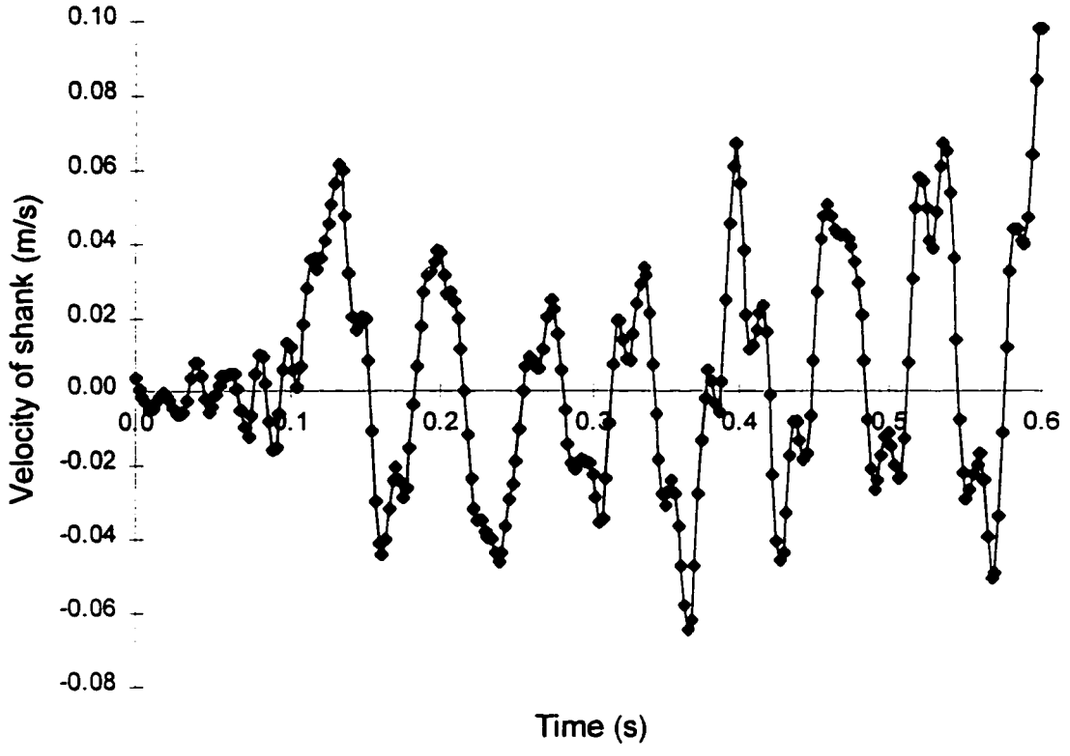

Figure 7.16 Finite element solution of velocity

under soil bin cutting resistance at speed 3.2 km/h

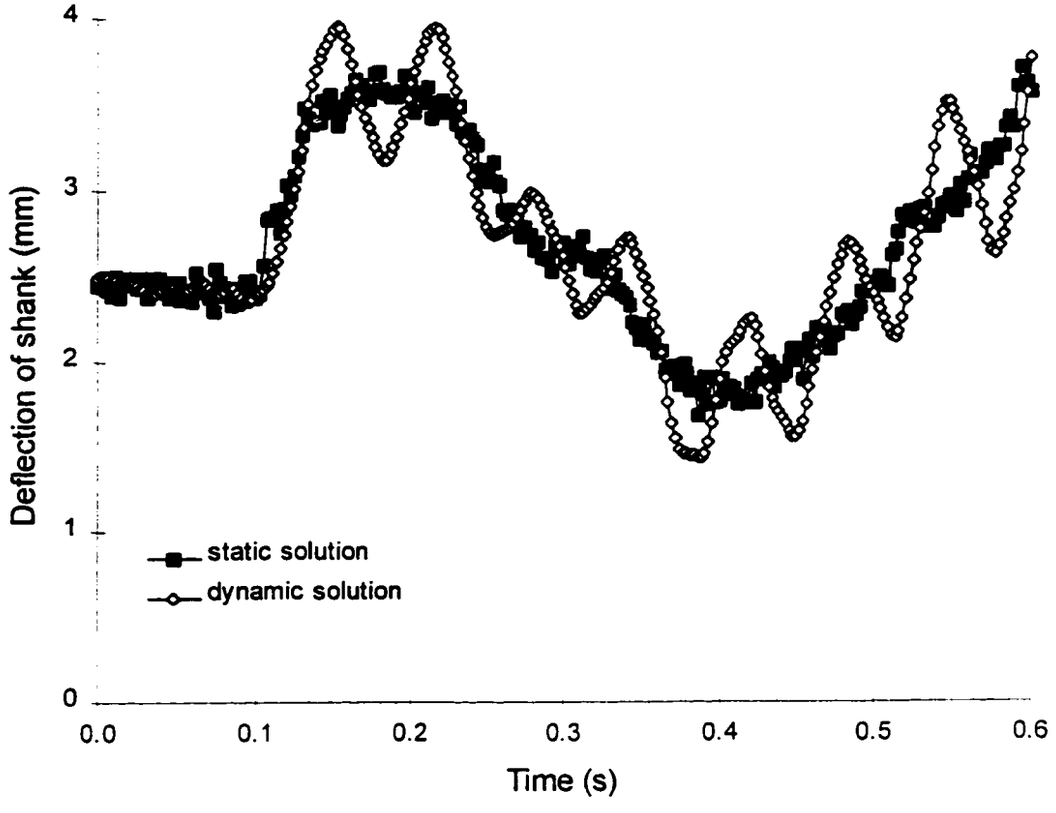

Figure 7.17 Comparison of the finite element solution of deflection with the static solution under soil resistance at speed 3.2 km/h

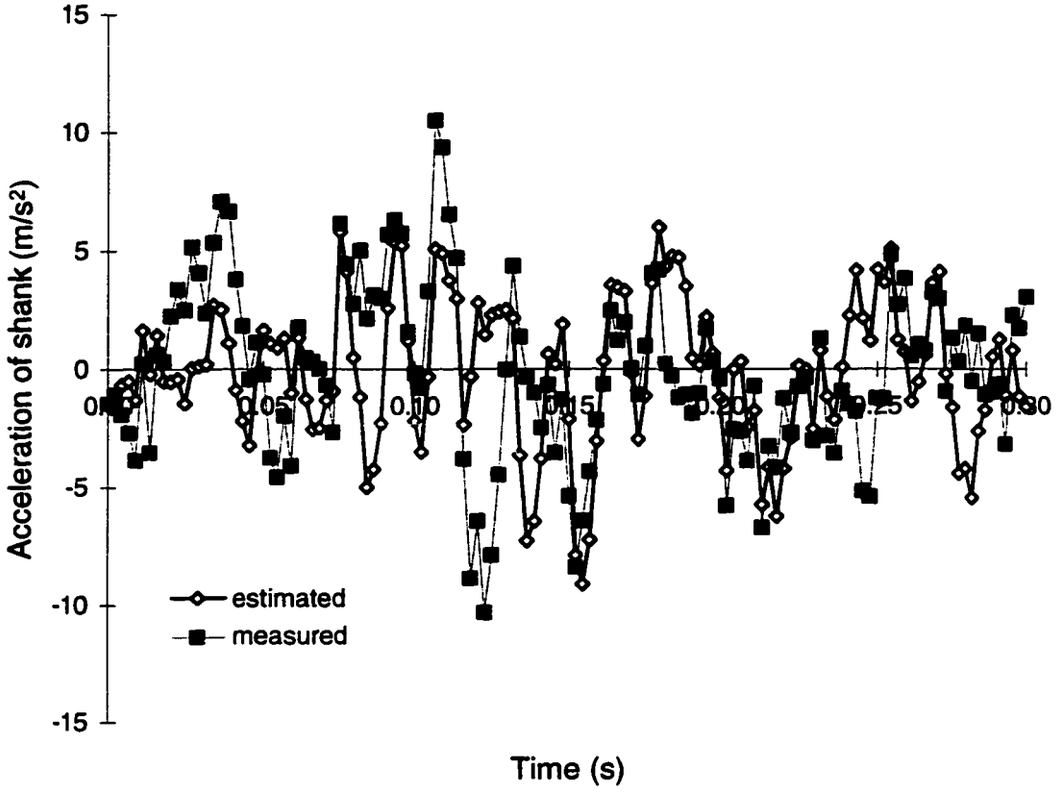

Figure 7.18 Comparison of the finite element solution of acceleration with the measured value at speed 3.2 km/h

As the soil resistance increases, the deflection of the shank increases, and more elastic energy is stored in the stressed beam until the dynamic system is balanced. The energy stored in the beam tends to be released as long as the soil resistance decreases and the shank begins to move forward relative to the frame, while the dynamic system reaches a new equilibrium state. The vibration of the system involves the transfer of its potential energy to kinetic energy and kinetic energy to potential energy, alternately. When the tool operates in the field, the soil resistance is passively applied to the tool. It is due to the movement of the tillage tool which encounters soil resistance. Hence, the soil cutting resistance is determined by the movement of the tillage tool. When the shank moves forward relative to the implement, the soil resistance tends to increase to restrict its movement. When the shank moves backward relative to the implement, the soil resistance tends to decrease so the stored elastic energy in the stressed beam is released to confine its movement. This kind of confinement created by the soil cutting resistance corresponding to the movement of the shank keeps the system relatively stable. For the finite element model prediction, although the measured soil cutting resistance was applied, the draft does not correspond to the predicted movement of the shank. It is an independent time sequential observation for the prediction model. The finite element model gives a good agreement for the deflection and acceleration at the first few points of prediction shown in Fig 7.19. Beyond the first few estimations of the finite element model, the difference between the simulation and field test gradually increases. The vibration system detects a higher fluctuation in deflection and acceleration compared with the observed values as shown in Figs. 7.12, 7.13, 7.17, and 7.18 as the shift of the prediction accumulated. Some of the parameters, including the mass variation of the system, measurement error of soil cutting resistance, and natural frequency shift of the system, will cause the shift and error in the finite element calculation. A change in amount of soil, adhered to the tool during the tillage operation, will affect the inertia force of the system and also alter the system natural frequency.

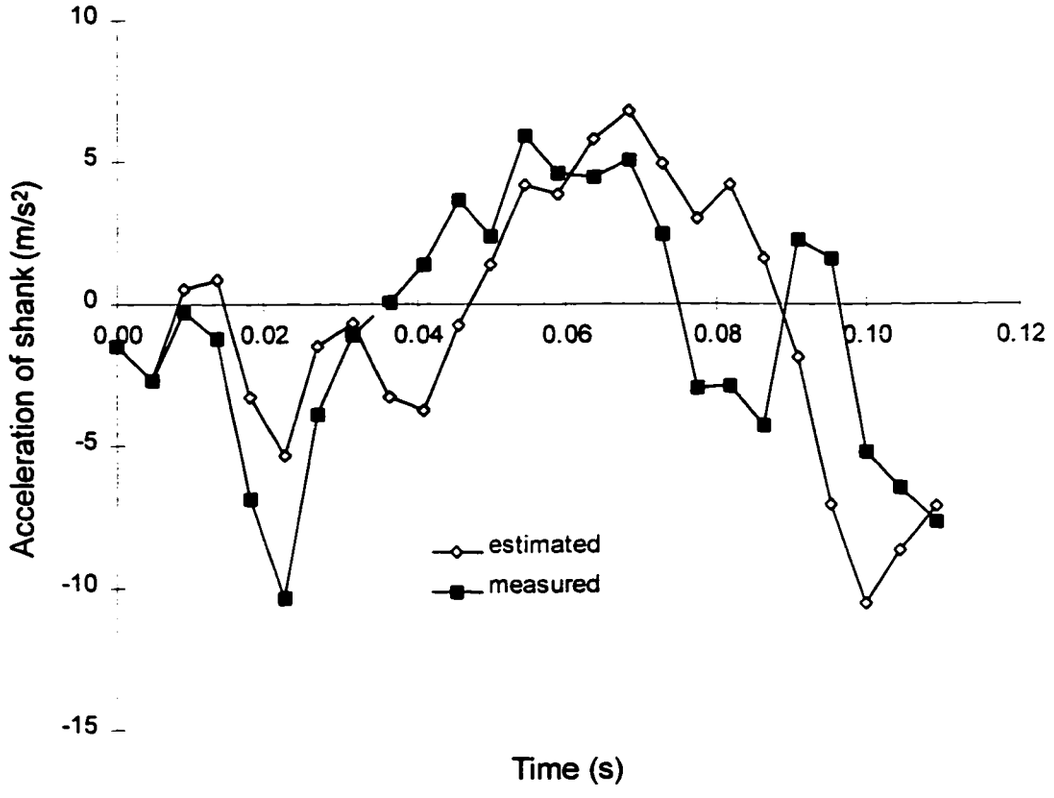

Figure 7.19 Comparison of the finite element solution of acceleration with measured value at first few points at speed 1.6 km/h

7.5 Data Analysis

Data analysis was necessary to provide the useful information and to confirm that the measurement procedure was not contaminated.

7.5.1 Fourier transfer analysis of finite element estimation

The dynamic responses of the tillage shank under the action of the soil cutting resistance were associated with some frequencies which are dependent on the characteristics of the tool implement and the type of soil.

Figure 7.20 shows the finite element solution of deflection output in the frequency domain. The FFT analysis of acceleration and velocity output in the frequency domain is presented in Figs 7.21 and 7.22, respectively. The dominant frequency is seen to be about 14 Hz. Note that the amplitude increases in the high frequencies for the velocity and acceleration output since their outputs are proportional to ω and ω^2, respectively.

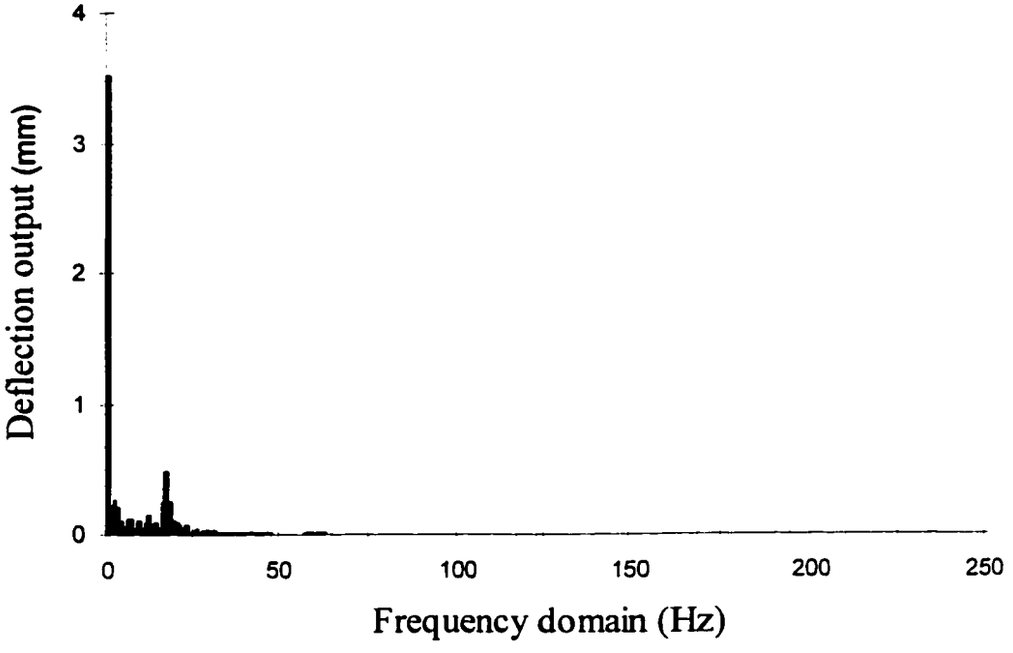

Figure 7. 20 FFT analysis of finite element solution of deflection under soil bin cutting resistance at speed 1.6 km/h

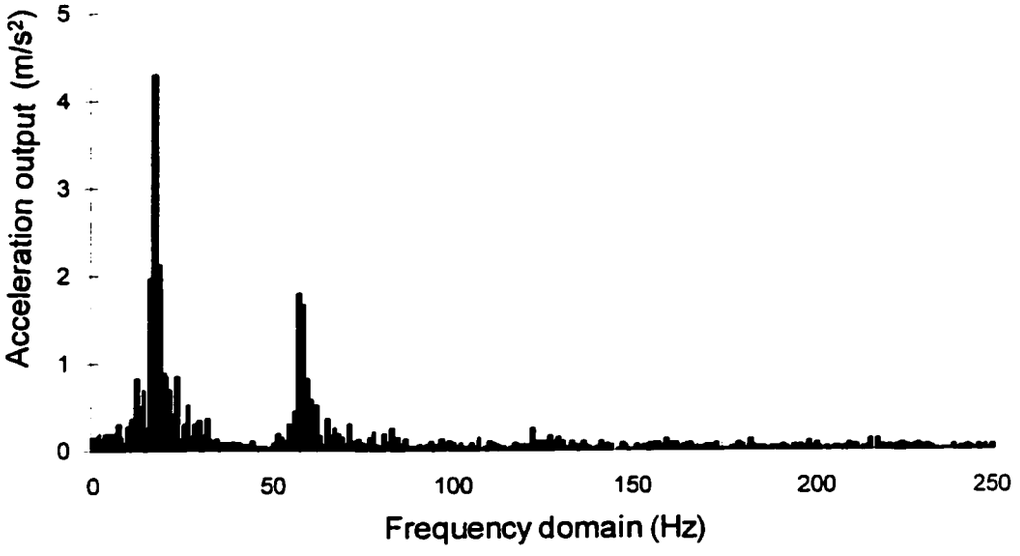

Figure 7.21 FFT analysis of finite element solution of acceleration under soil bin cutting resistance at speed 1.6 km/h.

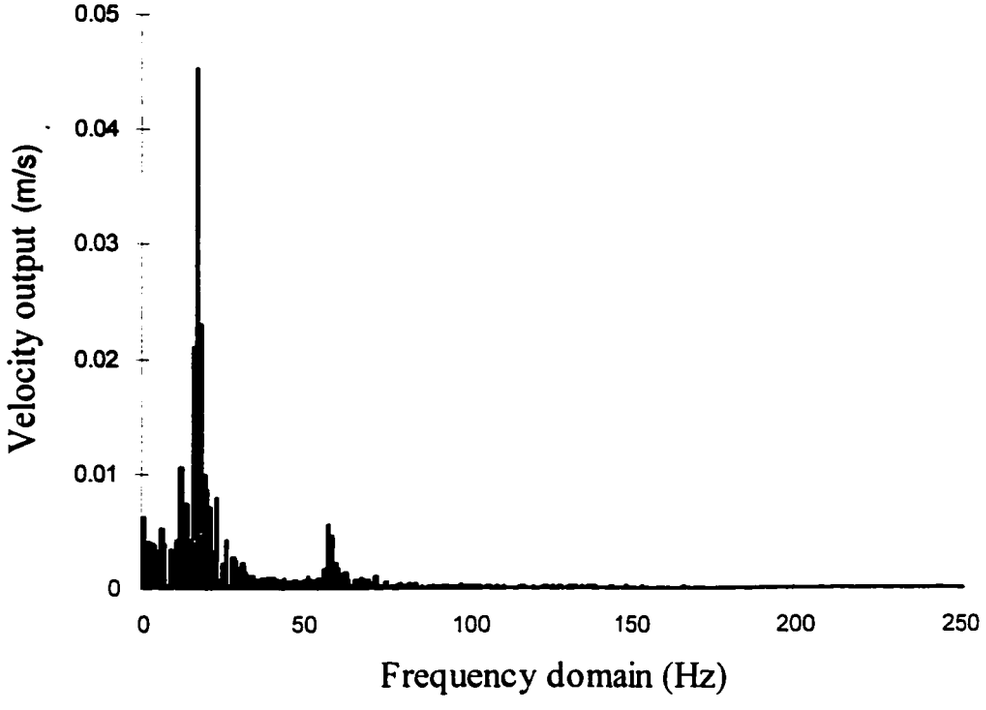

Figure 7.22 FFT analysis of finite element solution of velocity under soil bin cutting resistance at speed 1.6 km/h.

7.5.2 Aliasing analysis

Before any series of data can undergo digital signal processing, the data must be windowed and sampled. The rate at which the data is sampled determines how well it is defined and how close the discrete representation is to the analog original. The rule governing proper sampling is referred to as the Nyquist theorem (Bendat and Piersol 1986), which states that the sampling rate must be at least twice the frequency of the highest frequency component in the waveform being sampled. In other words, there must be at least two samples per cycle for any frequency component to be defined. If the sampling rate is less than twice the highest frequency component aliasing occurs. If the curve frequency is greater than the 1/2 of the sampling rate, the components fold around the edges of the FFT magnitude display and move back to a lower frequency area. It is the representation of a high frequency component by a low frequency component.

Figures 7.23 and 7.24 present the FFT analysis output of the soil cutting resistance on the frequency domain at speeds 1.6 and 3.2 km/h, respectively. It can be seen that the sampled signal drops to an insignificant level at high frequency, which indicates that there is no aliasing existing for the test data. Also the signals beyond 200 Hz were filtered using a low pass filter.

It is not possible to have a sampling rate that ensures two samples per cycle for all frequencies in the data series. This causes a considerable number of frequencies with insignificant magnitude which could exist in the high frequency area.

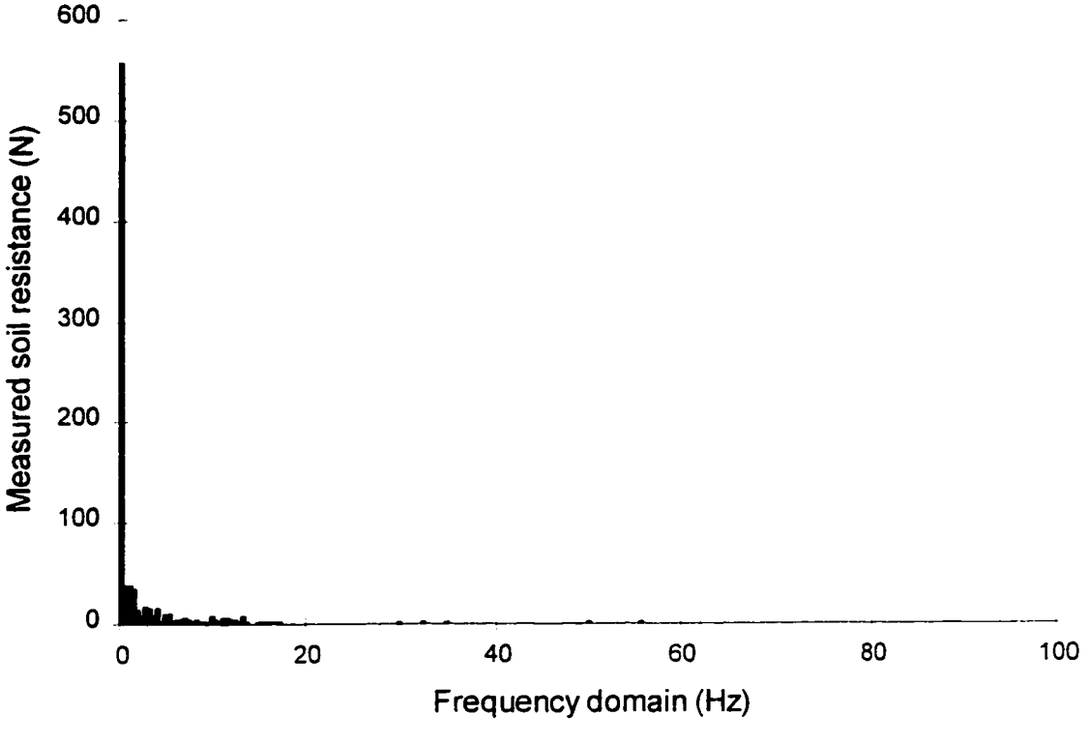

Figure 7.23 FFT analysis of soil bin cutting resistance at speed 1.6 km/h

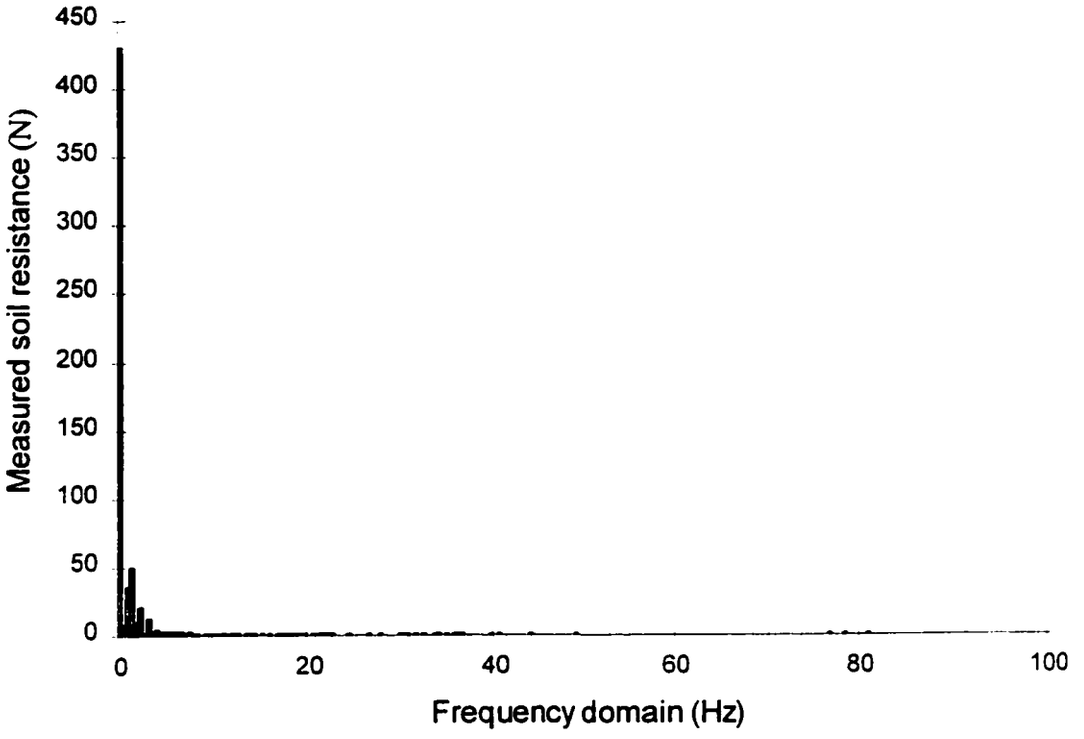

Figure 7.24 FFT analysis of soil bin cutting resistance at speed 3.2 km/h

CHAPTER 8

SUMMARY, CONCLUSIONS, AND SUGGESTIONS FOR FUTURE WORK

8.1 Summary

A theoretical investigation for soil cutting by forced oscillation and self-excited oscillation was presented. A model was developed to predict energy consumption of the forced oscillatory operation. A finite element model was developed to simulate the responses of the shank and tool under the transverse soil cutting resistance for the self-excited oscillation. The model was verified from experiments in an indoor soil bin.

For the forced oscillatory soil cutting, a model was developed to represent the force relationship of the vibrating system. The energy consumption model was suggested considering the oscillator driver and the tractor drawbar power. Utilizing the phenomena of soil resistance change by the effect of vibration velocity, the total energy consumption was obtained by using the numerical integration over the vibratory cycle. A comparison in energy consumption between the oscillatory and non-oscillatory case was presented with respect to the change of frequency and amplitude of the oscillatory system. An optimum frequency and amplitude were suggested to minimize the total energy consumption for the given parameters of the vibratory system.

Draft power plus the power needed to drive the vibrator constituted the total power consumption. Oscillatory operation generally resulted in a reduction of average soil cutting resistance. However, the draft reduction was achieved at a substantial increase of the overall power requirement.

The energy consumption for the soil cutting portion decreased as the vibratory frequency and amplitude increased. The energy needed to drive the vibrator increased with the increase of the vibratory frequency and amplitude. As a result, the total energy consumption was found to increase in the forced oscillatory operation. A nearly unit energy consumption ratio (the energy consumption of forced oscillation over the non-oscillatory operation) can be realized by optimizing the vibratory system.

For the self-excited soil cutting operation in the field, the tillage tool encounters periodic fluctuations of cutting resistance owing to the nonhomogeneous characteristics of soil. The fluctuations cause the shank of the tillage tool to move backward and forward relative to the implement. This phenomenon indicates that the actual tillage tool operation is a vibration process. Contrary to the forced vibration, this kind of process is called self-excited vibration.

Fast Fourier analysis of the measured soil resistance indicated that the draft fluctuated in a periodic manner with the associated frequencies up to 5 Hz. The dominant frequency was found at about 1 Hz. Draft forces for a sweep in the soil bin varied typically ±30% of the mean value.

The general differential equation of motion for the transverse vibration of the beam was used to describe the movement of the shank and tool relative to the frame. A sweep bolted at the end of shank was considered as a lumped mass attached to the beam (shank).

A finite element model was developed based on the fourth differential equation of the lateral vibration of the beam. The tillage tool was considered as a cantilever beam with lumped mass subjected to a transverse load acting on the tool. The results from the

finite element analysis included the deflection, slope, velocity, and acceleration of the shank at each node at various time intervals. The Newmark direct integration method was employed in the finite element model to obtain the transient values of the time intervals.

A constant soil cutting force was first considered as transverse load acting on the tool in the finite element analysis. The results of the finite element calculation indicated that the movement of the tillage tool was determined by its own characteristics and the applied transverse soil resistance. A sinusoidal load with 1 Hz frequency was then considered in the finite element analysis. The responding movement of the dynamic system was related to the frequency of the applied soil resistance. The results indicated that two dominant frequencies were associated with the curves of deflection, slope, velocity, and acceleration. One was the frequency of the applied soil resistance and the other was the fundamental frequency of the system. The resonant vibration occurred as the frequency of applied soil resistance was close to the natural frequency of the system.

A parametric sensitivity analysis was carried out to provide the basis for selecting the parameters that determine the performance of the vibration system. The deflection and velocity of the system were proportional to the length of the shank while the acceleration value decreased slightly as the length of the shank increased. The deflection and velocity decreased with an increase in flexural rigidity of the shank. There was no apparent change in the acceleration as the flexural rigidity are varied. The tillage tool was considered as the lumped mass attached on the shank. The attached mass tended to reduce the natural frequency of the vibration system.

Soil bin tests were carried out to verify the calculation of the finite element model by comparing the acceleration between measured and estimated data under the same soil

cutting resistance. Soil cutting resistance was obtained by measuring the strain change on the shank. The strain is directly related to the bending moment generated there. For the static problem, the bending moment is induced by the transverse load on the shank. The transverse load on the shank can be obtained by proper calibration through the measurement of the strain. For the dynamic system, the acceleration of the mass also added a bending moment component to the shank. Hence, the soil cutting resistance was obtained by solving the dynamic equation governing the lateral motion of the beam considering the effect of the inertia term. The soil cutting resistance obtained by this procedure was used for the dynamic analysis and evaluation of the finite element model of the tillage shank operation.

Comparing the acceleration between measured and estimated data, there was an apparent correlation between the finite element model estimations and the test results. In general, a good agreement was achieved in terms of acceleration at the first few points of the calculation. Beyond the first few points, the predicted data had a high fluctuation at a speed of 1.6 km/h. However, a close prediction was obtained in terms of acceleration at a travel speed 3.2 km/h. The better prediction was attributed to a small Δt used in the finite element analysis due to the high sampling rate of 440 Hz. Differences in the results from finite element method and the test results could be attributed to the error accumulation and shift of the estimation.

The finite element model was also used to predict the fluctuation of movement of the dynamic system assuming soil was homogenous and cutting resistance was linearly dependent on velocity. The results indicated that the fluctuation of the dynamic system gradually stabilized since the soil acted as a damping media to restrict the movement of the tillage tool. However, under the field conditions, the variations in soil resistance

would induce the vibration of the system although the vibration was restrained in both the soil bin tests and the finite element analysis.

8.2 Conclusions

1. A dynamic model was successfully used to predict the total energy consumption by considering the energy required for the soil cutting and for driving the oscillator.

   a) A forced oscillatory operation resulted in a decrease in the average soil cutting resistance. However, the draft reduction was achieved with additional power required for driving the oscillator. The overall total energy consumption was found to increase with the oscillator operation.

   b) The soil cutting energy consumption decreased as the amplitude and frequency increased while the energy consumption of the oscillator increased with increase of the amplitude and frequency of the system.

   c) The total energy consumption can be minimized by selecting a proper frequency and amplitude of the oscillatory system.

2. A finite element model was successfully used to simulate the responses of the tillage shank and tool under the transverse soil cutting resistance. The results from the finite element model included the deflection, slope, velocity, and acceleration of the shank at each node in the time intervals.

   a) The Fast Fourier analysis of the results of the finite element calculation indicated that the movement of tillage tool corresponded to the applied

transverse soil resistance. Two dominant frequencies were associated with the curves of deflection, slope, velocity, and acceleration. One was the frequency of the applied soil resistance and the other was the fundamental frequency of the system.

b) Resonant vibration will occur if the frequency of the soil resistance is close to the natural frequency of the dynamic system.

3. The corresponding motion of the tillage shank was determined by the properties of the beam and the applied soil resistance.

a) The deflection and velocity of the system were proportional to the length of the shank while the acceleration value decreased slightly as the length of the shank increased.

b) The deflection and velocity decreased with an increase in flexural rigidity of the shank. These results indicated that the length of the shank was the most sensitive parameter in determining the response of the shank movement.

c) The mass of the tillage tool tends to decrease the frequency of the vibrating system.

4. The verification of the model was in good agreement in terms of the acceleration for the first few points of comparison. A higher sampling rate provided a better agreement between the test data and the model estimations.

a) Both of the finite element results and soil bin test indicated that the soil media had the tendency to restrict the movement of the tillage tool. The movement of the self-excited vibratory operation was confined.

b) Draft forces for a sweep in the soil bin varied ±30% of the mean value with the associated frequencies up to 5 Hz.

8.3 Suggestions for Future Work

For the forced oscillatory soil cutting, a further experiment should be conducted to verify the energy consumption model considering the optimum frequency and amplitude. To match the frequency and amplitude for minimum energy consumption, a variable amplitude and stiffness spring system are suggested.

The finite element model has been developed based on the differential equation governing the motion of transverse vibration beam subjected to a point load on the end of the shank. In real tillage operation, different kinds of assembly other than the simple beam construction are used. A curved shank with a suspension spring connection is a common configuration. A more sophisticated two dimensional equation should be considered to describe the motion of the curved tillage assembly.

The work reported in this research project is still in a preliminary stage. To provide information for the optimum design of tillage assembly, more tests should be conducted under different conditions, such as various field conditions, different configurations of the tillage assembly, different travel speeds, etc. The best combination can be selected to provide a satisfactory soil structure for seed emergence and crop growth with a minimum of energy input.

The oscillatory tillage tool produces smaller soil aggregates than a rigid one. For self-excited oscillatory operation, further investigations are needed to considering the effects of amplitude and frequency on the aggregate size of soil.

REFERENCES

Adams, B. A. 1996. Critical state behavior of an agricultural soil. Unpublished Ph. D. thesis. Department of Agricultural & Bioresource Engineering, University of Saskatchewan, Saskatoon, Sask.

Bendat, J. S. and A. G. Piersol. 1986. *Random Data Analysis and Measurement Procedures,* 2nd ed. New York: John Wiley & Sons, Inc.

Blekhman, I. I. 1954. An investigation into the process of vibrational driving of piles and sheet piles. Inzy. Sb., Inst. Mekh. Acad. Nauk. U.S.S.R. 19:54-64.

Boccafogili, A., G. Busatti, F. Ghfrard, F. Malaguti and R. Paoluzzi. 1992. Experimental evaluation of cutting dynamic models in soil bin facility. *Journal of Terramechanics* 29(1):95-105.

Boyd, B. H. and C. L. Nalezny. 1967. A model of vibratory soil cutting. Society of Automotive Engineers Paper No. 670750.

Brown, J. M. 1978. Soil excavation improvement from bulldozer blade oscillation. Society of Automotive Engineers Paper No. 780776.

Buckingham, F. 1976. *Tillage, Fundamentals of Machine Operation.* Deere & Company, Moline, Illinois.

Buston, M. J. and D. MacIntyre. 1981. Vibrating soil cutting I; Soil tank studies of draught and power requirements. *Journal of Agricultural Engineering Research* 26:409-418.

Buston, M. J. and D. H. Rackham. 1981. Vibratory soil cutting II; An improved mathematical model. *Journal of Agricultural Engineering Research* 26:419-439.

Choa, S. L. and W. J. Chancellor. 1973. Optimum design and operation parameters for a resonant oscillating subsoiler. *Transactions of the ASAE* 16(6):1200-1208.

Cooper, A. W. and W. F. McCreery. 1961. Plastic surfaces for tillage tools. ASAE Paper No. 61-649. St. Joseph, MI:ASAE.

Cowper, G. W. 1966. The shear coefficient in Timoshenko's beam theory. *Journal of Applied Mechanics* 33:335-340.

Dubrovskii, A. A. 1968. *Vibration Engineering in Agriculture*. New Delhi:Indian National Scientific Documentation Center. Published for the U. S. Department of Agriculture (translated from Russian).

Eggenmuller, A. 1958. Field experiment with an oscillating plow body. *Grundlagen der Landtechnik.* 10:89-95.

Garber, M. 1983. Energy expenditure in cycle-loading processes. *Journal of Terramechanics* 19:257-267.

Gill, W. R. and G. E. Vanden Berg. 1967. Soil dynamics in tillage and traction. In *Agriculture Handbook, Superintendent of Documents*, U.S. Government Printing Office, Washington DC.

Goryachkin, V, P. 1898. The graphical theory of the plow. Collected works in Three Volumes Vol. II:6-55. Moscow:Kolos Publishing House, Republished 1968. (translation No. TT 71-50087 by the USDA and the National Science Foundation, Washington, D. C., 1971).

Gunn, J. T. and V. N. Tramontini. 1955. Oscillation of tillage implements. *Journal of Agricultural Engineering* 36(11):725-729.

Gupta, C. P. and D. S. Rajput. 1993. Effect of amplitude and frequency on soil break-up by an oscillating tool in a soil bin experiment. *Soil & Tillage Research* 25:329-338.

Hendrick, J. G. and W. F. Buchele. 1963. Tillage energy of a vibrating tillage tool. *Transactions of the American Society of Civil Engineers* 6(3):213-216.

Irwin, J. D. and E. R. Graf. 1979. *Industrial Noise and Vibration Control.* Englewood Cliffs, N. J:Prentice-Hall, Inc.

Ji, C. Y., M. N. Chen and J. Z. Pan. 1986. Approach and instrumentation for predicting sinkage of wetland vehicle based on rheological characteristics of paddy soils. *Transaction of the Chinese Society of Agricultural Machinery* 17(1):21-31.

Johnson, C. E. and W. F. Buchele. 1969. Energy in clod-size reduction of vibratory tillage. *Transactions of the ASAE* 12(3):371-374.

Kezdi, A. 1974. *Handbook of Soil Mechanics, Vol. 1.* Soil physics, Amsterdam:Elsevier.

Kondner, R. L. 1960. A non-dimensional approach to the vibratory cutting, compaction and penetration of soils. Technical report 8. Waterway experiment station.

Kushwaha, R. L., L. Chi and J. Shen. 1993. Analytical and numerical models for predicting soil forces on narrow tillage tools-A review. *Canadian Agricultural Engineering* 35(3):183-193.

Kushwaha, R. L. and C. Roy. 1989. Investigations with plasma-sprayed coating of agricultural tools. *Proceedings of the 5th ACOT Research Seminar.* Pointe Claire, Quebec.

Licsko, Z. J. and H. P. Harrison. 1988. Acquisition and processing of soil reaction forces on tillage tools. *Transactions of the ASAE* 31(2):315-318.

Mackson, C, J. 1962. The effect of electro-osmosis on soil to steel gliding friction as influenced by speed, voltage, and soil moisture. ASAE Paper No. 62-650. St. Joseph, MI:ASAE.

Malaguti, F. 1995. System identification and "impendence" of soil cutting. *Proceedings of the 5th International Society for Terrain-Vehicle Systems Conference/Workshop*, 233-238. Saskatoon, SK, May 10-12.

McKyes, E. 1989. *Agricultural Engineering Soil Mechanics.* Amsterdam:Elsevier.

McKyes, E. and O. S. Ali. 1977. The cutting of soil by a narrow blade. *Journal of Terramechanics* 14(2):43-58.

Mink, A. L. 1964. Effects of an air slide on soil engaging tools-results from ammonia knives in artificial soil. ASAE Paper No. 64-105. St. Joseph, MI:ASAE.

Mogami, T. and K. Kubo. 1953. The behavior of soil during vibration. In *Proceedings. of the Third International Conference of Soil Mechanics and Foundation Engineering,* V.I 152-155.

Newmark, M. M. 1959. A method of computation for structural dynamics. *Journal of Engineering Mechanics* 85:67-94.

Nichols, M. L. 1925. The sliding of metal over soil. *Agricultural Engineering* 6(4):80-84.

NRC. 1986. A strategy for tribology in Canada. NRCC 26556, National Research Council Canada, Ottawa.

Olson, D. J. and J. A. Weber. 1966. Effect of speed on soil failure patterns in front of model tillage tools. *Transactions of Society of Automotive Engineers* 74(4):298-310.

Panagiotopoulos, N. 1962. Investigation into the variation of cutting resistance of dozer blades under effect of oscillation. Second international conference of International Society for Terrain-Vehicle Systems.

Reddy, J. N. 1984. *An Introduction to the Finite Element Method.* McGraw-Hill. New York.

Reece, A. R. 1965. The fundamental equation of earth-moving mechanics. Symposium on Earth-Moving Machinery, In *Proceedings of Mechanical Engineers,* 179(3f):16-22.

Salokhe, V. M., M. S. Islam and M. N. Sakalaine. 1994. Power spectral density analysis of draft and torque fluctuations of a PTO powered disk tiller. *Journal of Terramechnics* 31(3):163-171.

Savchenko, I. 1958. The effect of vibration on internal friction in sand. Soil dynamics collection of papers No. 32, State Publishing House on Construction and Constraction Materials, Mosco, NTML translations.

Senator, M. 1967. Vibratory penetration of soils. *Transactions of the American Society of Mechanical Engineering, Journal of Engineering for Industry* 89(4):759-765.

Senator, M. and R. E. Warren. 1971. Penetration rates of fore-aft vibrating plows. *Transactions of the ASAE* 14(1):242-247.

Shabana, A. A. 1991. *Theory of vibration, Vol II:Discrete and continuous system.* New York, NY:Springer-Verlag.

Shkurenko, N. S. 1960. Experimental data on the effect of oscillation on cutting resistance of soil. *Journal of Agricultural Engineering Research* 5(2):226-232.

Simens, J. C., J. A. Weber and T. H. Thornburn. 1965. Mechanics of soil as influenced by model tillage tools. *Transactions of the ASAE* 8(1):1-7.

Singh, N., G. Singh and V. M. Salokhe. 1991. Cyclic variation in moldboard plow draft and its effect on implement control system. *Soil & Tillage Research* 21(3):273-286.

Smith, J. L. and A. M. Flikke. 1972. Theoretical analysis of vibratory tillage. *Transactions of the ASAE* 15(5):831-837.

Spektor, M. 1987. Minimum energy consumption of soil working cyclic processes. *Journal of Terramechanics* 24:95-107.

Stafford, J. V. and S. C. Young. 1986. Sensing soil failure mode for dynamic implement control. ASAE paper No. 86-1045. St. Joseph, MI:ASAE.

Sulatisky, M. T. and P. R. Ukrainetz. 1972. Draft reduction by vibratory soil cutting. *Transactions of the Canadian Society of Mechanical Engineering* 1(4):175-181.

Summers, J. D., M. F. Kocher and J. B. Solie. 1985. Frequency analysis of tillage tool forces. In *Proceedings of International Conference on Soil Dynamics* 2:384-399. Auburn, Alabama.

Szabo, B., F. Barnes, S. Sture, and H. Y. Ko. 1994. Effectiveness of vibrating bulldozer and plow blades on draft force reduction. ASAE Paper No. 941535. St. Joseph, MI:ASAE.

Timoshenko, S. P. 1921. On the correction for shear of the differential equation for transverse vibration of prismatic bars. *Philosophical Magazine, Series 6* 41:744-746.

Upadhyaya, S. K., T. X. Ma, W. J. Chancellor, and Y. M. Zhao. 1987. Dynamics of soil-tool interaction. *Soil & Tillage Research* 9:187-206.

Verma, B. P. 1971. Oscillating soil tools - A review. *Transactions of the ASAE* 14(6):1107-1115.

Winterkorn, H. F. 1954. Dynamic testing soils. Special technical publication. No 156, 77-89. :American Society of Testing Materials.

Young, S. C., C. E. Johnson and R. L. Schafer. 1984. Real-time quantification of soil condition. ASAE Paper No. 84-1037. St. Joseph, MI:ASAE.

Zhang, J. and R. L. Kushwaha. 1995. A modified model to predict soil cutting resistance. *Soil & Tillage Research* 34:157-168.